



POLITECNICO
MILANO 1863

**SCUOLA DI INGEGNERIA INDUSTRIALE E
DELL'INFORMAZIONE**

Laurea Magistrale in ingegneria Meccanica

Transmission and multibody simulation of an electric formula SAE

Supervisor: Prof. Edoardo Sabbioni



POLITECNICO
MILANO 1863

Lorenzo Mario Vitella

836852

Academic Year 2019/2020

Acknowledgements

I am particularly grateful for the assistance given by Michele Vignati.

Table of Contents

1	Introduction	7
2	Layout change	9
3	Transmission	12
3.1	Transmission assembly	12
3.2	Chainring assessment.....	17
3.3	Cover assessment (analytic solution)	19
3.3.1	Bolt joint friction assessment.....	21
3.3.2	shear bolted joints assessment.....	22
3.3.3	Plastic deformation of the hole.....	23
3.4	Chainring bracket.....	24
3.4.1	Mesh creation	25
3.4.2	Loads and constraints	28
3.4.3	Interactions	31
3.4.4	Results	33
3.5	Cover (numerical solution)	37
3.6	Tripod joint.....	38
3.6.1	Static assessment	38
3.6.2	Fatigue assessment.....	42
4	Multibody model of the car	44
4.1	Characteristics of a multibody model.....	44
4.2	Generality of the complete vehicle model	46
5	Pneumatic model study	55
5.1	Pneumatic model description.....	55
5.1.1	Contact forces calculation.....	58
5.1.2	Calculation of the torques on the wheels.....	65
5.1.3	Operating of the closed loop	66
5.2	Description of the simplified tire model	68
5.3	Vertical load behavior	71
5.4	Transverse force depending on the slip angle	73
5.5	Transverse force depending on the sliding coefficient.....	75
5.6	Response to camber variations.....	76
6	Full model study	78
6.1	Steady state maneuvers.....	78
6.1.1	Constant speed cornering	78
6.1.2	Constant cornering radius	82

6.1.3	Constant steering radius	83
6.2	Transient maneuvers.....	85
6.2.1	Braking in a turn.....	85
6.2.2	VDA test.....	86
7	Conclusions	90
8	Bibliography.....	94

1 Introduction

The aim of this thesis is to report two main steps in the conversion of a combustion Formula SAE into an electrical one.

- First step: The conversion of a transmission, designed to operate with a combustion motorbike engine, to another one that can operate with two electric motors.
- Second step: design a multibody model that can be anticipate the real behavior of the new car layout.

To contextualize this thesis it is important to shortly describe what are mean to ATA, formula SAE, formula EI and Dynamis PRC.

The inheritance of ATA (Associazione Tecnica dell'Automobile) born in 1948 was took by ANFIA in the 2016 (Associazione Nazionale Filiera Industria Automobilistica). The aim of ATA and after ANFIA is to increase the motoring culture in Italy. The focus is on the technical aspects, research and training.

Formula SAE Italy, for example, is an activity promoted by ATA.

It is quoted the description on the official site:” *Formula SAE Italy & Formula Electric Italy is a competition for engineering universities only, from all over the world. They have to design and to put together a prototype of a racing car (combustion or electric), following the Society of Automotive Engineers (SAE) rules.*”

The Polytechnic of Milan team that competes in the formula SAE is the Dynamis PRC (Polimi Reparto Corse).

Dynamis PRC born in 2004 tanks to professor Federico Cheli and professor Francesco Braghin. The first developed car, the DPRC 574 BT, designed and built in approximately three years won first place among the Italians team.



Figure 1-1. Dynamis DPRC 574 BT

During the year between 2006 and 2010 were designed and realized four cars with fluctuating results.

This team starts to have a strong organization and better resources after 2010. They designed and realized the car called DP5 during the biennium 2010-2012.



Figure 1-2. Dynamis DP5

This prototype has been chosen like base to develop a car that can be race in the Formula Electric. This choice has been made first of all for the availability of the car itself and for the characteristic of its frame.

The DP5 has a carbon steel tubes frame on the contrary of the newest cars that have a carbon fiber one or an anterior part in carbon fiber and a posterior one in carbon steel tubes.

A steel frame allow to make modification and added new brackets easily. For example to add new brackets for the battery it was enough to weld new tubes to the previous frame. This procedure would have been more difficult with a carbon frame.

It is important underline that the aim of the new prototype is to develop and test the new powertrain that it's going to use in an electric formula car. This actual prototype doesn't respect the rules of formula electric, so it could never take part in an official race.

2 Layout change

In this chapter will be explained the main modify at the frame. The DP5, like already discussed in the previous chapter, has a carbon steel tube chassis.

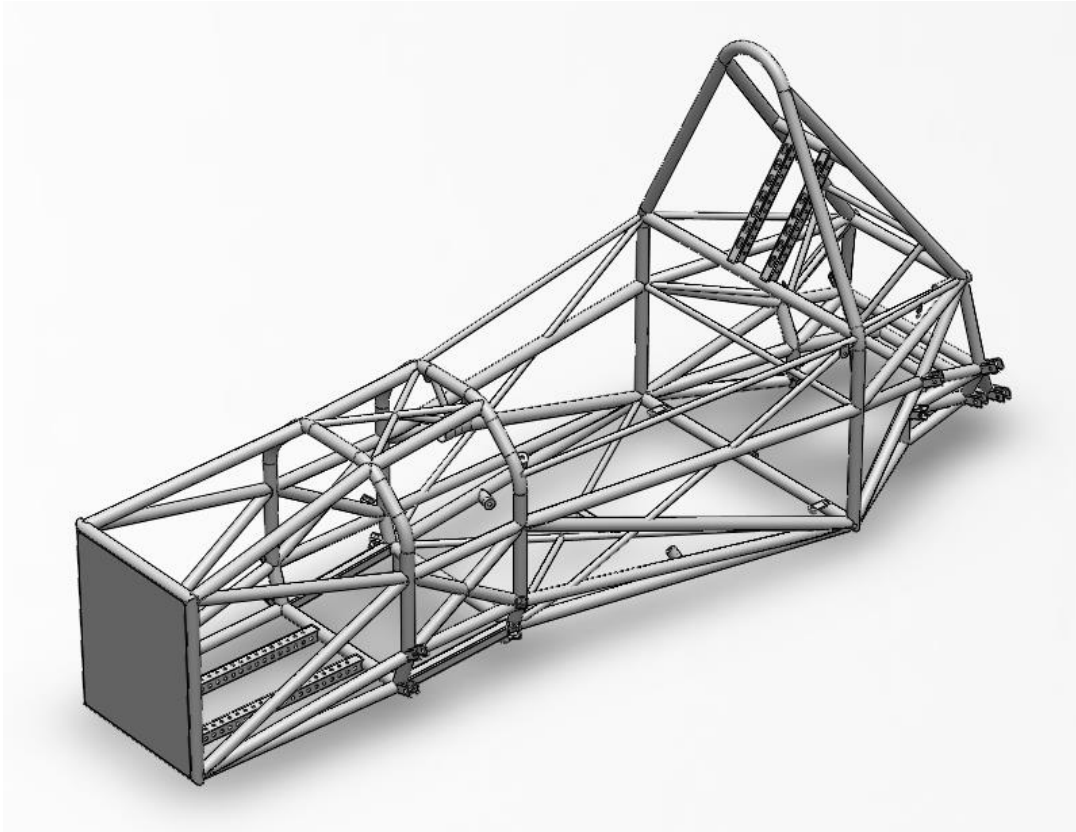


Figure 2-1. DP5 frame

This frame didn't have the space for batteries while the motors and all the component for the electronic control and actuation are positioned inside the previous petrol engine space through new brackets. To allow the housing of the batteries it was necessary to weld two new lateral frame to the main one.

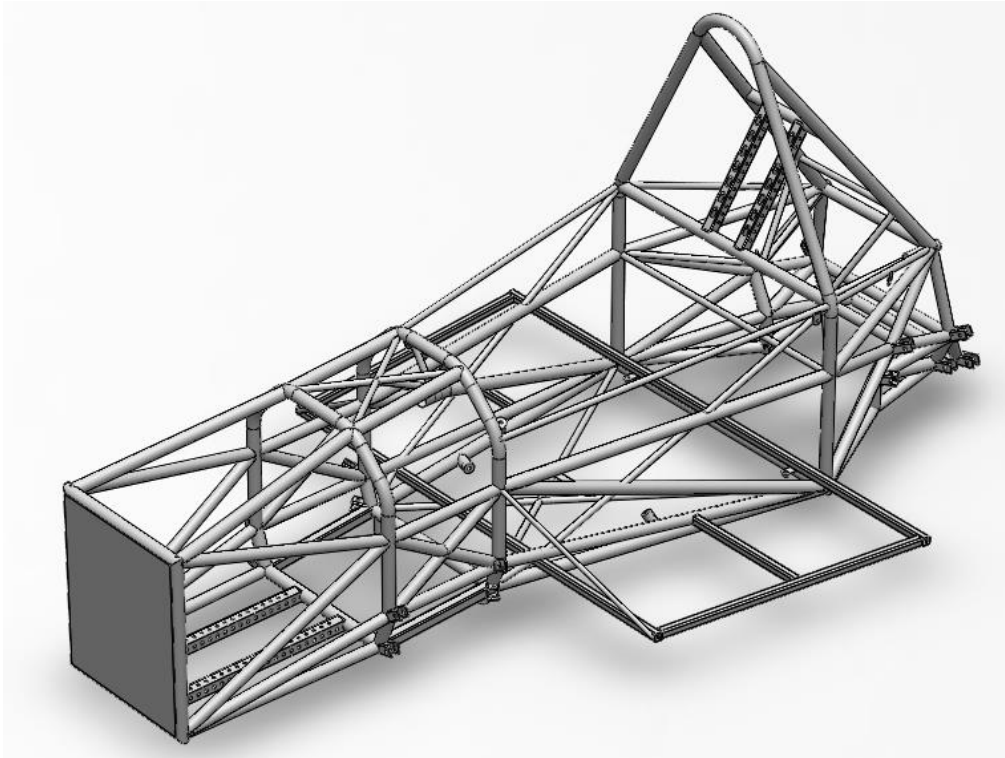


Figure 2-2. Frame with battery brackets

To use the batteries original fixing points it has been welding steel plates that successively was holed.



Figure 2-3. Battery brackets with steel plates

The weight of the two batteries is approximatively of 136 kg. The DP5 original weight was about 200 kg so the inertial properties drastically change in the new prototype and also the mass distribution is totally different.

Moreover the total weight of the new prototype is estimated about 300 kg.

For time and cost reason it is impossible to change the links between frame and suspension but only hydraulic dampers and springs.

To find the right values of stiffness and damper before finishing the prototype it is necessary to make a multibody model for predict the behavior of the new layout, however this part will be treated in the subsequent part of the thesis.

3 Transmission

Moving from the configuration with one combustion engine to one with two electric motor it was be necessary to update the transmission. The aim of this design phase is to maintain the major possible quantity of old components to reduce cost and time, in terms of design and making.

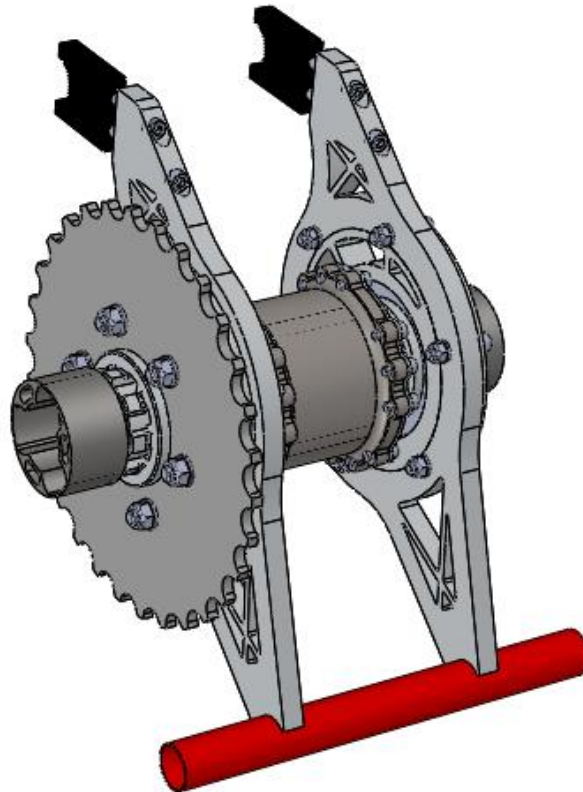


Figure 3-1. Old transmission

The new transmission will be described in the next paragraphs. This new unit has the aim to test the new electric configuration of the car. An optimization will not be done in terms of weight reduction but the main aim is to have a secure and reliable unit minimizing expense and time.

3.1 Transmission assembly

In this section it will be shown the new complete transmission instead in the next one it will be explained the analysis of the new components and the old ones because there will be the need to have a secure testing configuration.

The car has two equal transmission (one for each motor), one specular respect to the other. For sake of simplicity the analysis will be shown only for one transmission.

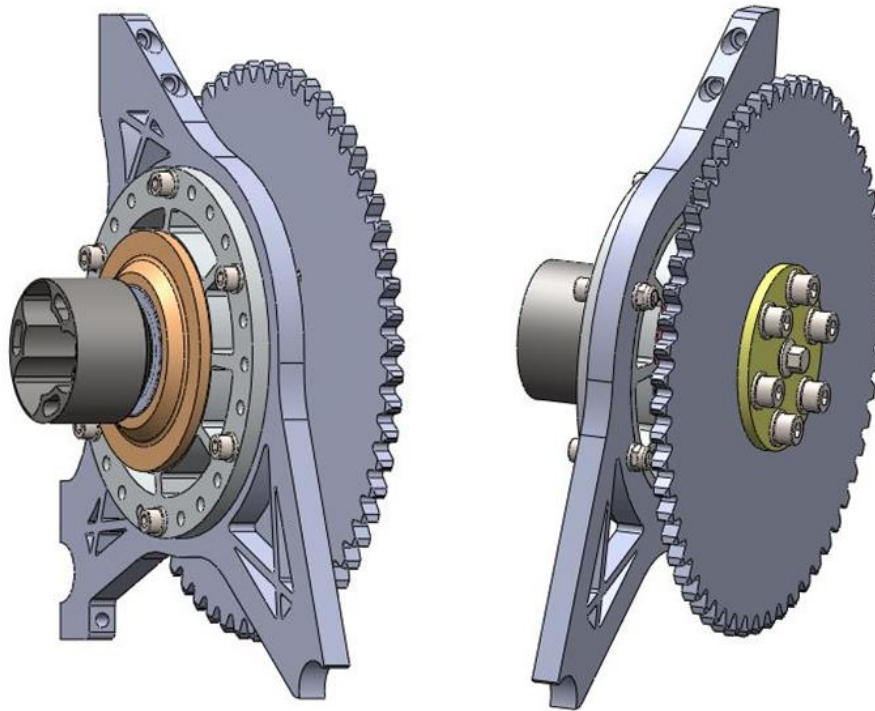


Figure 3-2. New transmission

In the figure below we can find the interaction between the transmission block and the rest of the vehicle. The transmission bracket was already used in the old one. It is fixed to the frame through four bolts. In the figure we can see the two superior holes and below there are other two. In the front of the transmission we can find an half-moon hollow that was fixed to the jacking bar, not present in the figure.

This bar is a red painted tube to lift the car. We can find it in the old transmission figure (see above).

The chainring houses the chain that transfers the motion from the motor to the tripod joint. This joint houses the drive shaft that ends with the tripod. Drive shaft transfers the motion to the wheel.

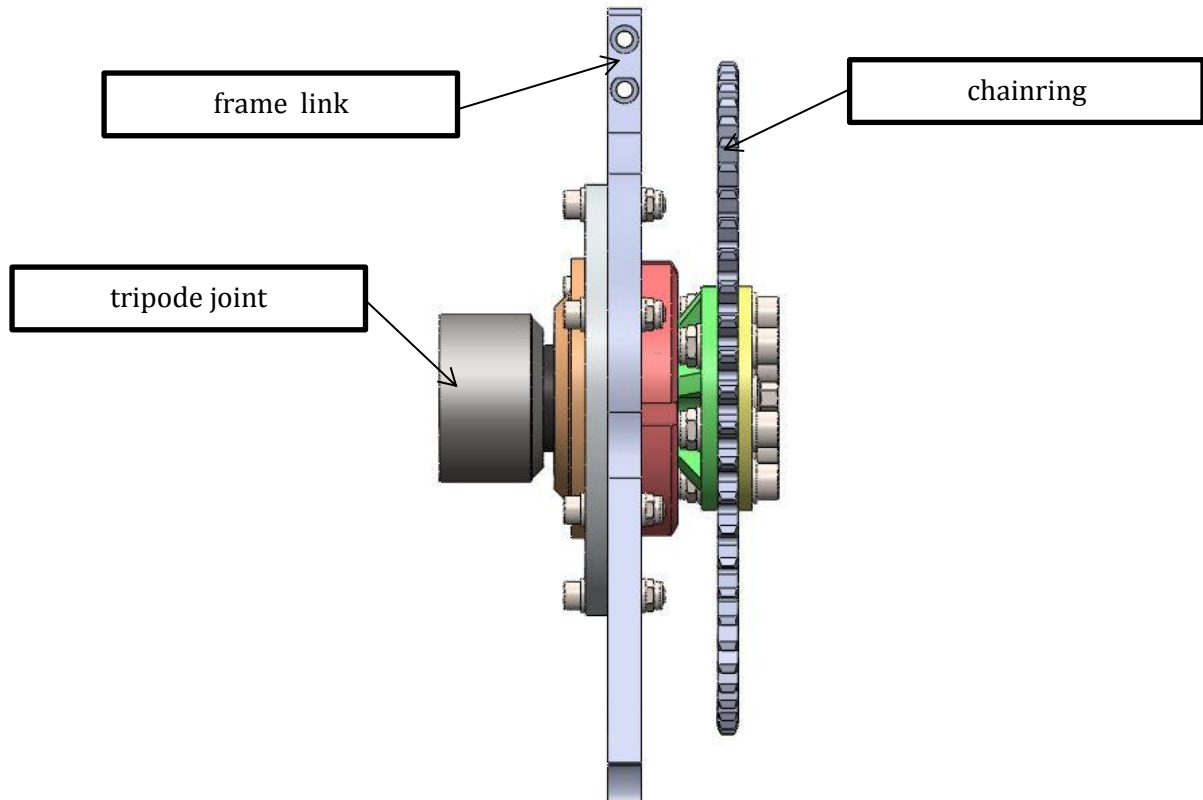


Figure 3-3. Transmission assembly

In the next part it is shown a section of the assembly and it is possible to find the position of bearings and the details of the assembly.

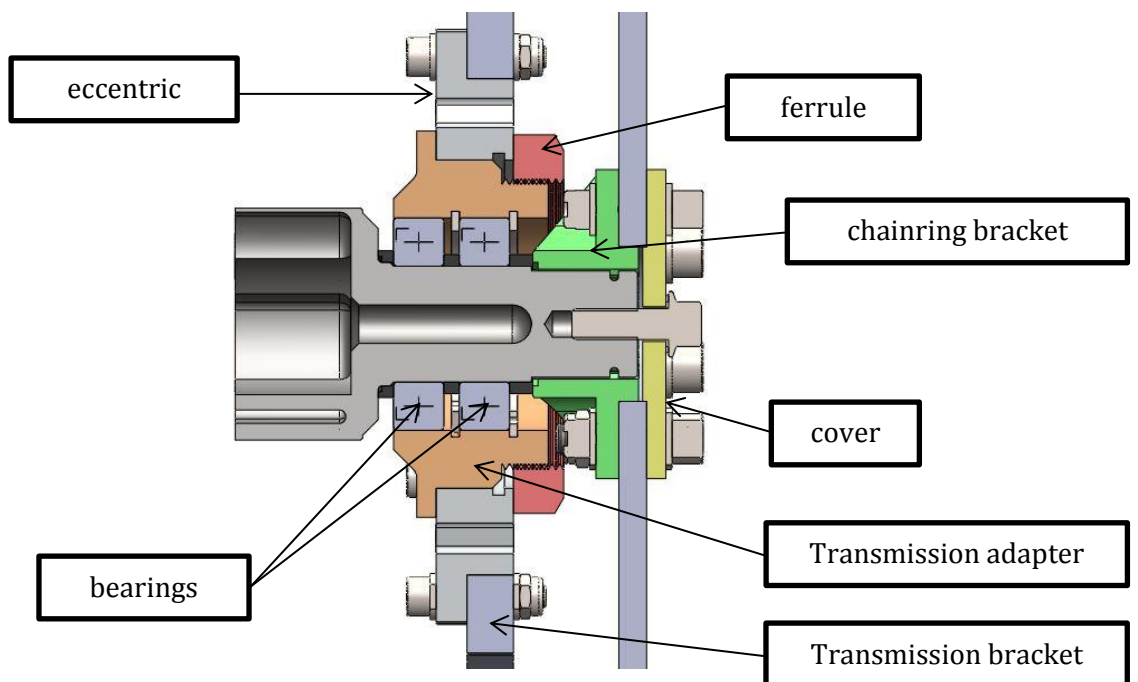


Figure 3-1. Section of transmission assembly

The ferrule compress the adapter on the eccentric. Between ferrule and adapter there is a backlash to avoid the possibility of a double connection.

The cover and the chainring bracket compress the chainring through bolts. The cover is link to the tripod joint through a central screw.

The bearings are fixed through seegers (represented in white) and spacers (represented in black). Seeing the sketch, it can be noted that all the backlashes are designed to guarantee the tightening on a unique surface.

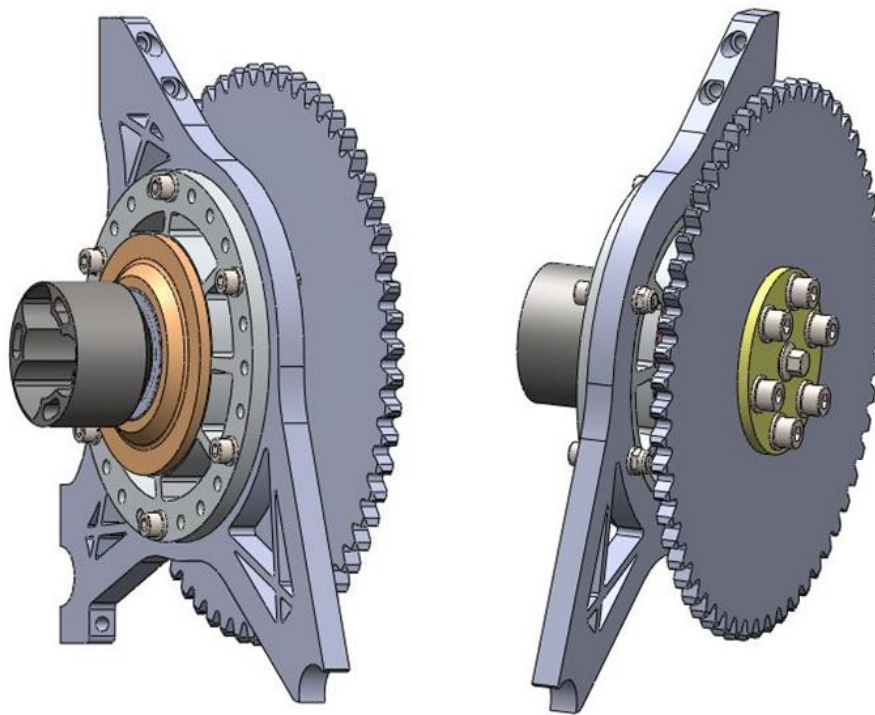


Figure 3-2. Transmission assembly isometric views

Screwing and unscrewing the screws of the eccentric in a different way it is possible to set the pull of chain while for a more detailed setting it is possible to add spacers between transmission bracket and frame.

Below are reported two exploded views that clarify the geometry of components of the transmission.

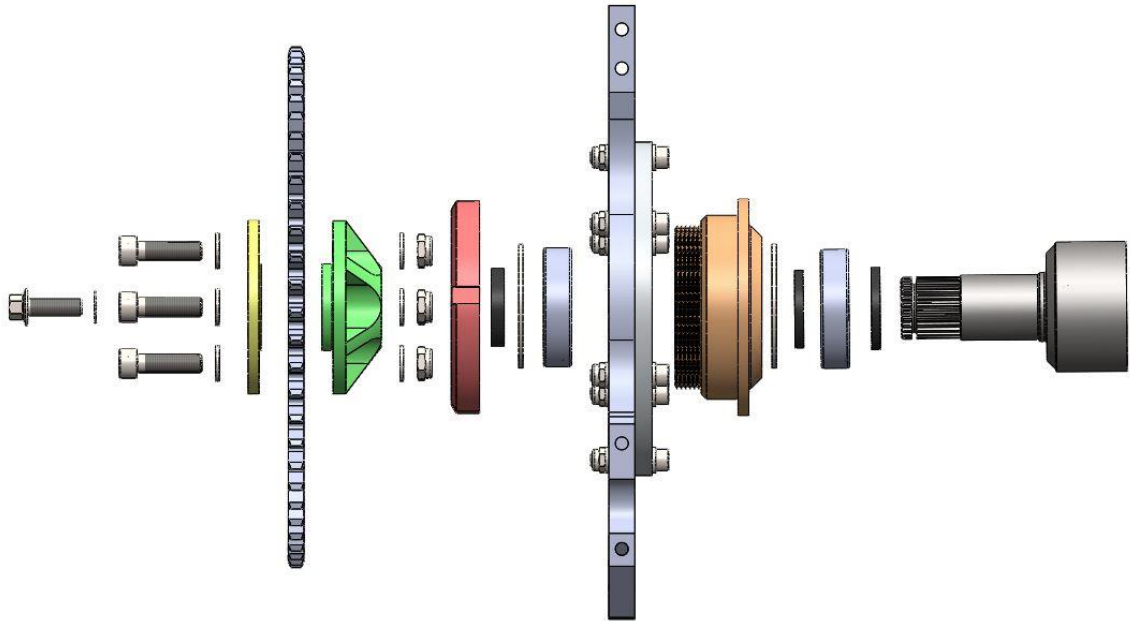


Figure 3-3. Transmission assembly exploded view

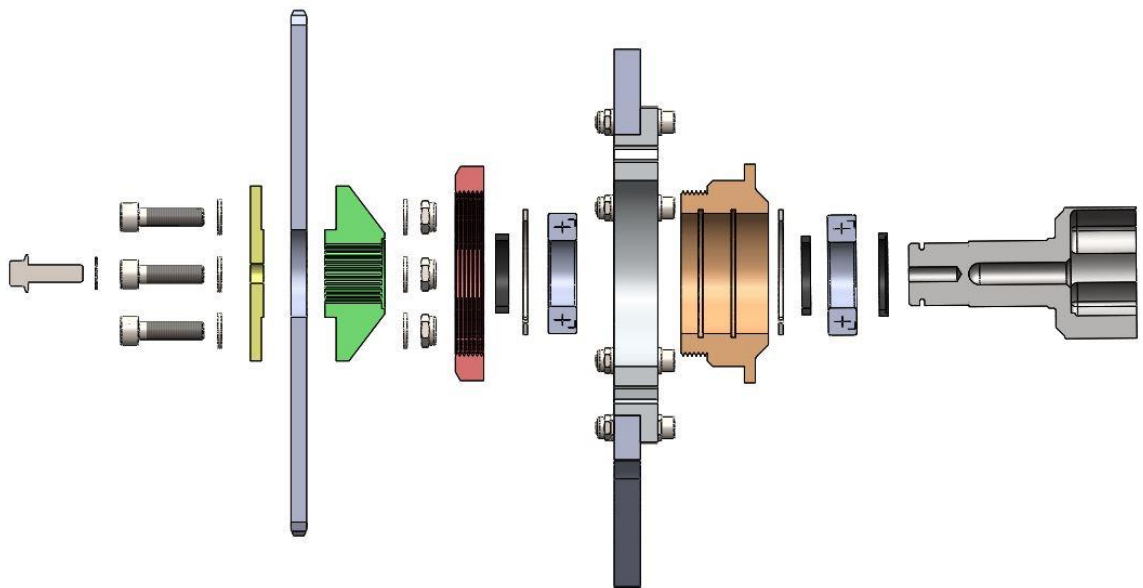


Figure 3-4. Section of transmission assembly exploded view

In the figure below we can see the disassembly of the chainrings.

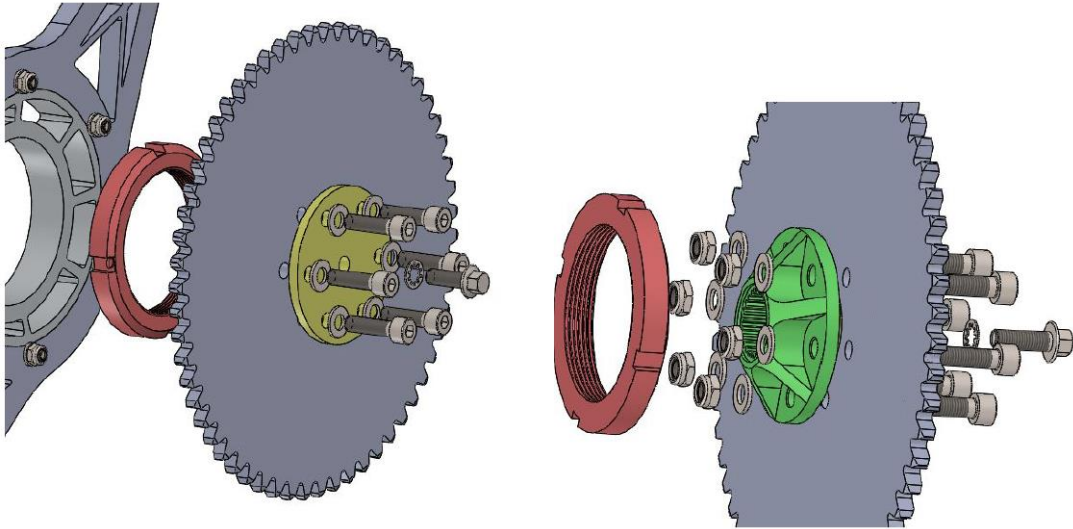


Figure 3-5. Detail of chainring disassembly

In the figure below we can see the disassembly of the tripod joint.

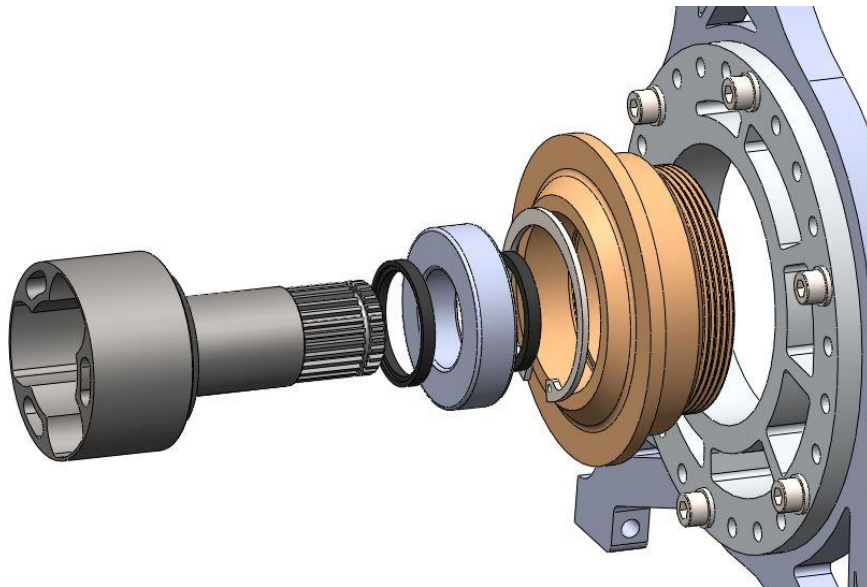


Figure 3-6. Detail of the tripod joint disassembly

In the next sections will be explained the analytic and numerical assessments to validate the geometry of the transmission components.

3.2 Chainring assessment

It starts with transmission components already bought in a previous phase. In detail, we speak about chainring, chain and pignon.

The pignon is the component QCS08B1-015, the chainring the QCS08B1-058 and the chain 08B1. All components bought by the company SIT S.p.A that respects the standard DIN 8187 ISO/R 606.

All the calculation about the chain pull is it made "from catalogue" of the company itself.

It is calculate the primitive diameter of pinion:

$$D_p = \text{primitive diameter} = p * \frac{1}{\sin\left(\frac{\pi}{Z_p}\right)} = 61.08 \text{ mm}$$

With:

$$p = \text{chain pitch} = 12.7 \text{ mm}$$

$$Z_p = \text{number of pinion teeth} = 15$$

It is possible to calculate the design power:

$$P_p = \text{design power} = P_n * F_s$$

Where P_n is the nominal power estimated in 19 kW and F_s is the service factor assumed as 1.5. This value has a range between 1 and 1.5 in the electric motors. In our case a value was chosen at the upper end of the range because in this type of transmission the power is delivered in a discontinuous way. The pilot pulls and releases the accelerator impulsively in a typical formula SAE dynamic event.

We proceed to the calculation of the chain pull, first calculating the linear velocity of the chain:

$$V = \text{chain linear velocity} = \frac{\pi * D_p * n}{60} = 8.63 \frac{m}{s}$$

Like n was used 2700 rpm, which is the motor speed at the maximum power.

$$T = \text{chain pull} = \frac{75 * P_p * 1.35962 * g}{V} = 3301 \text{ N}$$

It is possible to obtain the centrifugal force:

$$F_c = \text{centrifugal force} = W * V^2 = 52 \text{ N}$$

With $W = 0.7 \frac{kg}{m}$ defined as chain linear weight per linear unit.

It is possible to calculate the total force acting on the chain:

$$F_c = \text{total force} = T + F_c = 3354 \text{ N}$$

This force, from now, will be used for all subsequent assessments.

The safety coefficient is now calculated to evaluate the correctness of the chain selection.

$$k = \text{safety factor} = \frac{R_t}{F_{tot}} = 5.37$$

With an $R_t = 18000$ N for the selected chain.

The company recommends a safety factor k greater than 8 for normal applications and 5 for high quality chains (as in our case). Consider that in our application the chain will work for short periods and therefore we accept this solution.

3.3 Cover assessment (analytic solution)

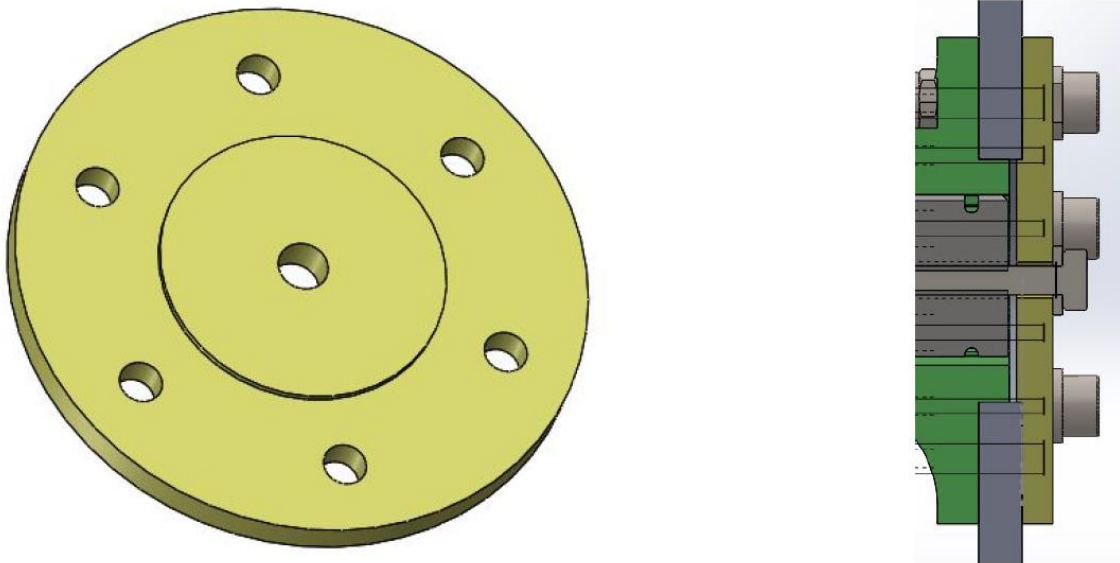


Figure 3-7. Cover

As it can be seen from the image the central screw has the purpose of connecting the tripod joint with the cover. The only contact surface is between the washer and the cover itself, while for the other bolts there are 2 contact surfaces (steel / steel). Furthermore, its position has a 9 mm hole instead of 8 mm, as for the other bolts, to make centering easier. For these reasons I do not consider this bolt in the verification of the bolted joint. This simplification is however conservative therefore it is considered acceptable.

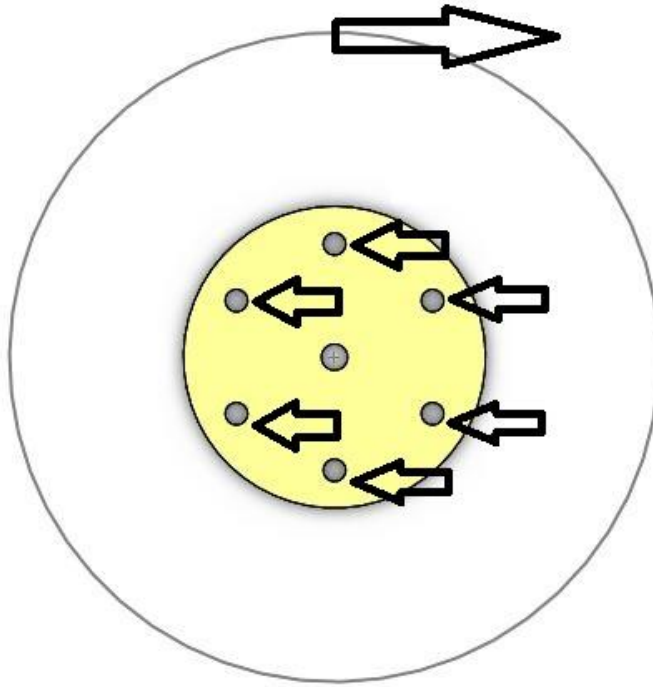


Figure 3-8. Horizontal forces equilibrium

As for the balance of horizontal components, the force acting on the single bolt is calculated as follows:

$$F_{b\text{-horizontal}} = \frac{F_{tot}}{n_b} = 559 \text{ N}$$

With $n_b = 6$ and $F_{tot} = 3354 \text{ N}$ already calculated previously.

We now proceed to the calculation of the force component due to the equilibrium of the moments.

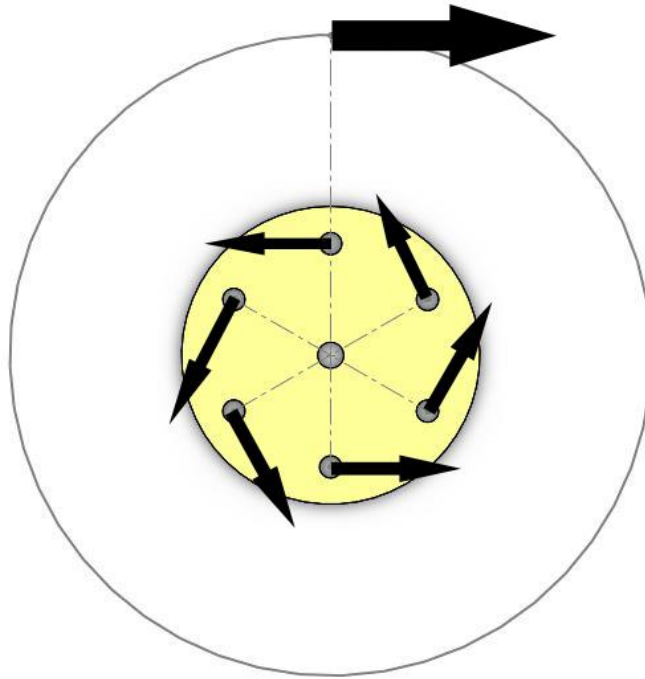


Figure 3-9. Momentums equilibrium

It is calculate the primitive diameter of chainring:

$$D_c = \text{chainring primitive diameter} = p * \frac{1}{\sin\left(\frac{\pi}{Z_p}\right)} = 234.58 \text{ mm}$$

With:

$$Z_c = \text{number of chainring teeth} = 58$$

$$F_{b\text{-momentum}} = \text{force due by moments} = \frac{F_{\text{tot}} * D_c}{2 * n_b * d} = 2185.3 \text{ N}$$

With $d = 30 \text{ mm}$ that is the distance between central screw and external bolts.

The most stressed bolt takes a force:

$$F_b = \text{force on the most stressed bolt} = F_{b\text{-horizontal}} + F_{b\text{-momentum}} = 2744.3 \text{ N}$$

Once the forces on the component have been obtained, it is possible to carry out all checks in accordance with the CNR-UNI 10011 standard.

3.3.1 Bolt joint friction assessment

The resistance of the bolted friction joint is evaluated first.

When working the component must always work in this condition while the shear check is done only as a further safety in the case in which, for example for an incorrect tightening of the bolts, the calculated friction condition is less.

Having used class 8.8 M8 screws we use the following values:

$$f_{k,N} = \text{admissible bolt stress} = 560 \frac{\text{N}}{\text{mm}^2}$$

$$A_{res} = \text{bolt resistance section} = 36.6 \text{ mm}^2$$

The force perpendicular to the surface and the friction force can be calculated.

$$V_0 = \text{force perpendicular to the surface} = 0.8 * f_{k,N} * A_{res} = 16397 \text{ N}$$

$$F_{friction} = \text{friction force} = f * V_0 * n_f = 0.3 * V_0 * 2 = 9838.1 \text{ N}$$

Using as values of $f = 0.3$ that is the steel friction coefficient and $n_f = 2$ since the surfaces in contact are those crown\cover and crown\support.

It is therefore necessary that the following condition is satisfied:

$$F_b = \text{bolt force} < \frac{F_{friction}}{1.25} = F_{lim} = 7870.5 \text{ N}$$

In our case this relationship is satisfied and therefore the junction will work in friction mode. We now proceed to the calculation of the safety coefficient regarding this condition:

$$C_s = \text{safety factor} = \frac{F_b}{F_{lim}} = 2.868$$

The tightening torque to be applied to these bolts to ensure the correct operation of the joint will be:

$$T_s = \text{tightening torque} = 0.2 * V_0 * d(M8) = 26.2 \text{ Nm}$$

3.3.2 shear bolted joints assessment

If the friction between the components were not present, the six bolts would be found to work in shear. Their resistance to this type of stress then occurs. It must be remembered that there is no guarantee that all bolts receive the same load in equal measure. This is due to possible lack of precision on the holes and on the bolts themselves.

To avoid excessive production costs and times, a simplification is accepted (non-conservative) and after each use it will be verified that the joint has worked in friction mode and not in shear one.

$$\tau = \text{shear stress} = \frac{F_b}{A_{res}} = 74.98 \text{ MPa}$$

For a class 8.8 screw the $\tau_{adm} = 264 \text{ MPa}$. It is therefore possible to calculate its *safety factor* also in this case.

$$C_s = \text{safety factor} = \frac{\tau_{adm}}{\tau} = 3.52$$

3.3.3 Plastic deformation of the hole

Another important assessment to be carried out is on the resistance of the cover itself if the bolt works in shear.

$$\sigma = \text{normal stress} = \frac{F_b}{t * (H - d)} = 19.96 \text{ MPa}$$

With $H = 35.5 \text{ mm}$. See the image below to understand the dimension.

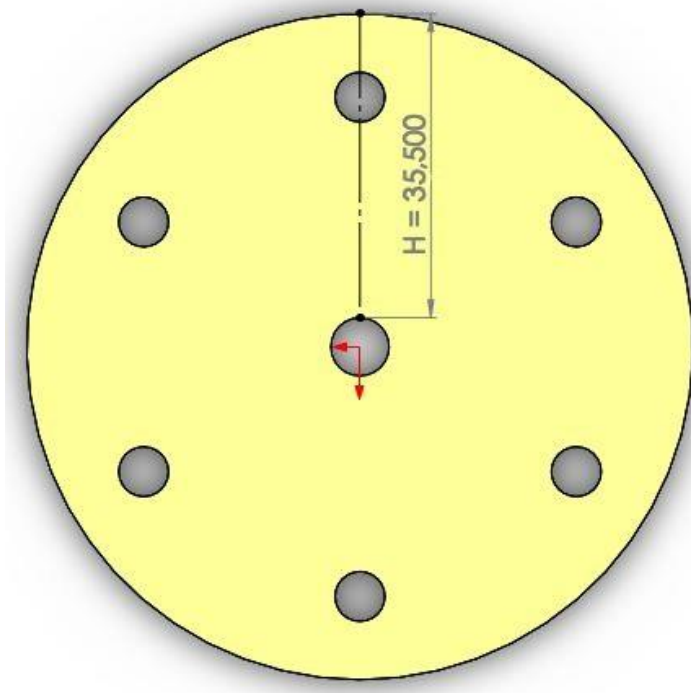


Figure 3-10. H dimension

It is therefore used as a resistant section ($t * (H - d)$).

It continues with the calculation of the safety factor:

$$C_s = \text{safety factor} = \frac{\sigma_{adm}}{\sigma} = 8.02$$

As we note we are very conservative on this component. This choice was made to support the strongly impulsive dynamics that the transmission will be called to support during use.

3.4 Chainring bracket

We will now proceed to the assessment of the chainring bracket.

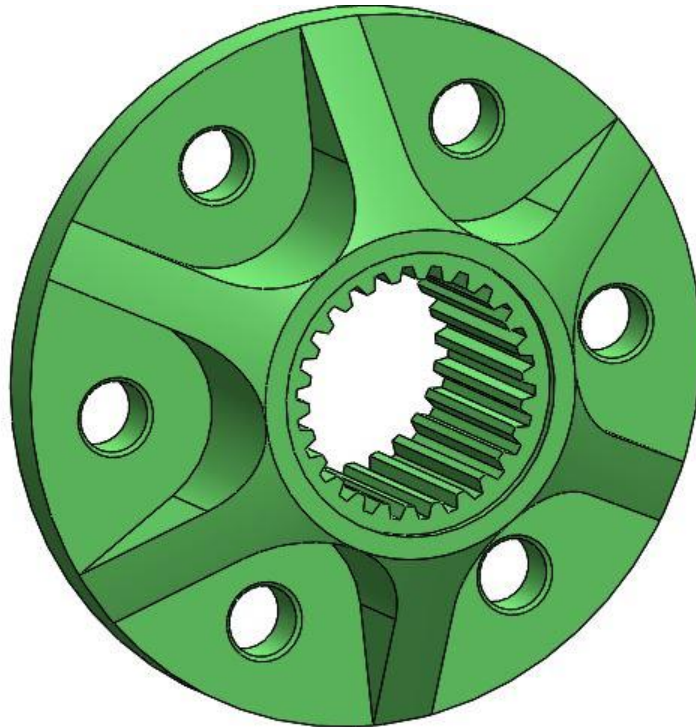


Figure 3-11. Chainring bracket

A finite element analysis was carried out for this component using the Abaqus program.

To simplify the simulation the position for the splined profile and the fillet were omitted. The chainring assembly (without teeth), cover, bolts and chainring bracket were used. The components are axial-symmetrical, so it is possible to analyze only one segment, reducing the calculation time.

Now it is reported an image of the FEM assembly:

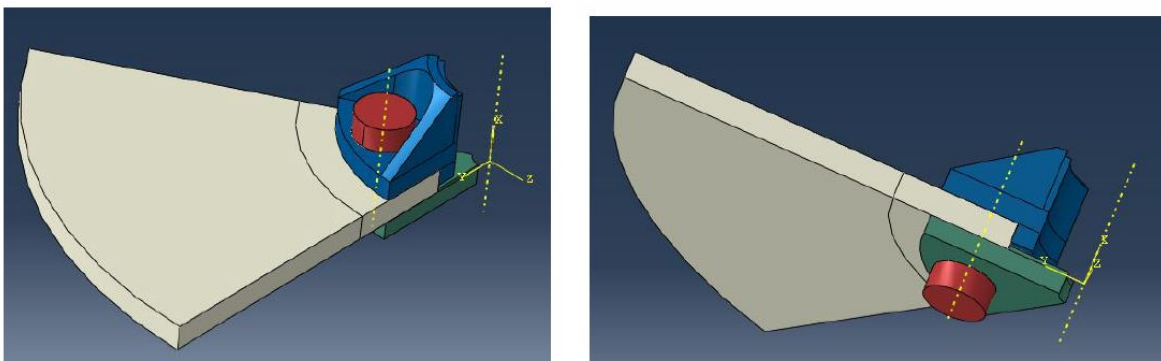


Figure 3-12. FEM assembly

In the figure below, it is possible to see a section of the analyzed segment.

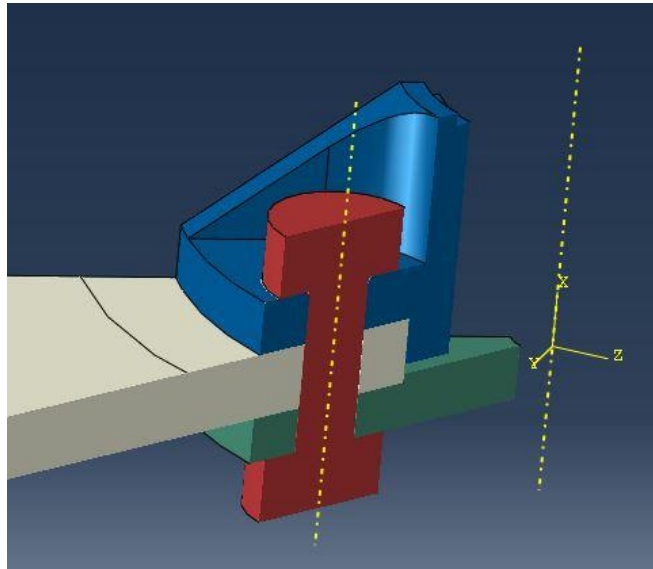


Figure 3-13. FEM assembly section

3.4.1 Mesh creation

After having shown the geometry that constitutes the model we will go on to describe its discretization (definition of the mesh).

C3D10 elements were used for the chainring bracket. Quadratic tetrahedral elements at ten nodes. Partitions were made in the circular seats of the bolts and in the central part, since they represent the parts of application of the loads and the constraints. The bodies must be discretized in order to allow the application of the constraints and loads in a right way.

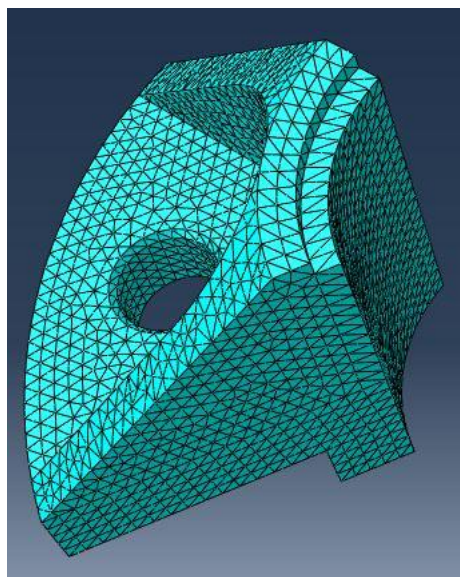


Figure 3-14. Chainring bracket mesh

For bolts, simplified for simulation, a mesh with C3D8R elements was used. Linear hexagonal at eight nodes.

Given the geometry, as far as possible, we have tried to give a development that respects the axial-symmetry.

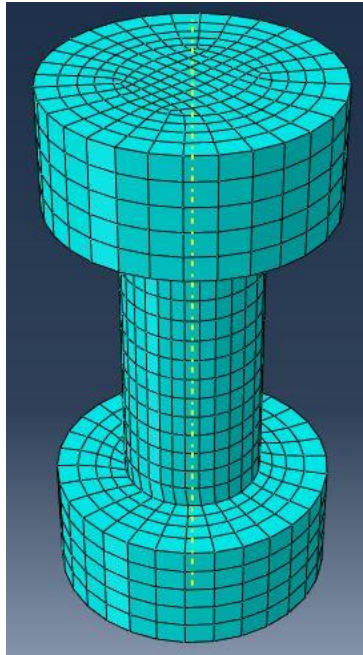


Figure 3-15. Bolt mesh

A mesh with C3D8R elements was also used for the cover, trying to remain pertinent to the geometry.

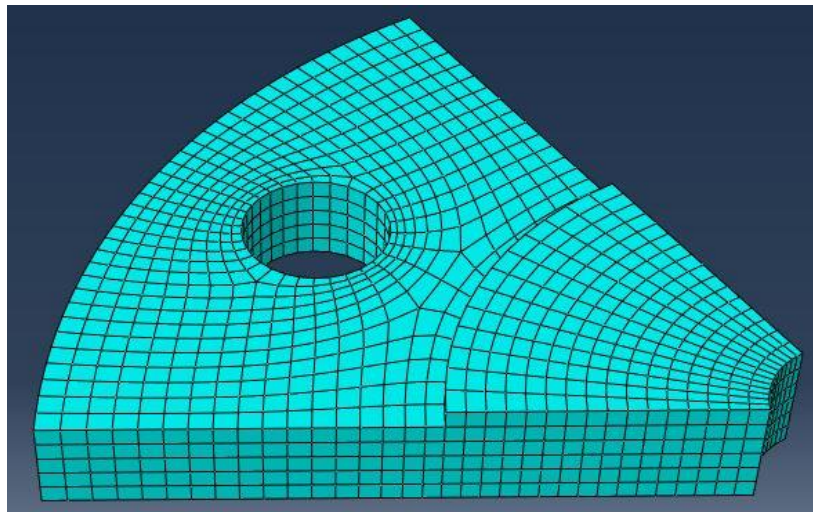


Figure 3-16. Cover mesh

The same type of element was also used for the chainring.

Note that near the holes the mesh has been thickened, as well as in the cover, to represent in more detail the intensification of the effort near the notches.

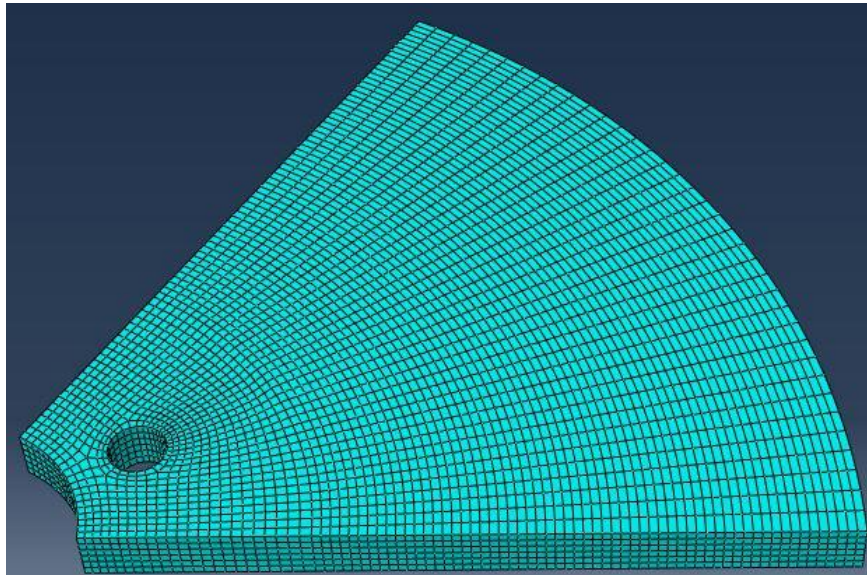


Figure 3-17. Chainring mesh

3.4.2 Loads and constraints

We move on to the definition of the system of loads and constraints to be applied to the model.

The load used in the simulation is the chain pull, divided by the number of segments (6):

$$T = \text{chain pull} = \frac{F_{\text{tot}}}{6} = 555 \text{ N}$$

This force was considered as point-like and applied perpendicularly to the chainring, along the Z direction.

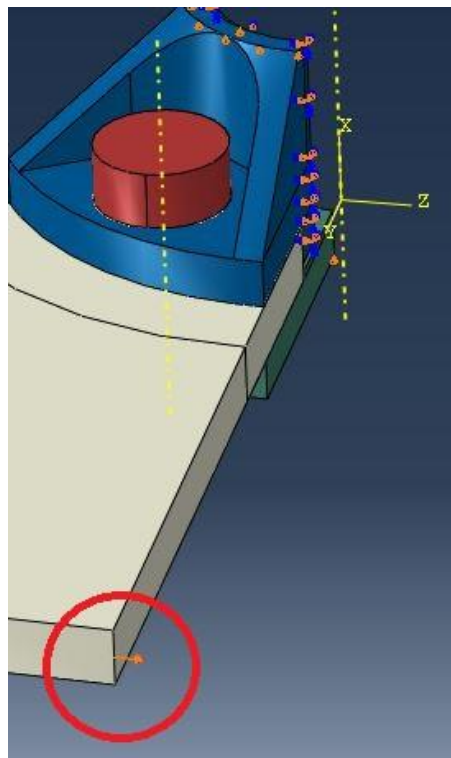


Figure 3-18. Chain pull force

As other load was considered the preload on the bolt, inserted in Abaqus with the bolt load command. The value used is the one already calculated previously, always considering M8 bolts of class 8.8:

$$V_0 = \text{force perpendicular to the surface} = 0.8 * f_{k,N} * A_{res} = 16397 \text{ N}$$

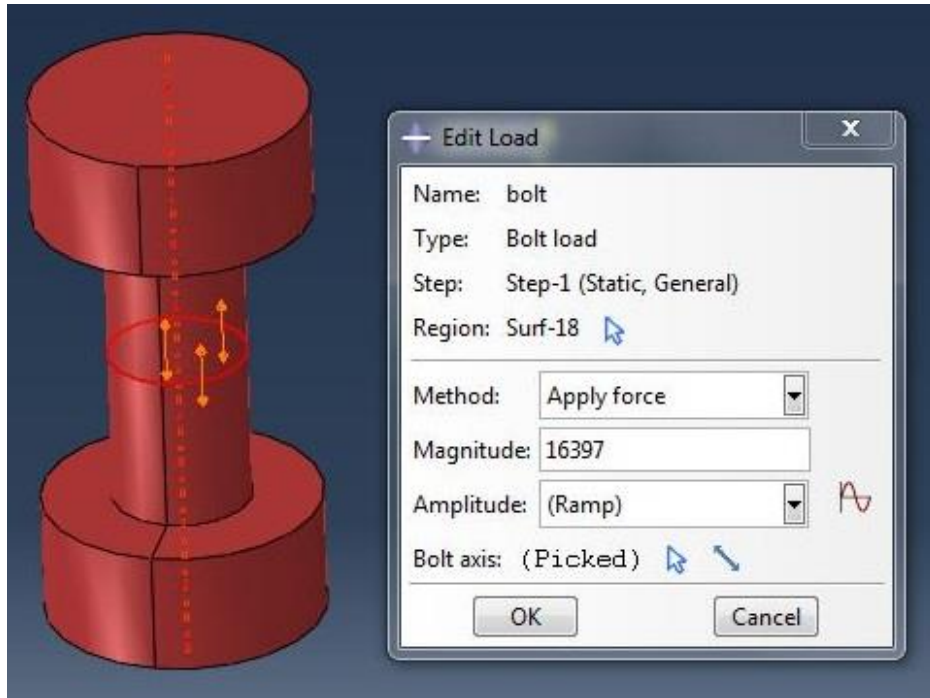


Figure 3-19. Bolt load

It is used three constraints. The vertical movements along the X have been inhibited at the upper surface of the chaining bracket and at the lower edge of the cover, as shown in the two figures below.

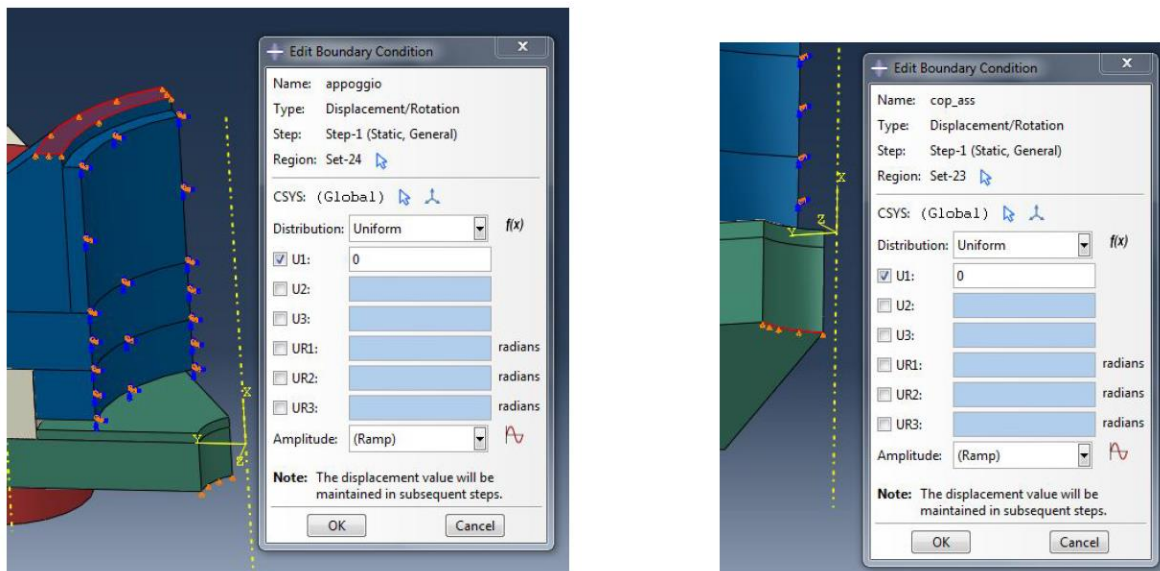


Figure 3-20. FEM Boundary conditions

At the surface of the spline joint, on the other hand, all the movements except the vertical one have been suppressed.

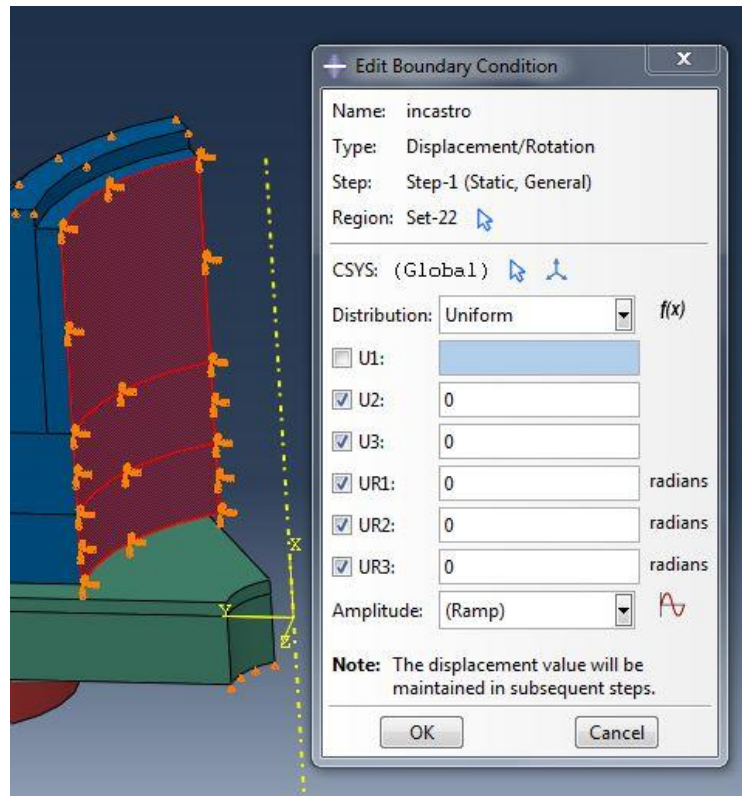


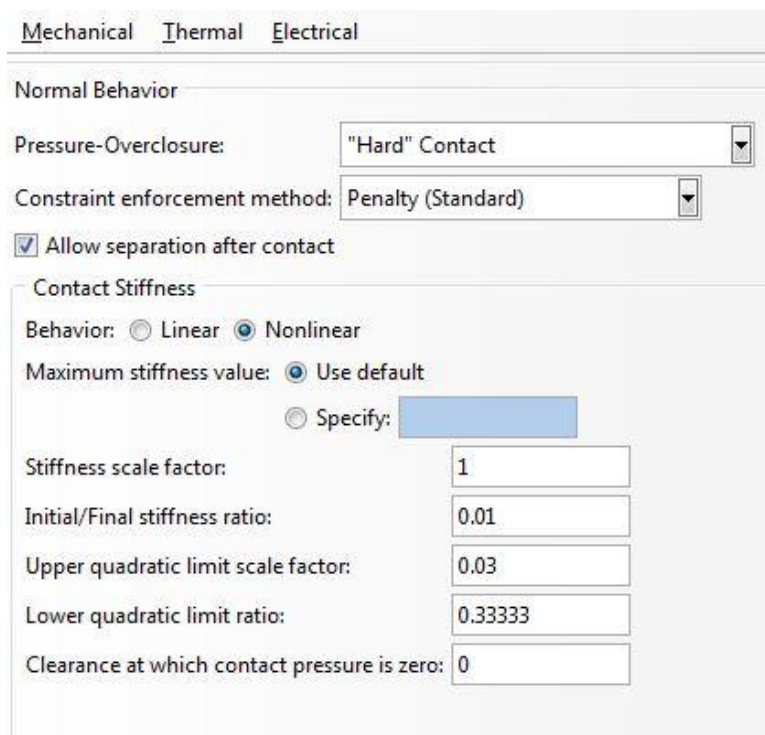
Figure 3-21. Surface FEM boundary condition

3.4.3 Interactions

In addition to the constraints and loads, because we wanted to simulate an assembly, it was necessary to define the interactions between the various components.

The real situation was considered, with the contacts between the various surfaces of the four components: Bolts, chainring bracket, chainring and cover. For each contact a non-linear model was used during normal contact, due to the application of forces perpendicular to the surface from time to time considered. The non-linearity concerns the variation of the stiffness of the material subjected to a pressure by another component. This variation was considered non-linear.

Afterwards it is possible to observe the factors introduced for the description of the law that describes the aforementioned contact.



Mechanical Thermal Electrical

Normal Behavior

Pressure-Overclosure: "Hard" Contact

Constraint enforcement method: Penalty (Standard)

Allow separation after contact

Contact Stiffness

Behavior: Linear Nonlinear

Maximum stiffness value: Use default Specify: []

Stiffness scale factor: [1]

Initial/Final stiffness ratio: [0.01]

Upper quadratic limit scale factor: [0.03]

Lower quadratic limit ratio: [0.33333]

Clearance at which contact pressure is zero: [0]

Figure 3-22. Normal contact non-linear law

As regards the tangential behavior and therefore the exchange of shear stresses, a linear friction model with a factor of 0.7 was used. This value was considered appropriate for a non-lubricated steel / steel static friction.

It should be noted that in the analytical assessment a much more conservative value of 0.3 was considered. Furthermore, no limits were imposed on the transmitted shear stresses. This behavior is justified by the fact that the previous check on the bolted joint by friction gave

very conservative results. We are therefore reasonably sure of being in a static and non-dynamic field.

Below there are the values entered to describe the linear model of the tangential friction.

The screenshot shows the 'Tangential Behavior' dialog box in Abaqus. The 'Friction formulation' is set to 'Penalty'. Under the 'Friction' tab, 'Directionality' is set to 'Isotropic'. Three checkboxes are present: 'Use slip-rate-dependent data', 'Use contact-pressure-dependent data', and 'Use temperature-dependent data', all of which are unchecked. The 'Number of field variables' is set to 0. A table at the bottom shows a 'Friction Coeff' of 0.7.

Friction Coeff
0.7

Figure 3-23. Tangential contact linear law

It must be remembered that Abaqus considers, as default, an elastic slip as a fraction of the surfaces. This aspect will be noted in the results subsequently.

The screenshot shows the 'Tangential Behavior' dialog box with the 'Elastic Slip' tab selected. Under 'Specify maximum elastic slip (Standard only)', the 'Fraction of characteristic surface dimension' is set to 0.005. Under 'Elastic slip stiffness (Explicit only)', the 'Infinite (no slip)' option is selected.

Figure 3-24. Elastic slip

3.4.4 Results

We now move on to the description of the results resulting from the assessments set with the data reported in the previous sections.

We report the stress of Von Mises:

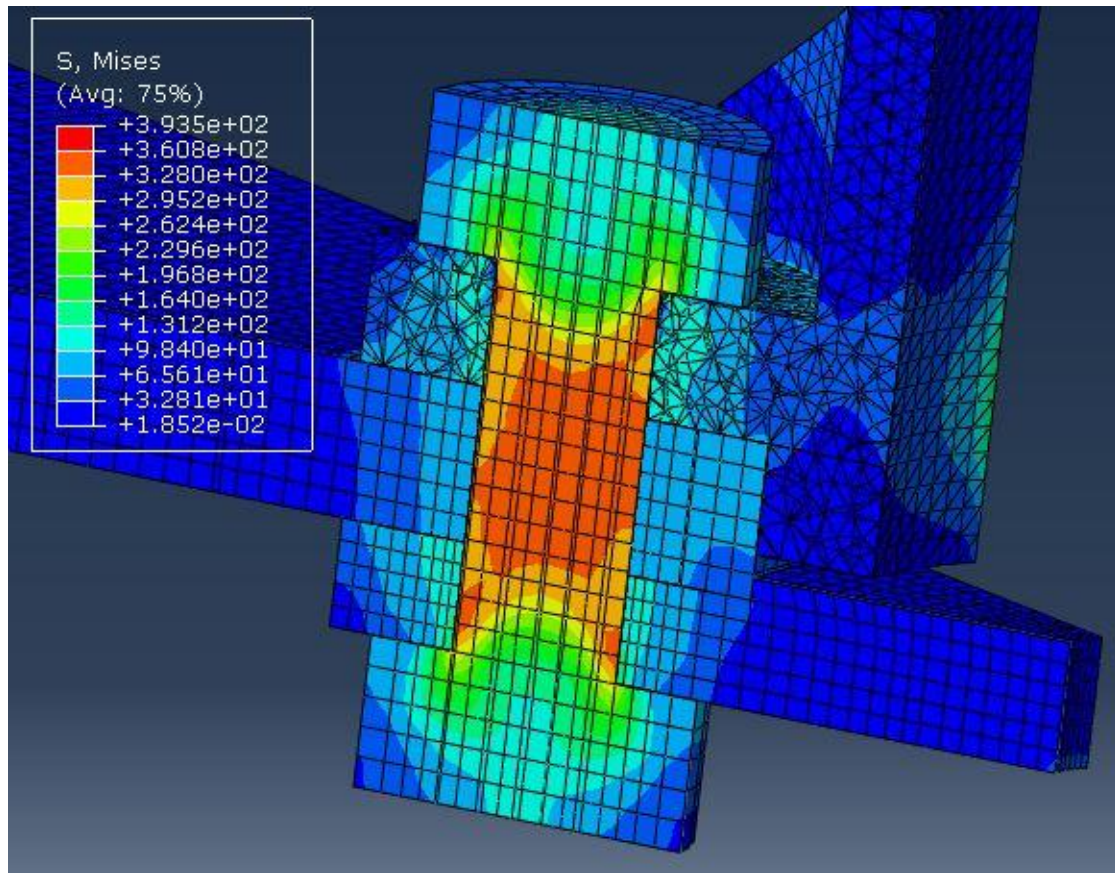


Figure 3-25. Bolt Von Mises Stress

From the figure it is understood that the greater stress are given by the bolt preload. Efforts of 393MPa that are however well below the yield values of bolts class 8.8 (640MPa).

By analyzing the chainring bracket:

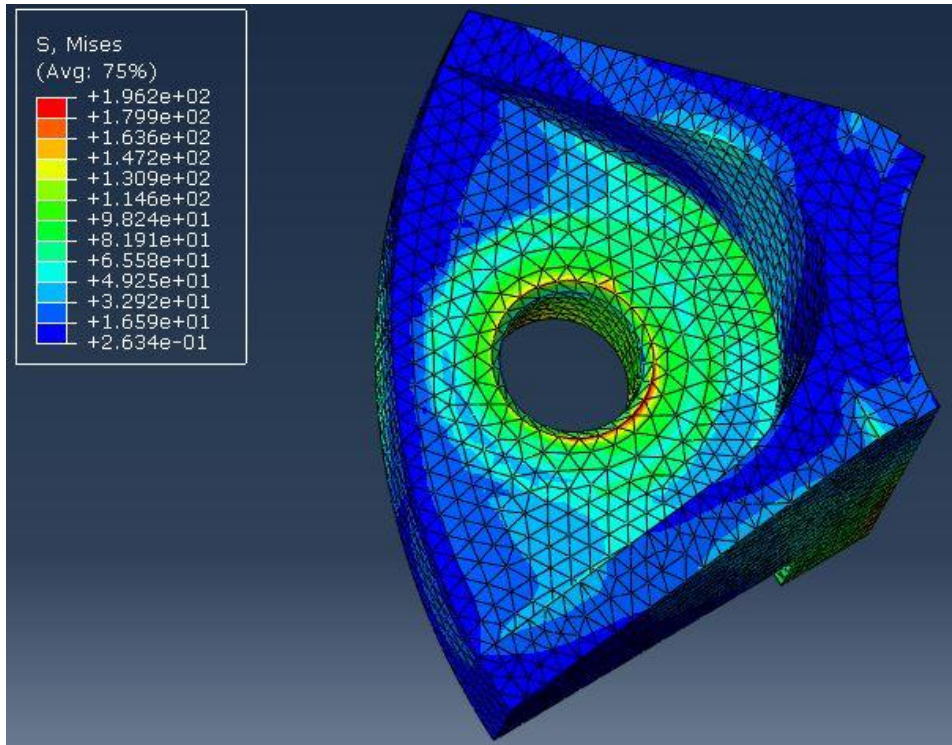


Figure 3-26. Chainring bracket Von Mises stress (upper view)

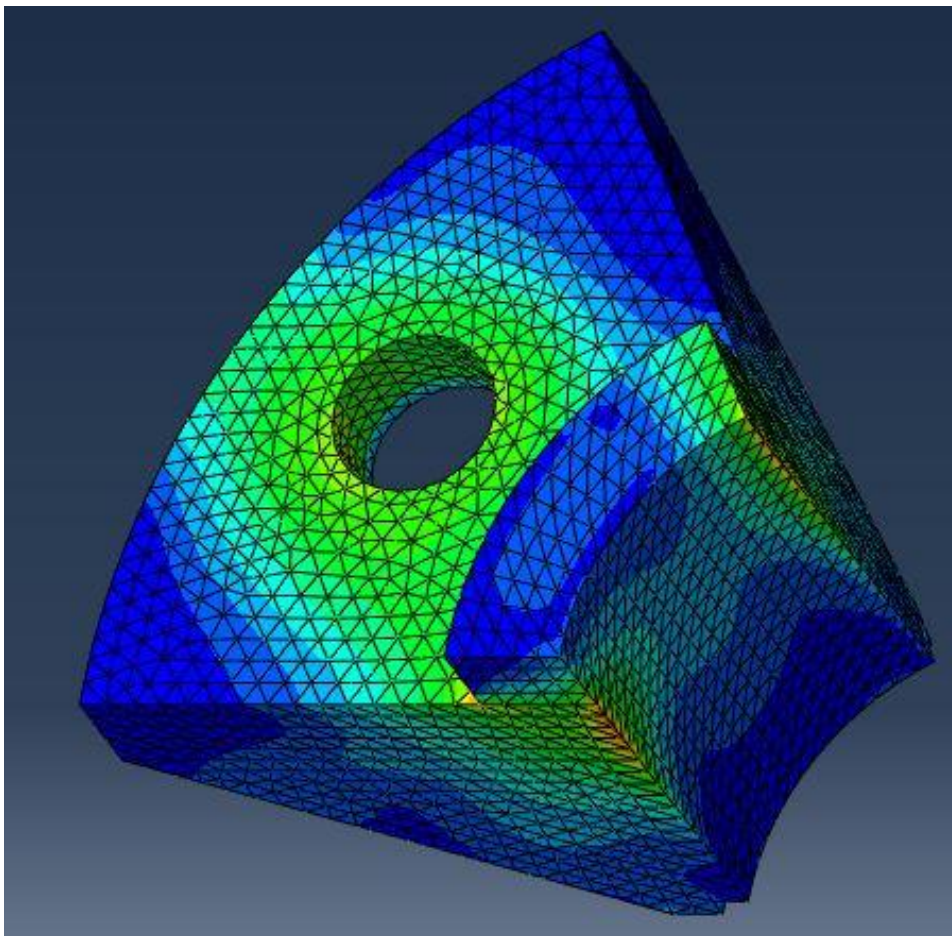


Figure 3-27. Chainring bracket Von Mises stress (bottom view)

Looking at the images above we can see that the most stressed parts are those in contact with the bolt and with the constraint represented by the splined profile. However, the maximum Von Mises stress stands at 196 MPa, well below the limit of the material.

It is also interesting to evaluate the relative displacements between the chainring bracket and the chainring itself. Abaqus provides this data along two components, perpendicular to each other (CSLIP1 and CSLIP2). From the figures it can be seen how these displacements are very contained and due to the deformation of the material (elastic slippage) and not to an absence of friction between the components. Let us remember that the defined friction model is static.

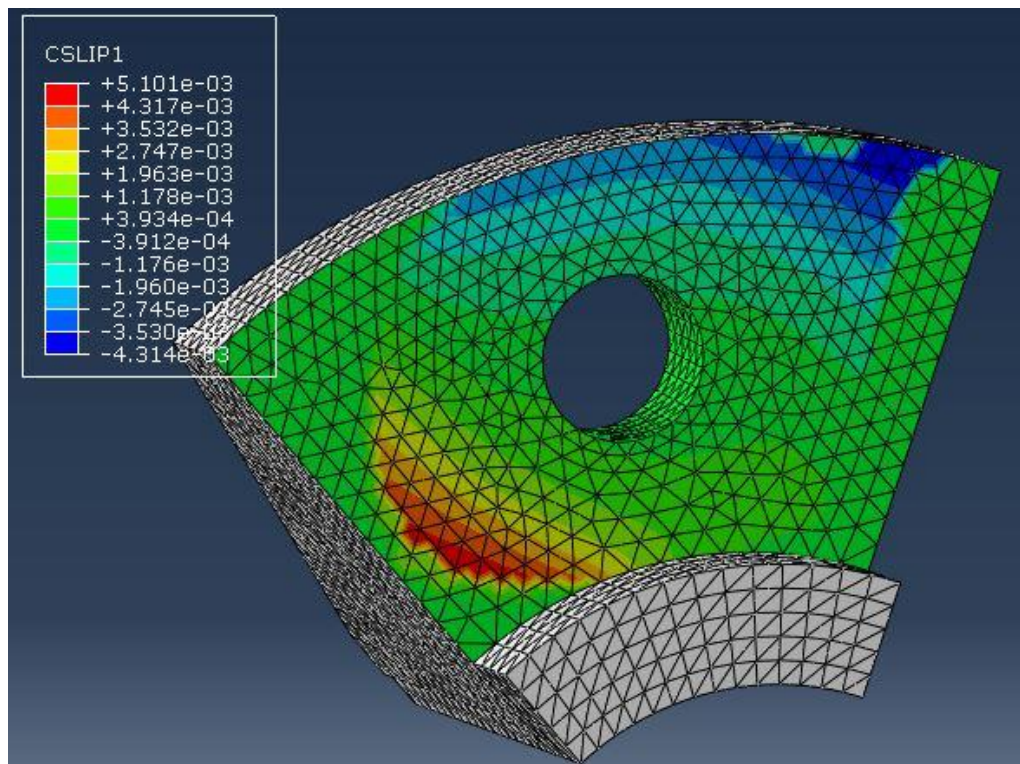


Figure 3-28. CSLIP1

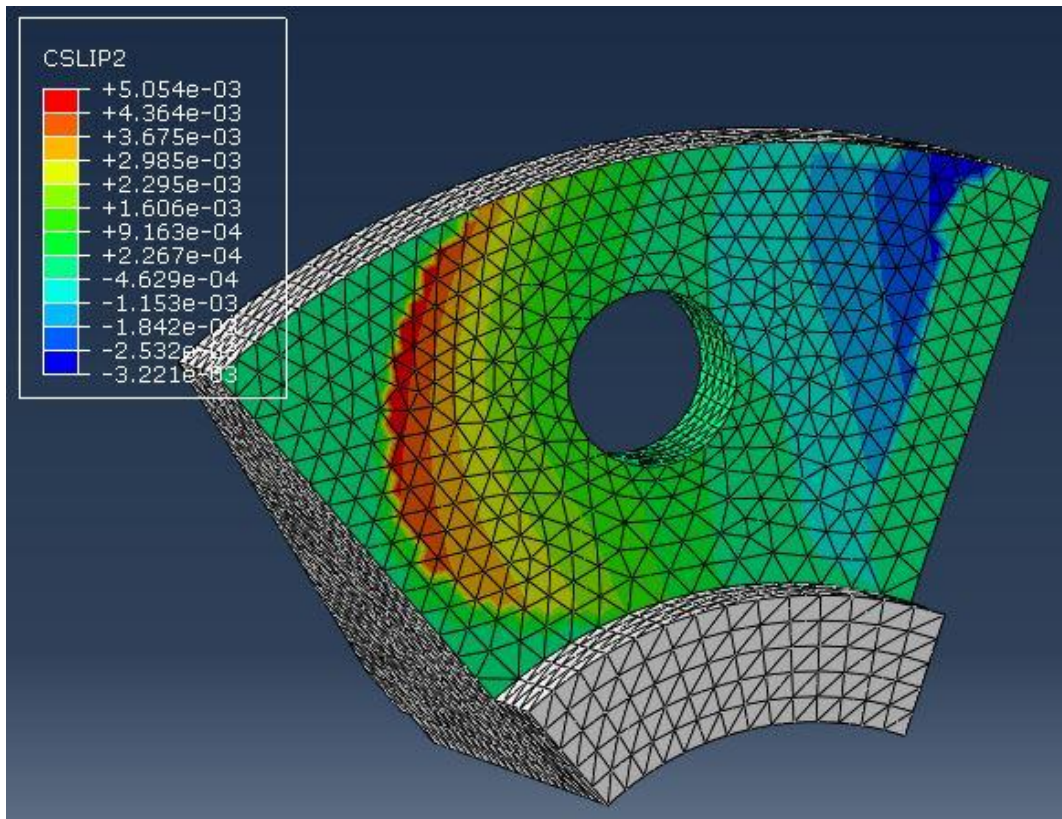


Figure 3-29. CSLIP2

From the data obtained, the choice to use a C40 steel is considered safe. This material in fact has a yield stress of more than 260 Mpa. However, surface treatments will be necessary on the sliced profile. The choice of this part was however leaved to the supplier.

3.5 Cover (numerical solution)

For the cover the results are similar to the chainring bracket. The maximum stress is 183 MPa. Also in this case we choose to use a C40 steel. However, it is necessary to evaluate, both in this and in the previous component, that the friction coefficient between the various materials is at least 0.3.

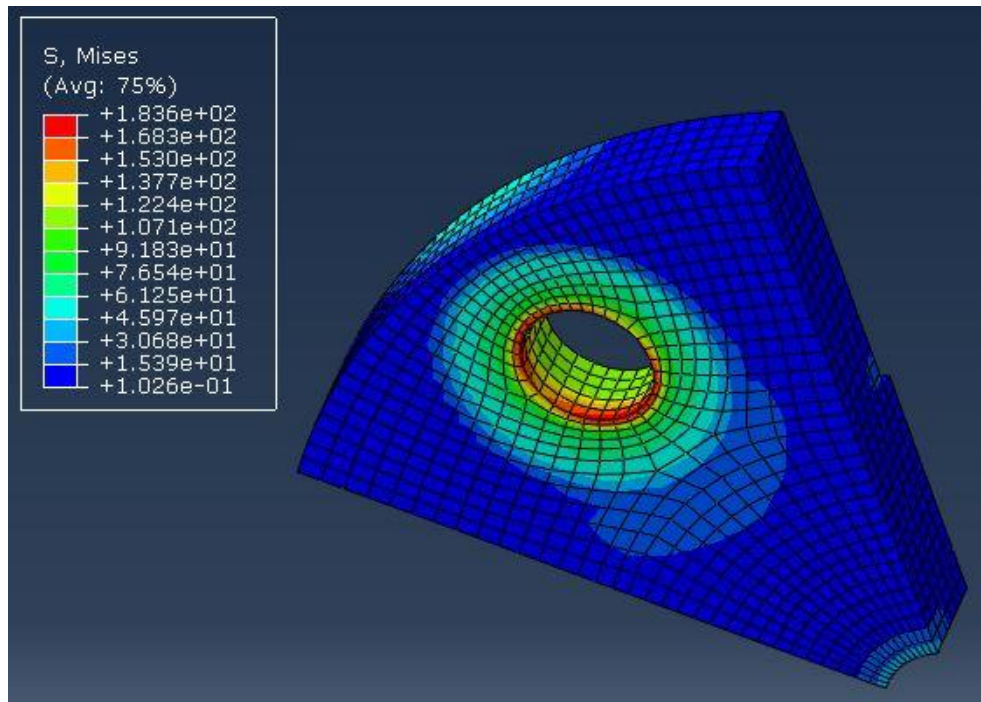


Figure 3-30. Cover Von Mises stress

3.6 Tripod joint

We now see the verification of the tripod joint, a component already present "in stock", but to be reworked to adapt it to the new needs of the electric car.

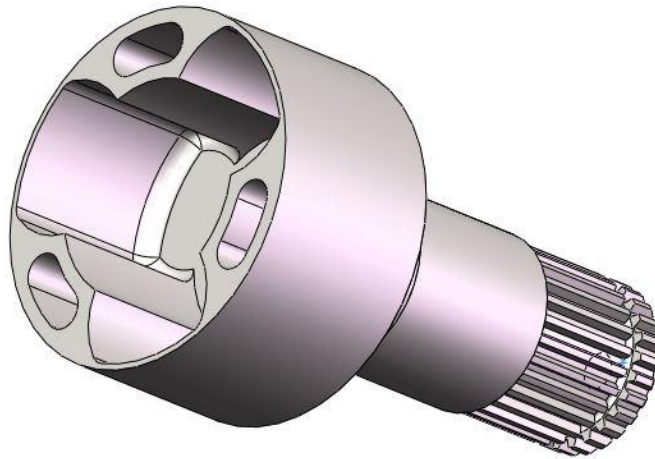


Figure 3-31. Tripod joint

3.6.1 Static assessment

We started by making a simplified schematization of the component. The chain transmits a torque and a force through the chainring and splined profile.

These contributions, calculated previously, are:

$$M_t = \text{torque} = F_{tot} * \frac{D_c}{2} = 393360 \text{ Nmm}$$

$$F = F_{tot} = 3353.7 \text{ N}$$

For the constraint reactions, for how the position of the bearings were designed, we have a carriage and a hinge, indicated respectively with R1 and R2.

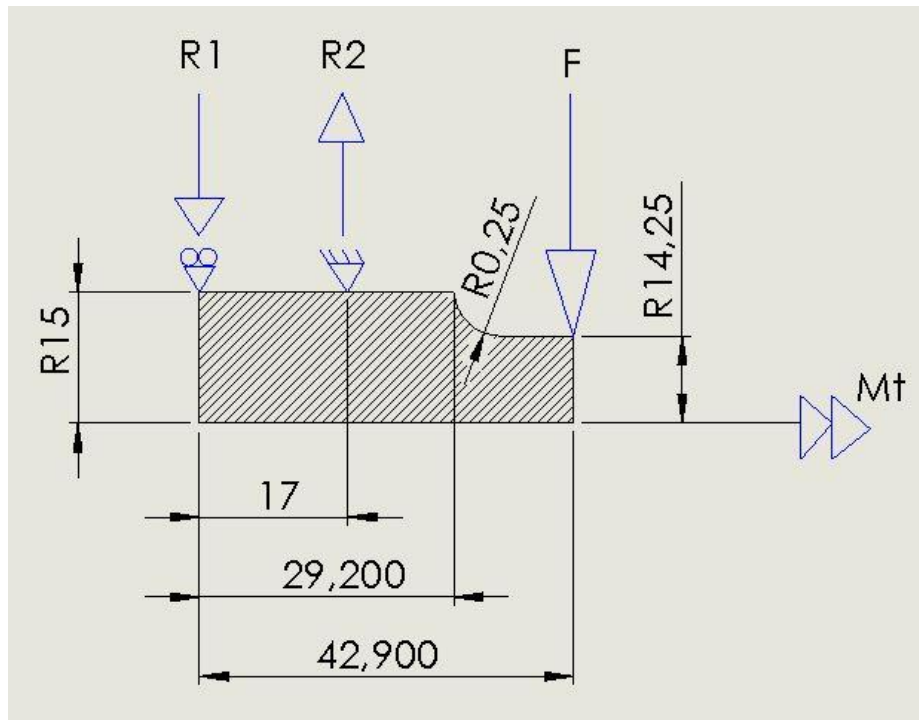


Figure 3-32. Tripod joint schematization

We proceed to the calculation of the constraints reactions by carrying out the balances of vertical forces and moments.

$$R1 = \text{constraint reaction } R1 = \frac{F * b}{a} = 5109.5 \text{ N}$$

$$R2 = \text{constraint reaction } R2 = F * \left(1 + \frac{b}{a}\right) = 8463.2 \text{ N}$$

With a and b respectively the distance between R1 and R2 and the distance between the force F and R2.

We now proceed to the calculation of the bending moment and of the torque along the structure.

It is shown in the graph below the trend of the bending and torque along the component.

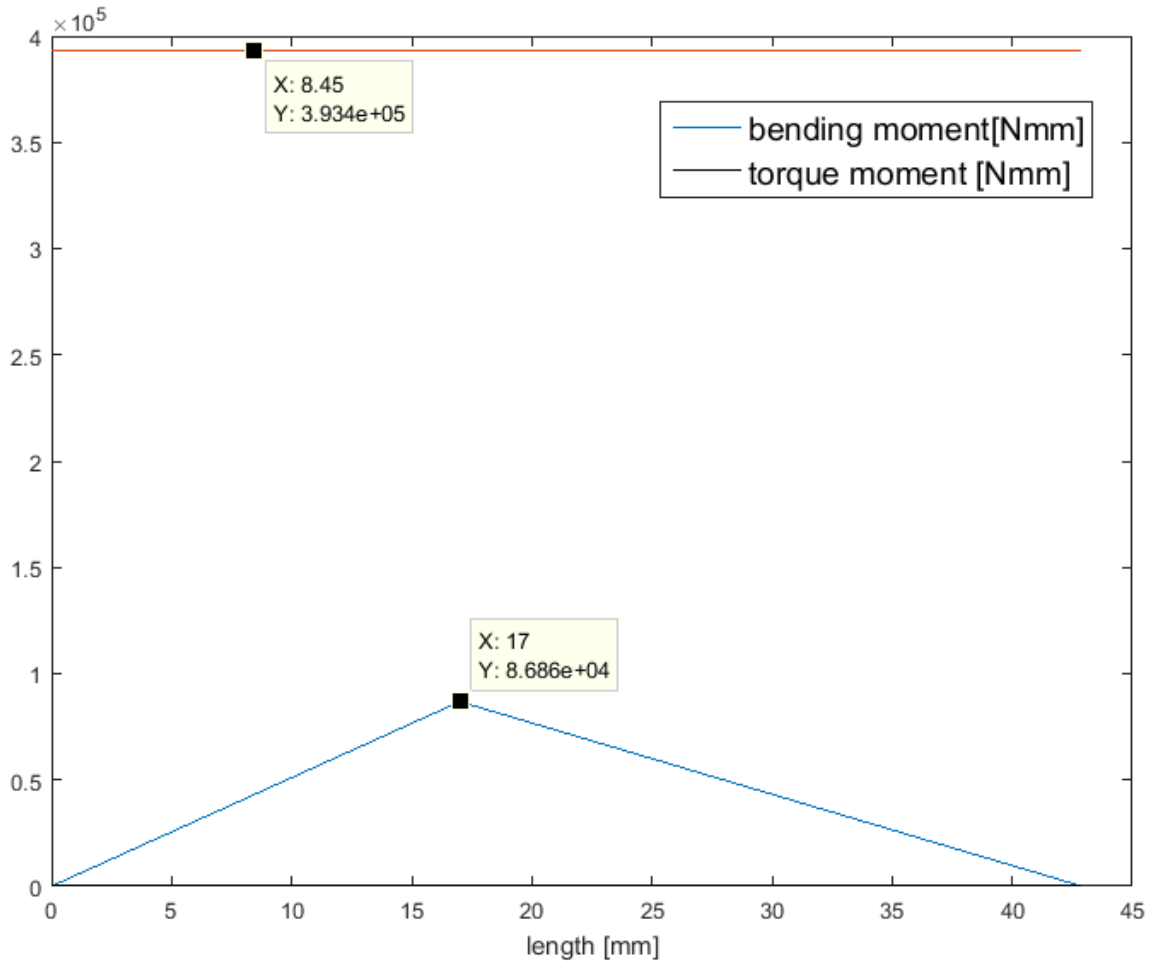


Figure 3-33. Tripod joint bending moment and torque.

Note that while the torque remains constant, the bending moment has a maximum in correspondence of the second bearing (constraint reaction R2).

We then proceed to the calculation of the stresses.

$$\sigma = \text{normal stress} = 32 * \frac{M_f}{\pi * d^3}$$

$$\tau = \text{shear stress} = 16 * \frac{M_t}{\pi * d^3}$$

The graph below shows the trend of the two stress components calculated along the component.

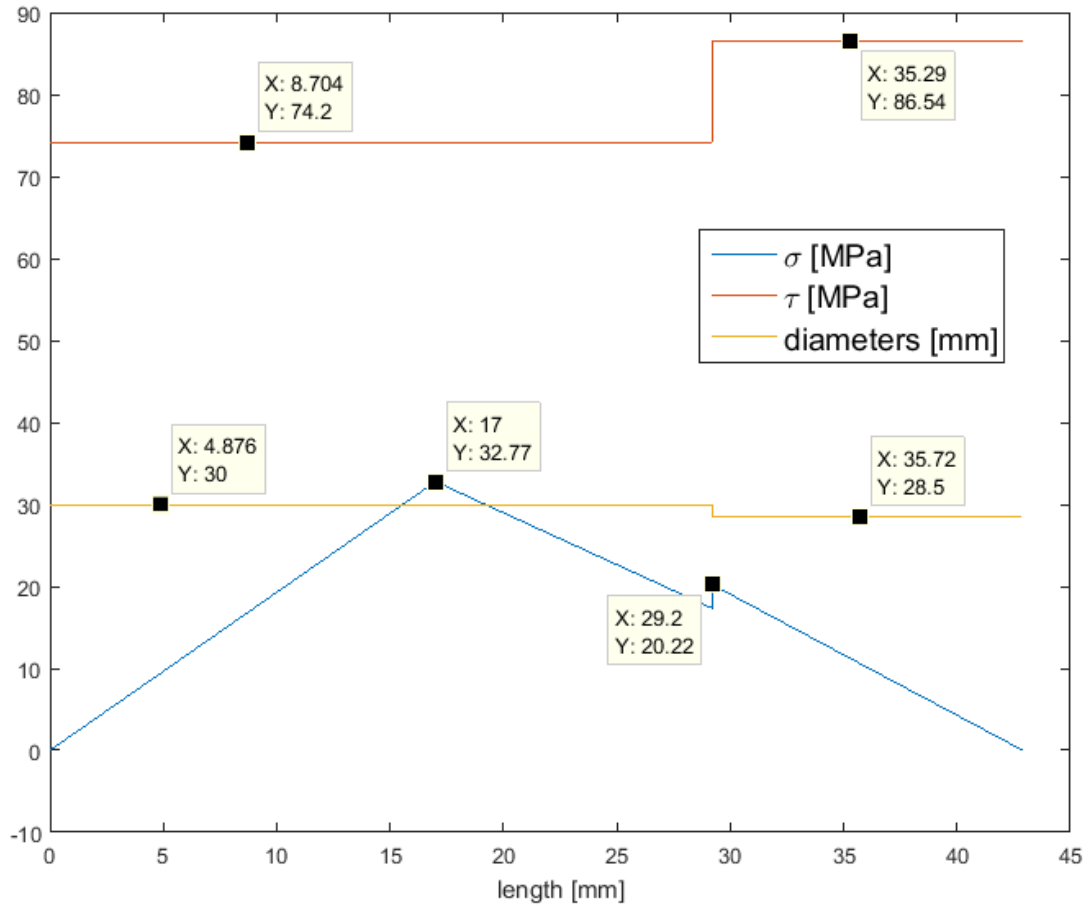


Figure 3-34. Tripod joint stresses

The Von Mises criterion is used to correctly evaluate both the contents of normal and shear stresses. The two contributions are combined to find an equivalent effort.

$$\sigma_{VM} = \text{Von Mises equivalent stress} = \sqrt{\sigma^2 + 3 * \tau^2}$$

The equivalent stress trend along the component is reported.

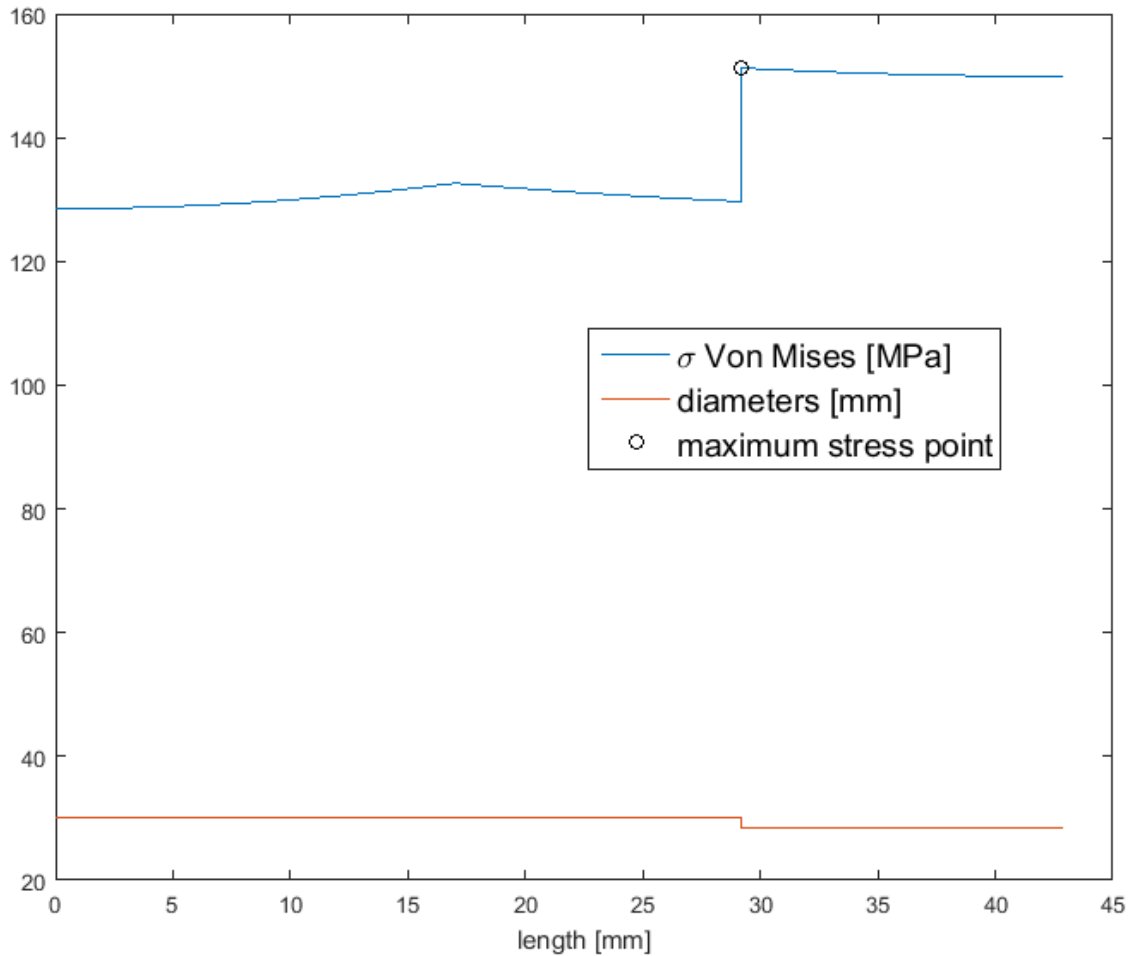


Figure 3-35. Tripod joint Von Mises stress

The most critical section is that in which the section is changed. Here the stress of Von Mises is about 151.3 MPa. As material it was considered a pure commercial grade 2 Titanium, having no further details on the material of the component in our possession. In this way, in a very generic case, it is therefore possible to calculate the safety factor.

$$CS = \text{safety factor} = \frac{\sigma_y}{\sigma_{VM}} = \frac{275}{151.3} = 1.8182$$

The static analysis is therefore satisfied. Note however that in the force F there are also the inertial components of the chain that in a static analysis should not be present. I therefore consider this contribution as an additional safety margin.

3.6.2 Fatigue assessment

Given the cyclical nature of the bending moment, a fatigue assessment, using Sines method, was also considered useful. In reality the car will almost never travel at a constant speed and therefore the risk of going against fatigue breaks is very low. However, it is decided, as a further security, to proceed with the assessment anyway.

We start to calculate the fatigue stress.

$$\sigma_e = \text{fatigue stress} = 0.5 * \sigma_u * m_s * m_d = 0.5 * 345 * 0.85 * 0.9 = 131.96 \text{ MPa}$$

m_s, m_d are coefficients linked respectively to the surface finish and to the size of the object to be checked with respect to the standard specimen, σ_u is instead referred to the material already considered previously.

We must now consider the intensification of the stress given by the change of section with connection. For this reason we consider $K_t = 1.025$.

Using Neuber formula:

$$q = \frac{1}{1 + \sqrt{\frac{\rho}{r}}} = \frac{1}{1 + \sqrt{\frac{0.16}{0.25}}} = 0.5556$$

Now we can calculate K_f .

$$K_f = 1 + q * (K_t - 1) = 1.0139$$

It is therefore possible to calculate the fatigue limit stress in the case of our component.

$$\sigma'_e = \text{fatigue limit stress} = \frac{\sigma_e}{K_f} = 130.15 \text{ MPa}$$

The equivalent stress of Sines in this case corresponds exclusively to the stress given by the bending moment, which is the only alternating component. The torque is instead constant and therefore generates only average stress components, but only tangential. So it is not taken into consideration by the Sines formulation.

$$\sigma_{Sines} = \text{equivalent Sines stress} = \sigma \text{ (nel cambio sezione)} = 20.21 \text{ MPa}$$

Now we can calculate the safety factor:

$$CS = \text{safety factor} = \frac{\sigma'_e}{\sigma_{Sines}} = 6.44$$

Given the value of the safety factor it can be said that even in this case the assessment is satisfied.

Once the part of planning, analysis and implementation of the transmission is over, we move on to the second macro-topic of this thesis. The study of the dynamic and kinematic behavior of the new electric vehicle.

4 Multibody model of the car

To study the dynamic and kinematic behavior of the vehicle, we started with the multibody model of the internal combustion vehicle, modifying its inertial and geometric characteristics.

However, the previous model was restricted to wheel hubs and its use was limited to applying forces or accelerations to the center of gravity. In this way the behavior of the suspensions could be studied.

What we wanted to achieve in this thesis is to add tire modules and release the vehicle from the global reference. In this way it is possible to simulate the behavior of the entire vehicle subject to the real torque of the two engines and the input of the steering.

We move from a vehicle linked to hubs without tires to a complete vehicle capable of simulating real driving conditions, even with approximations.

4.1 Characteristics of a multibody model

The need to study the behavior in space of complex systems that undergo macroscopic displacements has given origin to an approach called dynamic of multibody systems. These movements in space lead to strongly non-linear equations of motion.



Figure 4-1. Multibody simulation

With these resolution methods the real system is replaced by an alternative but equivalent model consisting of rigid or flexible bodies, connected to each other by elastic and dissipative bonds. Also bonds or constraints can have linear or non-linear behaviors.

A multibody system is characterized by multiple reference systems. In general there will be a global or inertial one. Compared to the global one, each rigid body will have its own local reference system, in solidarity with itself.

The motions of the bodies will be described by the trajectories of the local systems with respect to the global one.

A flexible body can be approximated by various rigid bodies with flexible bonds or alternatively a finite element analysis (FEM) can be incorporated into the multibody simulator. In our case, for example, we used the first approach for the tire schematization.

This approach requires the resolution of ordinary differential equations (ODEs) that describe the dynamics of the system and differential algebraic equations (AEDs) for the description of the constraints. Both types of equations must be solved numerically by computer.

The simulators described above have increasingly taken hold, due to the need, for companies, to reduce development times and have various advantages:

- The possibility to simulate dangerous and/or expensive situations (crashes).
- Going to the first physical prototype, already optimized, through virtual simulation.
- The reductions of practice tests, reducing develop cost and time.
- The possibilities to increase the possible tests.
- Being able to separate the effects of the variations of the single parameters more easily (sensitivity analysis).

Applications such as the Simulink multibody module also allow easy integration with control systems, such as ABS, stability control, torque vectoring, etc.

4.2 Generality of the complete vehicle model

The behavior of the complete vehicle model is now explained.

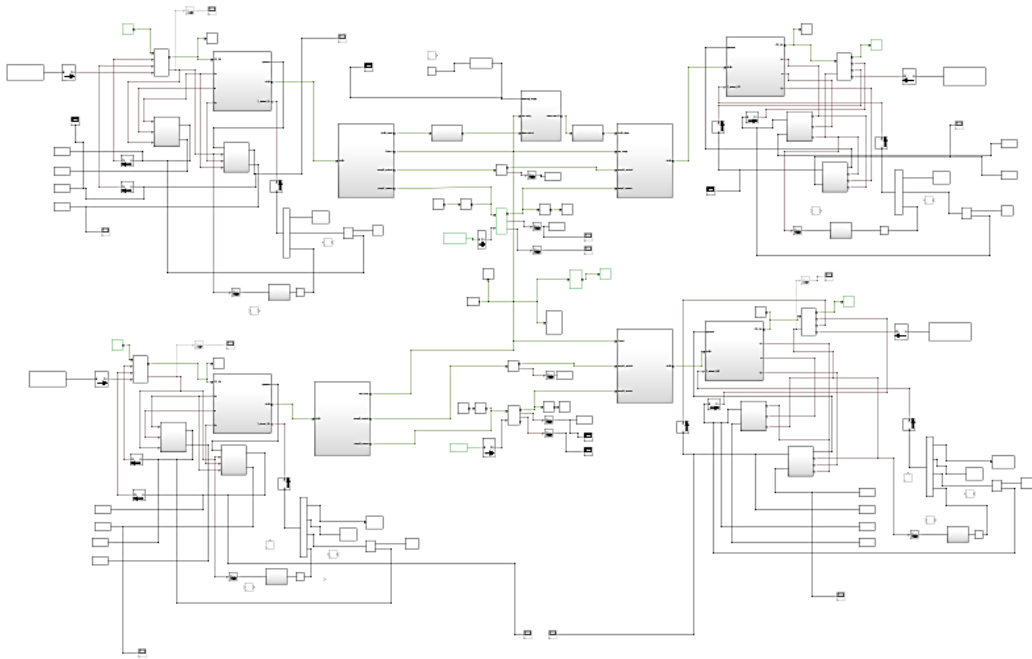


Figure 4-2. Complete model

The model can be divided into macro areas, with different functions.

We start from the three points of contact with the asphalt that we see marked in red. Contact forces are applied directly to these entities.

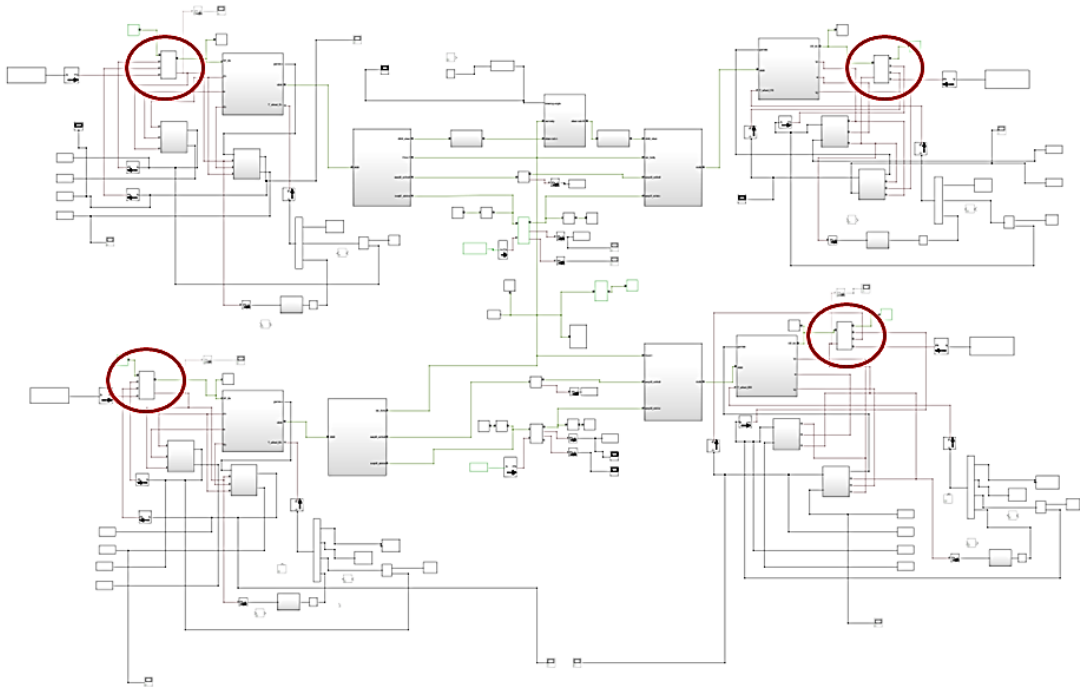


Figure 4-3. Contact point

The contact points are part of the macro areas of the tires that will be described in an exhaustive manner in the following parts.

Circled in blue you can see the areas that allow the simulation of all four wheel groups. Directly on the rear tires are attributed the torques coming from the engines, while the braking and dissipative ones on all wheels.

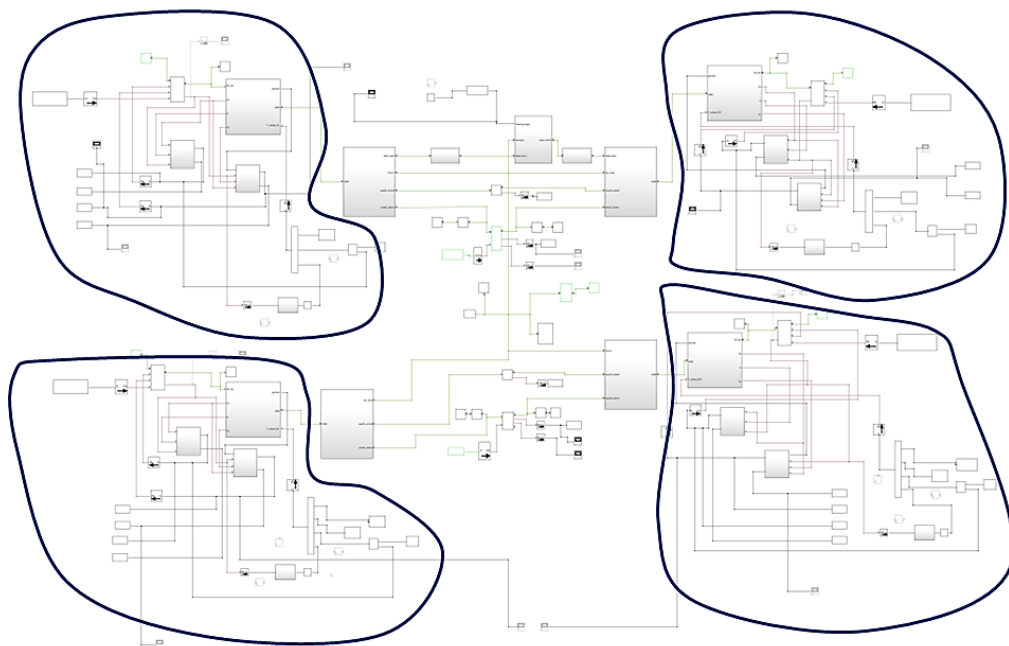


Figure 4-4. Wheel areas

There are also areas used for the simulation of suspensions circled in green, steering in orange and a part, circled in black, in which the inertial properties of the vehicle were inserted.

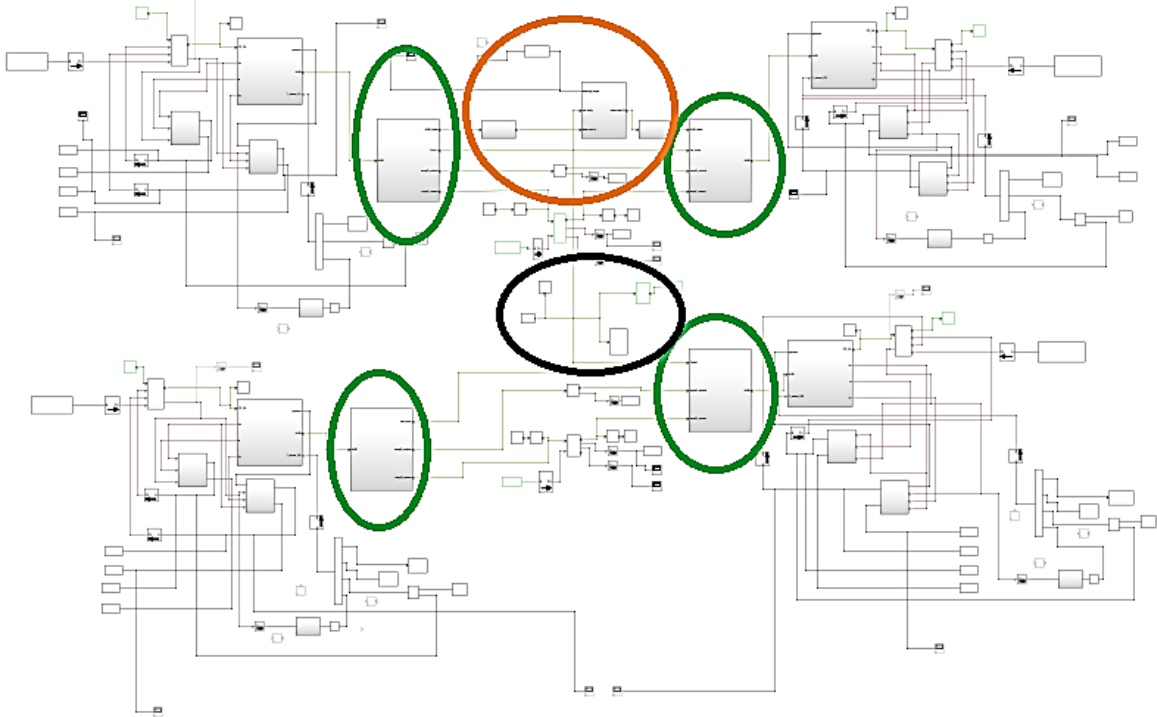


Figure 4-5. Car areas

The global reference system can be interpreted as a generic, fixed point, towards which the car has constrained and unconstrained degrees of freedom.

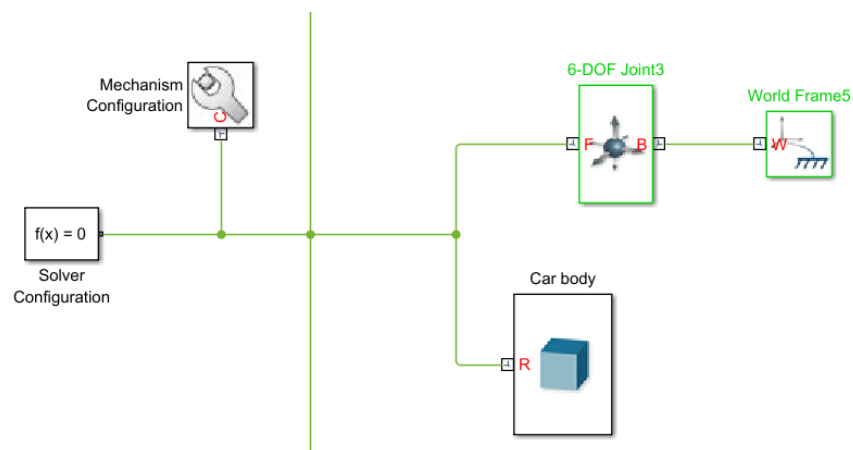


Figure 4-6. World frame

This global reference system is named "World frame" and is connected to the main body "Car body" (point-like but with all the inertial properties of the car) through a "6-DOF Joint" that is a constraint with 6 degrees of freedom. It allows any movement in space.

The vehicle can move freely in space although its movements are calculated starting from the global reference system. However, the development of the model made it necessary to introduce further constraints with respect to the same reference.

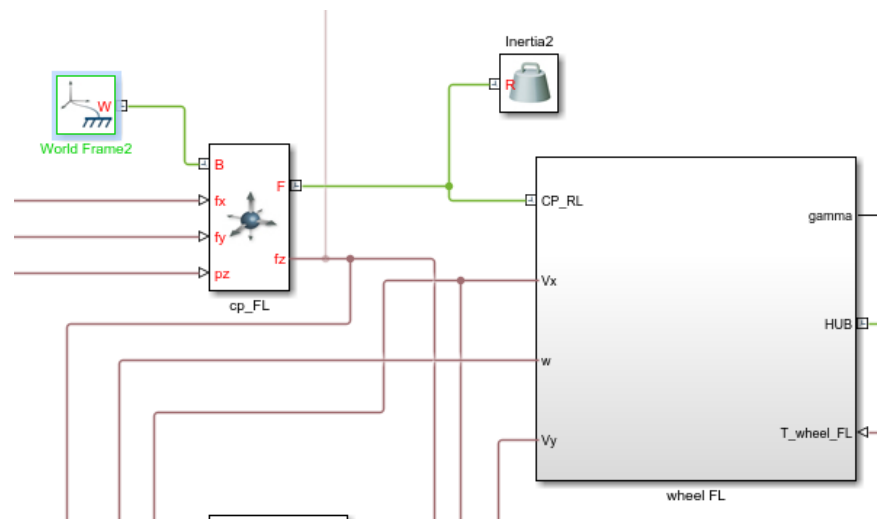


Figure 4-7. World frame link with CP

The points of contact, as will be described in detail in the section of the tire, undergo the suppression of the displacement with respect to the Z axis. In this way the plane of the road, on which the origin of world frame is positioned, cannot undergo relative vertical displacements with respect to the kinematic contact point of the tire. To better clarify the concept, see the contact points as entities that can only move on the (2D) plane of the road. This simplification was necessary to complete the model.

Without going into the detail of each individual sub block, we now explain the general approach with which the multibody model of the vehicle was generated, starting from the geometric dimensions of the 3D model. It should be noted that the suspension and steering parts are not included in the treatment of this thesis.

As an example will be explained the working of a part of the front left suspension, which in the model has the FL (Front Left) attribute. The image below, taken from the Simulink graphic interface, is underlined.

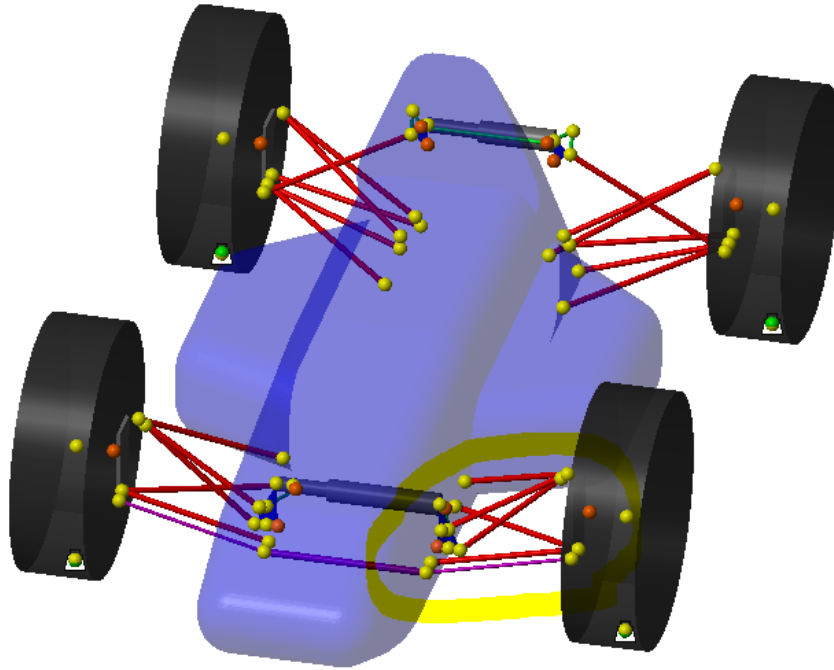


Figure 4-8. Suspension FL

The graphic interface has been built starting from entities, available on Simulink, that allow you to have immediate feedback on the movements of the model. Given the complexity and the number of moving parts, this approach proved to be indispensable even if it considerably weighs in terms of calculation times.

The upper triangle of the suspension, called “wishbone_upper”, is exposed.

This structure is composed of two connecting rods joined on one side to the body of the vehicle (frame) and on the other one to the hub and to the connecting rod, connected to the rocker.

The model part of the upper wishbone is shown.

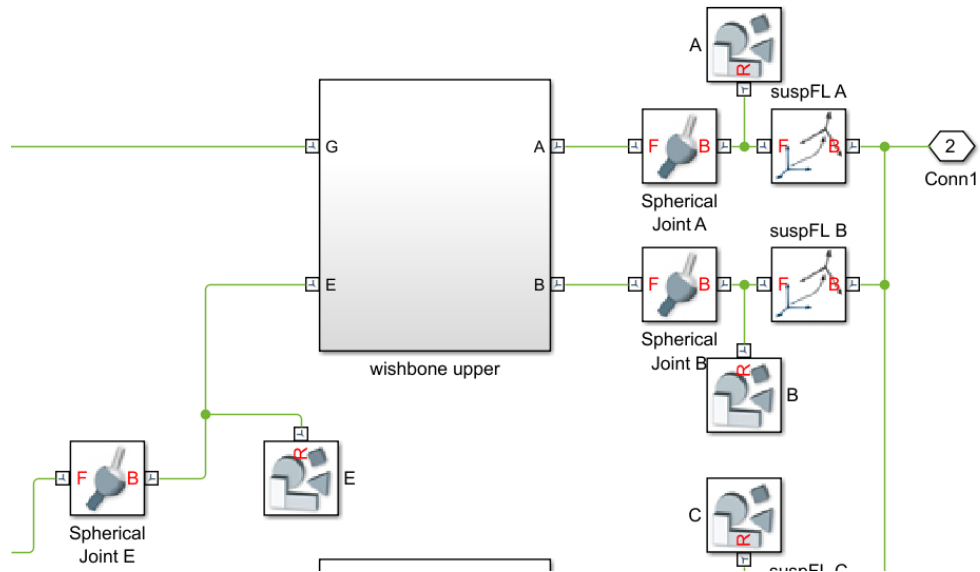


Figure 4-9. Wishbone upper

Spherical joints are 3D hinges that allow all rotations in space. Spherical joints A and B are connected to the car body, while E is at the hub. The point G of the wishbone upper is another hinge (not present in the diagram above) connected through a bar, highlighted in the figure below, to the rocker.

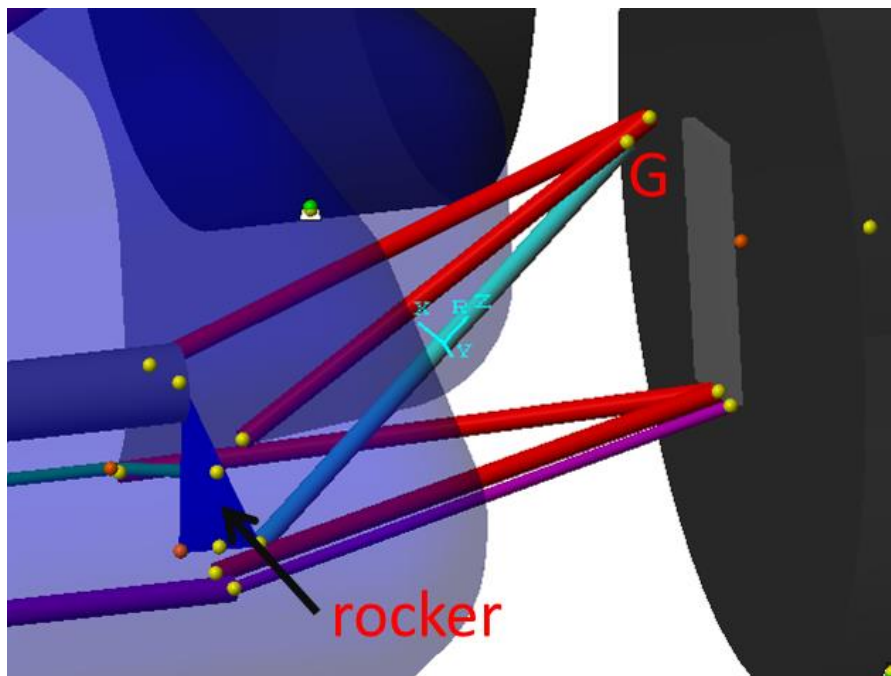


Figure 4-10. Rocker and spherical joint G

The yellow points are represented through blocks called “Graphic”. These entities, as mentioned earlier, have no dynamic or kinematic influence on the model. Their only purpose is the composition of the graphic interface.

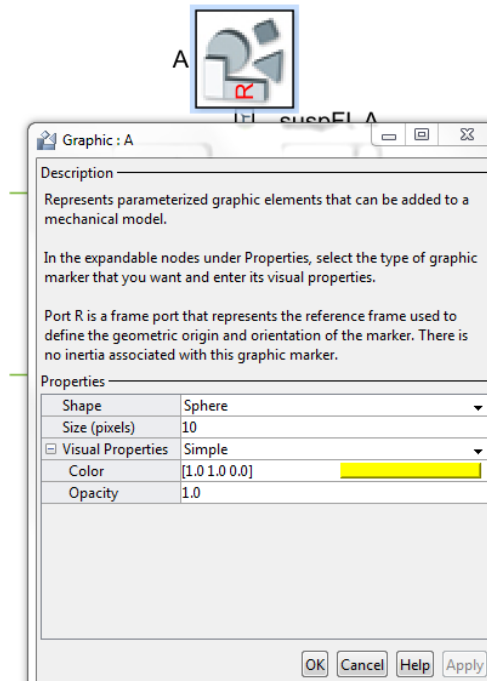


Figure 4-11. Graphic

We highlight, in an image, the other points that coincide with the spherical joints.

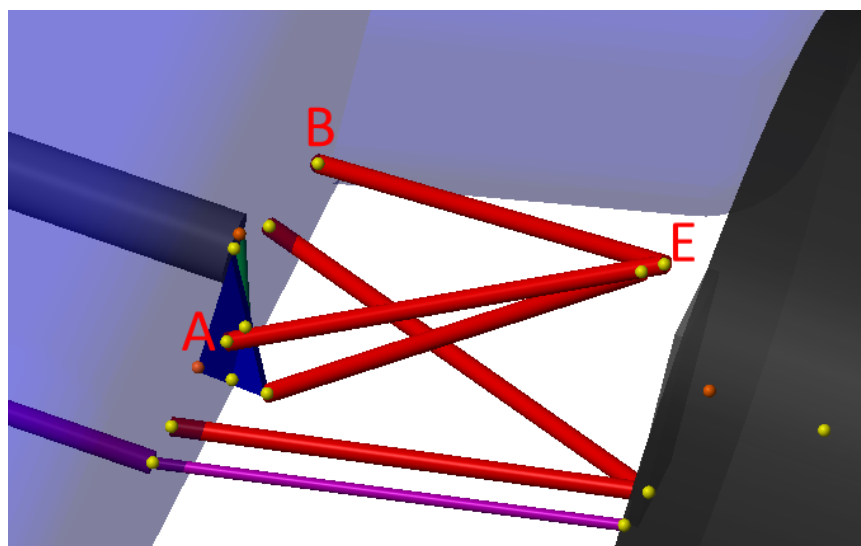


Figure 4-12. Point

Now we study in deep the multibody approach in the definition of points in space and bodies by going to see the definition of the two connecting rods of the upper triangle. We enter the Wishbone upper subsystem.

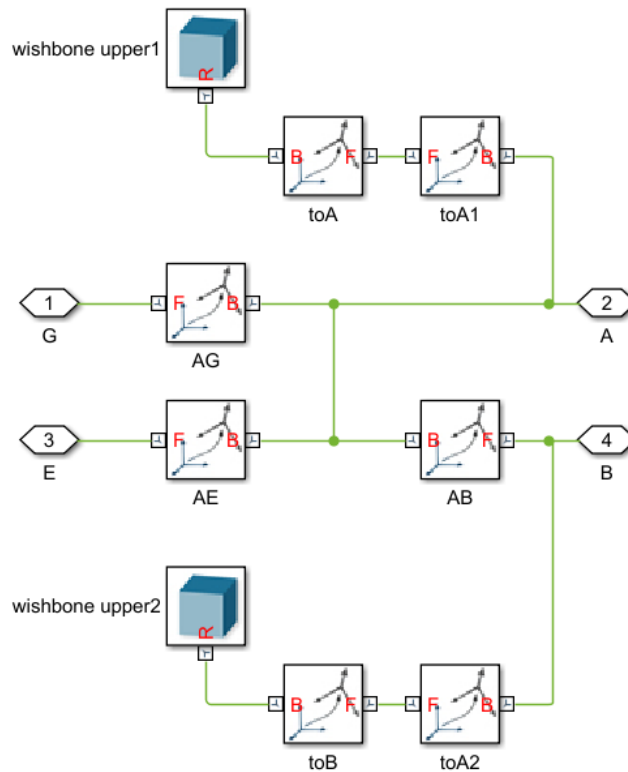


Figure 4-13. Wishbone upper structure

Analyzing the upper branch in the image above we find two blocks called "toA1" and "toA". These are rigid transformations. The diagram will be analyzed starting from point A, integral with the vehicle chassis, and going to the left.

The first block (toA1) operates a 3D rotation that allows to align the reference system with Z in the same direction as the suspension arm. The next block moves it, always along Z, into the central part of the arm where it is finally possible to associate the inertial properties of the component itself.

The block in which these properties are indicated is called "wishbone upper 1".

The hexagonal blocks named "A", "B", "G" and "E" are the inputs and outputs of the subsystem towards an higher level. Simulink is organized with blocks that can enclose others by creating subsystems or analytical functions written in Matlab code.

We summarize the steps previously explained with an image.

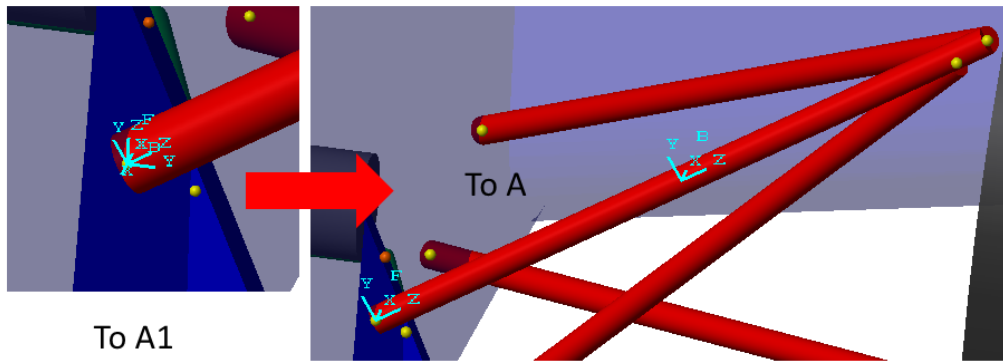


Figure 4-14. Rigid transform

In each rigid transformation the two reference systems are named “B” (Base frame) and “F” (Follower frame). “B” is the starting system that undergoes the transformation to become “F”. The transformation is defined with respect to “B”.

We will now proceed to the validation and description of the pneumatic model.

5 Pneumatic model study

To study the working of tire model it is decided to consider it separately from the rest of the car.

In order to guarantee a behavior that simulates the movements of the wheel in a coherent, but simplified, way with respect to the global reference system, we have added blocks that allow to control the movements in space.

5.1 Pneumatic model description

The tire model is linked to the hub and therefore to the suspension system through the hub. It leans on the asphalt.

In the case of the tyre model, the reference system, integral with the hub, has kinematic links directly with the global reference system. In detail with respect to the latter, it has three degrees of freedom; the three translations along the axes (cartesian joint).

The second bond of the tire is the one with the asphalt.

This bond is first described:

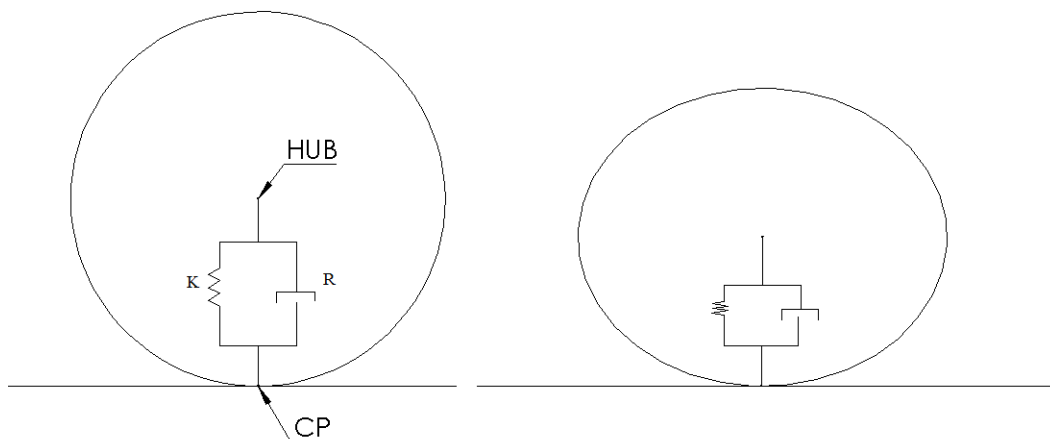


Figure 5-1. Tyre model

The point (kinematic entity), integral with the asphalt, is called CP (point of contact).

A concentrated mass is added to the CP, equal to 5.4 kg. This is the inertia of the contact area. A second load (of 16 kg) is then attributed to the rim / tyre assembly and represents the rest of the mass of the entire wheel.

Between CP and the absolute reference system (world_frame) a 6 dof bond (6-DOF joint) is inserted. Of these degrees of freedom the only one to be suppressed is the displacement of CP with respect to asphalt. This is a simplification in that the wheel, in reality, could detach from the asphalt.

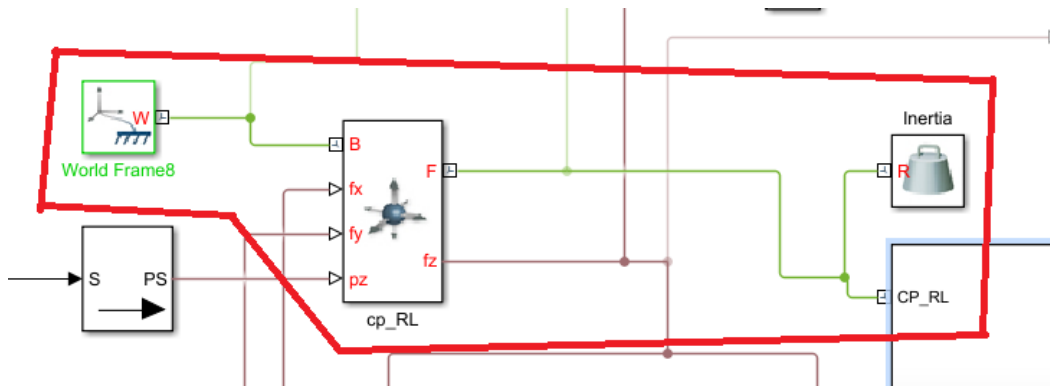


Figure 5-2. Link between world frame and CP

Entering the tire block we find the structure that allows rotation and deformation due to the vertical load.

A prismatic joint makes it possible to simulate the stiffness and damping of the tire. The characteristics assigned are the following:

$$k_{tyre} = 210000 \left[\frac{N}{m} \right]$$

$$r_{tyre} = 50 \left[\frac{N * s}{m} \right]$$

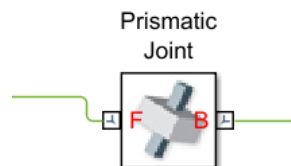


Figure 5-3. Prismatic joint symbol

This prismatic bond allows only the movement along the axis indicated in red in the figure. The Contact Point and the Hub can therefore move relative to each other by simulating the actual deformations of the tyre.

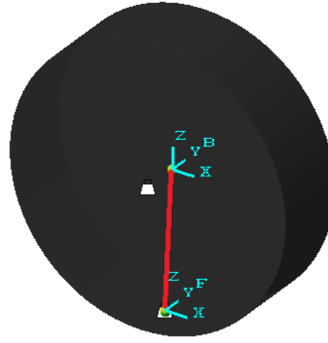


Figure 5-4. Prismatic joint

As for the rotation of the wheel a second link has been introduced between the HUB and the wheel itself, which is considered with an inertia in rotation but without a mass. This choice is justified by having already attributed its weight to the point of contact. Otherwise it would have been considered a double weight compared to the real one.

The link chosen is the “Revolute joint” that allows the rotation between two bodies.

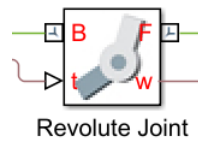


Figure 5-5. Revolute joint

The block diagram inside the wheel is now summarized.

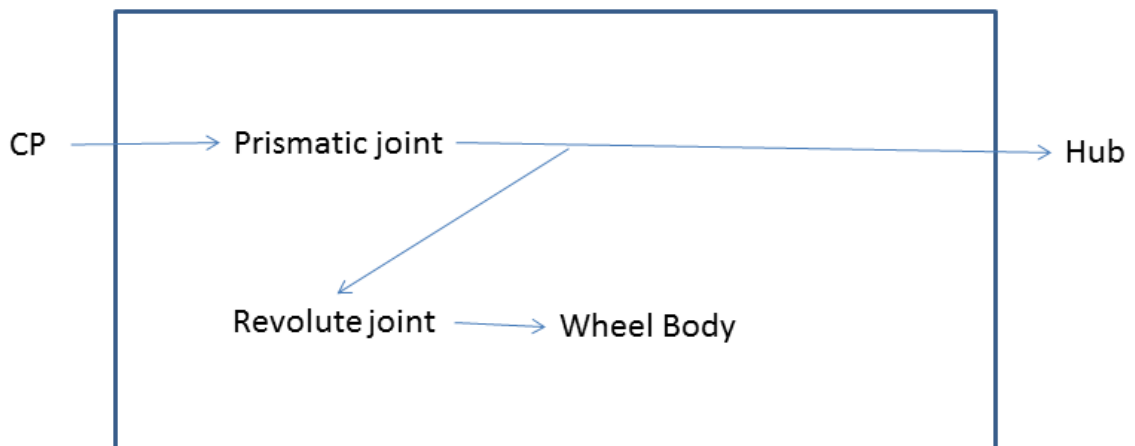


Figure 5-6. Wheel scheme

Now we define the flow of measured and calculated signals.

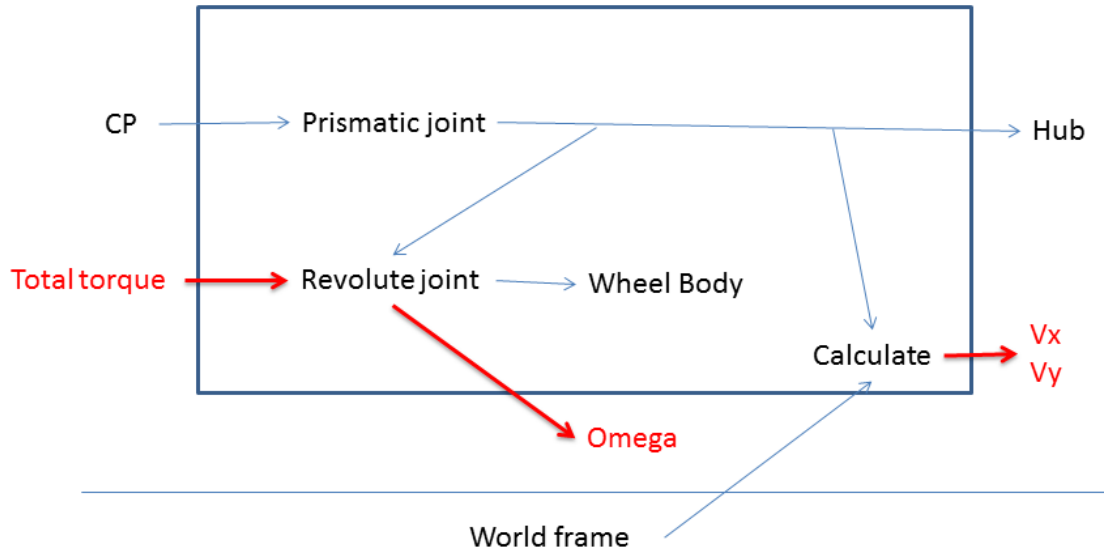


Figure 5-7. Wheel scheme with measurements

As input the revolute joint takes the total torque acting on the wheel while returning the angular speed of the wheel (Ω). The other outputs are the transverse and longitudinal speeds (respectively V_y and V_x) which are calculated starting from the relative displacements of the wheel with respect to the global reference.

Outside the main wheel block there are further blocks used to calculate contact forces.

The operation of these blocks will now be described.

5.1.1 Contact forces calculation

The Pacejka model was used for the calculation neglecting the contribution of the self-aligning moment and the combined actions. Therefore only pure drift and pure longitudinal slip are evaluated.

The function, that calculates the longitudinal force, takes the longitudinal speed (V_x), the angular speed of the wheel (w) and the vertical load (F_z) as input.

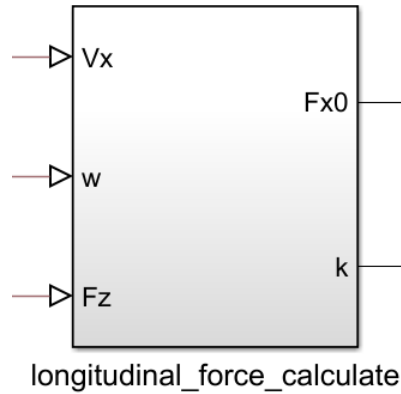


Figure 5-8. Longitudinal force calculate

The k , the longitudinal slip, is calculated.

$$k = \text{longitudinal slip} = \frac{\omega * r - V_x}{V_x}$$

With:

$V_x = \text{longitudinal speed}$

$\omega = \text{wheel angular speed}$

$r = \text{wheel undeformed radius}$

With the longitudinal slip it is possible to apply the Pacejka formula for calculating the longitudinal force.

As input in addition to k we need other features of the tyre.

We will have scale factors that are all set equal to 1 to avoid introducing further complications to the model.

$\lambda_{Fz0} = 1 = \text{scale factor of nominal load}$

$\lambda_{Cx} = 1 = \text{scale factor of } F_x \text{ shape factor}$

$\lambda_{Ex} = 1 = \text{scale factor of } F_x \text{ curvature factor}$

$\lambda_{Hx} = 1 = \text{scale factor of } F_x \text{ horizontal shift}$

$\lambda_{Kx} = 1 = \text{scale factor of } F_x \text{ slip stiffness}$

$\lambda_{\mu x} = 1 = \text{scale factor of } F_x \text{ peak friction coefficient}$

$\lambda_{Vx} = 1 = \text{scale factor of } F_x \text{ vertical shift}$

The scale factor is now applied to the nominal vertical force F_{z0} .

$$F'_{z0} = \lambda_{Fz0} * F_{z0} = 1 * 4850 = 4850 \text{ N}$$

The difference between the nominal load and the instantaneous one is:

$$dF_z = \frac{F_z - F'_{z0}}{F'_{z0}}$$

Now we calculate the horizontal offset (S_{Hx}), to be given to the Fx force curve, as a function of longitudinal slip. This offset depends on variations in the vertical load.

$$S_{Hx} = (P_{Hx1} + P_{Hx2} * dF_z) * \lambda_{Hx}$$

With:

$$P_{Hx1} = 0.0012297$$

= horizontal displacement of S_{Hx} in the case of nominal vertical load.

$$P_{Hx2} = 0.0004318 = \text{variation of } S_{Hx} \text{ respect to the vertical load.}$$

The horizontal offset is now assigned to the longitudinal sliding coefficient.

$$k_x = k + S_{Hx}$$

The longitudinal shape factor C_x is calculated. This factor determines the part of the sine function used by the curve and influences its shape.

$$C_x = P_{Cx1} * \lambda_{Cx}$$

With:

$$P_{Cx1} = 1.6411 = \text{shape factor for the longitudinal force.}$$

The longitudinal friction coefficient is calculated. Its variations are related to those of the vertical load.

$$\mu_x = (P_{Dx1} + P_{Dx2} * dF_z) * \lambda_{\mu x}$$

With:

$$P_{Dx1} = 1.1739 = \text{longitudinal friction coefficient } \mu_x \text{ in case of nominal vertical force.}$$

$$P_{Dx2} = -0.16395 = \text{variation of } \mu_x \text{ in function of the load.}$$

It is therefore possible to calculate the parameter D_x which represents the peak value of the longitudinal force.

$$D_x = \mu_x * F_z$$

The E_x parameter represents the curvature factor. It modifies the shape of the curve around the peak.

$$E_x = (P_{Ex1} + P_{Ex2} * dF_z + P_{Ex3} * dF_z^2) * (1 - P_{Ex4} * \text{sign}(k_x)) * \lambda_{Ex}$$

With:

$$P_{Ex1} = 0.46403$$

= longitudinal curvature E_x when subjected to the nominal vertical load.

$$P_{Ex2} = 0.25022 = \text{variation of } E_x \text{ depending on the load variation.}$$

$$P_{Ex3} = 0.067842 = \text{variation of } E_x \text{ depending on the square of the load variation.}$$

$$P_{Ex4} = -3.7604 * 10^{-5} = \text{factor that depend on the driving.}$$

The parameter K_x represents the longitudinal stiffness.

$$K_x = F_z * (P_{Kx1} + P_{Kx2} * dF_z) * e^{(P_{Kx3} * dF_z)} * \lambda_{Kx}$$

With:

$$P_{Kx1} = 22.303 = \text{longitudinal stiffness } \left(\frac{K_x}{F_z}\right) \text{ in the case of nominal load.}$$

$$P_{Kx2} = 0.48896$$

= variation of longitudinal stiffness $\left(\frac{K_x}{F_z}\right)$ depending on the vertical load.

$$P_{Kx3} = 0.21253$$

= exponential of the longitudinal stiffness $\left(\frac{K_x}{F_z}\right)$ depending on the vertical load.

It is possible to calculate B_x , stiffness factor, using the relationship that links it to the other parameters.

$$B_x = \frac{K_x}{C_x * D_x}$$

Now we can calculate the vertical offset (S_{Vx}) to be given to the F_x force curve as a function of the longitudinal slip. This offset depends on variations in the vertical load.

$$S_{Vx} = F_z * (P_{Vx1} + P_{Vx2} * dF_z) * \lambda_{Vx} * \lambda_{\mu x}$$

With:

$$P_{Vx1} = -8.8098 * 10^{-6} = \text{vertical slip } \frac{S_{Vx}}{F_z} \text{ calculated with the nominal load.}$$

$$P_{Vx2} = 1.862 * 10^{-5} = \text{variation of the vertical slip } \frac{S_{Vx}}{F_z} \text{ depending on the load.}$$

After obtaining all the necessary factors it is possible to calculate the longitudinal force.

$$F_x = D_x * \sin(C_x * \tan^{-1}(B_x * k_x - E_x * (B_x * k_x - \tan^{-1}(B_x * k_x)))) + S_{Vx}$$

We now describe the function which, again using the Pacejka model, allows the calculation of the transverse force.

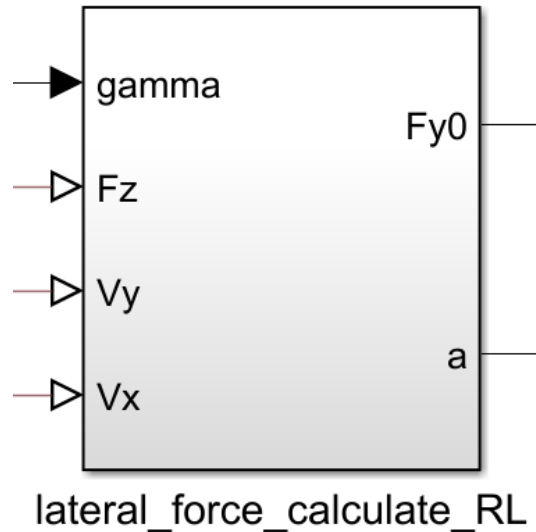


Figure 5-9. Lateral force calculate

The function that calculates the transverse force takes, as input, the longitudinal speed (V_x), the transverse speed (V_y), the camber angle (γ) and the vertical load (F_z).

Now we calculate α , the slip angle.

$$\alpha = \text{slip angle} = \tan^{-1}\left(\frac{V_y}{V_x}\right)$$

Also in this function we will have scale factors that are all set equal to 1 to avoid introducing further complications to the model.

$$\lambda_{Fz0} = 1 = \text{scale factor of nominal load}$$

$$\lambda_{Cy} = 1 = \text{scale factor of } F_y \text{ shape factor}$$

$$\lambda_{Ey} = 1 = \text{scale factor of } F_y \text{ curvature factor}$$

$$\lambda_{Hy} = 1 = \text{scale factor of } F_y \text{ horizontal shift}$$

$$\lambda_{Ky} = 1 = \text{scale factor of } F_y \text{ slip stiffness}$$

$$\lambda_{\mu y} = 1 = \text{scale factor of } F_y \text{ peak friction coefficient}$$

$$\lambda_{Vy} = 1 = \text{scale factor of } F_y \text{ vertical shift}$$

$\lambda_{GAy} = 1 = \text{scale factor of } F_y \text{ camber}$

We can calculate the camber angle:

$$\gamma_y = \gamma * \lambda_{GAy}$$

Now we calculate the horizontal offset (S_{Hy}) to be given to the F_y force curve as a function of the slip angle. This offset depends on variations in the vertical load and on the camber angle.

$$S_{Hy} = (P_{Hy1} + P_{Hy2} * dF_z) * \lambda_{Hx} + P_{Hy3} * \gamma_y$$

With:

$$P_{Hy1} = 0.0026747 = \text{horizontal shift of } S_{Hy} \text{ in the case of nominal vertical load.}$$

$$P_{Hy2} = 8.9094 * 10^{-5} = \text{variation of } S_{Hy} \text{ respect to the vertical load.}$$

$$P_{Hy3} = 0.031415 = \text{variation of } S_{Hy} \text{ respect to the camber angle.}$$

Offset is applied to the slip angle.

$$\alpha_y = \alpha + S_{Hy}$$

The parameter K_y represents the lateral stiffness.

$$K_y = P_{Ky1} * F_{z0} * \sin \left(2 * \tan^{-1} \left(\frac{F_z}{P_{Ky2} * F_{z0} * \lambda_{Fz0}} \right) \right) * (1 - P_{Ky3} * |\gamma_y|) * \lambda_{Fz0} * \lambda_{Ky}$$

With:

$$P_{Ky1} = -21.92 = \text{maximum value of stiffness } \frac{K_y}{F_{z0}}.$$

$$P_{Ky2} = 2.0012 = \text{valwhere } K_y \text{ reaches the maximum value.}$$

$$P_{Ky3} = -0.024778 = \text{variation of } \frac{K_y}{F_{z0}} \text{ depending on the camber angle.}$$

The cross-sectional factor C_y is calculated. This factor determines the part of the sine function used by the curve and influences its shape.

$$C_y = P_{Cy1} * \lambda_{Cy}$$

With:

$$P_{Cy1} = 1.3507 = \text{shape factor for the lateral force.}$$

The lateral friction coefficient is calculated. Its variations are related to those of the vertical load.

$$\mu_y = (P_{Dy1} + P_{Dy2} * dF_z) * (1 - P_{Dy3} * \gamma_y^2) * \lambda_{\mu y}$$

With:

$$P_{Dy1} = 1.0489$$

= longitudinal friction coefficient μ_y in the case of nominal vertical force.

$P_{Dy2} = -0.18033$ = variation of μ_y depending on the load.

$P_{Dy3} = -2.8821$ = variation of μ_y depending on the square of the camber angle.

It is therefore possible to calculate the parameter D_y which represents the peak value of the lateral force.

$$D_y = \mu_y * F_z$$

We calculate B_y , stiffness factor, using the relationship that links it to the other parameters.

$$B_y = \frac{K_y}{C_y * D_y}$$

The E_y parameter represents the shape factor. Therefore, modify the shape of the curve around the peak.

$$E_y = (P_{Ey1} + P_{Ey2} * dF_z) * (1 - (P_{Ey3} + P_{Ey4} * \gamma_y) * \text{sign}(\alpha_y)) * \lambda_{Ey}$$

With:

$P_{Ey1} = -0.0074722$ = lateral curvature E_y when subjected to the nominal vertical load.

$P_{Ey2} = -0.0063208$ = variation of E_y depending on the load variations.

$P_{Ey3} = -9.9935$ = constant linked to the dependence of E_y from the camber angle.

$P_{Ey4} = -7.6014 * 10^2$ = dependence of E_y respect to the camber angle.

It is calculated the vertical offset (S_{Vy}) to be given to the F_y force curve as a function of the slip angle. This offset depends on variations in the vertical load.

$$S_{Vy} = F_z * ((P_{Vy1} + P_{Vy2} * dF_z) * \lambda_{Vy} + (P_{Vy3} + P_{Vy4} * dF_z) * \gamma_y) * \lambda_{\mu y}$$

With:

$P_{Vy1} = 0.037318$ = vertical slip $\frac{S_{Vy}}{F_z}$ calculated with the nominal load.

$P_{Vy2} = -0.010049$ = variation of the vertical slip $\frac{S_{Vy}}{F_z}$ depending on the load.

$P_{Vy3} = -0.32931 = \text{variation of the vertical slip } \frac{S_{Vy}}{F_z} \text{ depending on the camber.}$

$P_{Vy4} = -0.69553$

$= \text{variation of the vertical slip } \frac{S_{Vy}}{F_z} \text{ depending on the camber and the load.}$

After obtaining all the necessary factors it is possible to calculate the longitudinal force.

$$F_y = D_y * \sin \left(C_y * \tan^{-1} \left(B_y * \alpha_y - E_y * \left(B_y * \alpha_y - \tan^{-1} (B_y * \alpha_y) \right) \right) \right) + S_{Vy}$$

5.1.2 Calculation of the torques on the wheels

In addition to the parts that calculate the contact forces (transversal and longitudinal), outside the wheel block, the torques are also calculated. These are then used as input in the revolute joint (inside the wheel block).

Now we show the Simulink scheme of the blocks used to calculate the various contributions leading to the total torque.

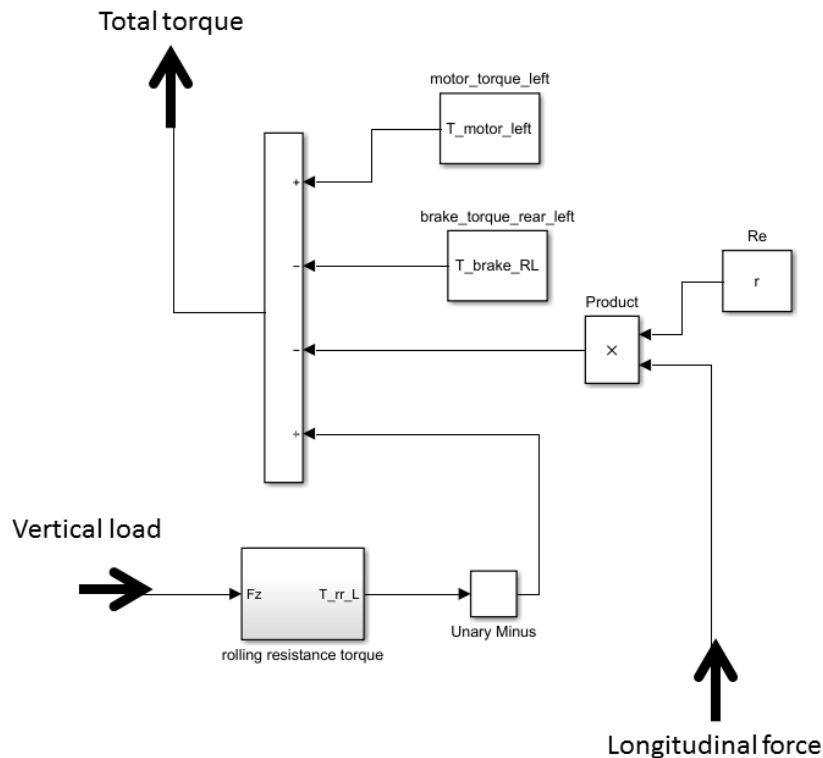


Figure 5-10. Total torque calculation

The torque given by braking is represented by a constant to give an equal contribution for the whole simulation. In this phase, it was decided not to further complicate the model by introducing functions that represented various types of braking.

The motor torque has been treated as the braking one. So with a constant value. It should be noted that leaving constant braking and acceleration, the transients in the implementation of the controls by the pilot were neglected. Important phenomena in the study of the dynamics of the entire car.

Regarding rolling resistance:

$$C_{rolling} = Q_{Sy1} * r * F_z$$

With:

$$Q_{Sy1} = 0.01 = \text{rolling resistance coefficient} .$$

$$r = \text{wheel radius}$$

Regarding the torque generated by the contact force:

$$C_x = F_x * r$$

The total torque acting on the wheel will therefore be:

$$C_{tot} = C_{motor} - C_{braking} - C_{rolling} - C_x$$

5.1.3 Operating of the closed loop

Described all the parts that compose the model it is useful to carry out its operation, paying attention to the closed loop that are used for the calculation of the contact forces.

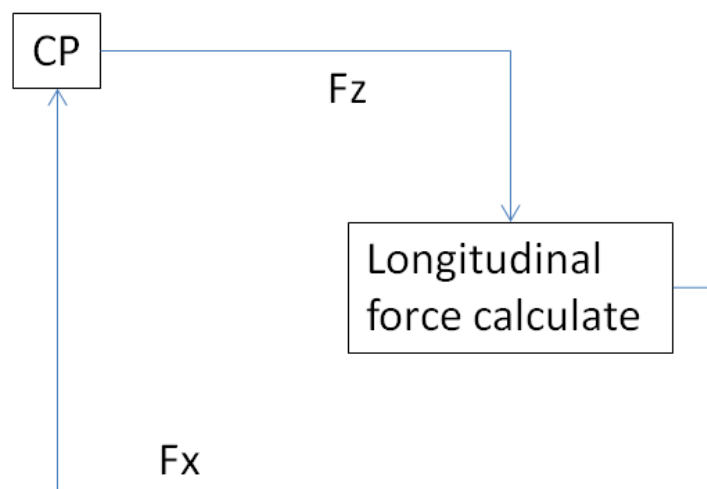


Figure 5-11. Longitudinal force loop

At the point of contact we calculate the vertical force and use it as input in the calculation block of longitudinal contact forces.

The output of this block is used at the entrance of the CP (contact point) to generate the motion of the wheel itself.

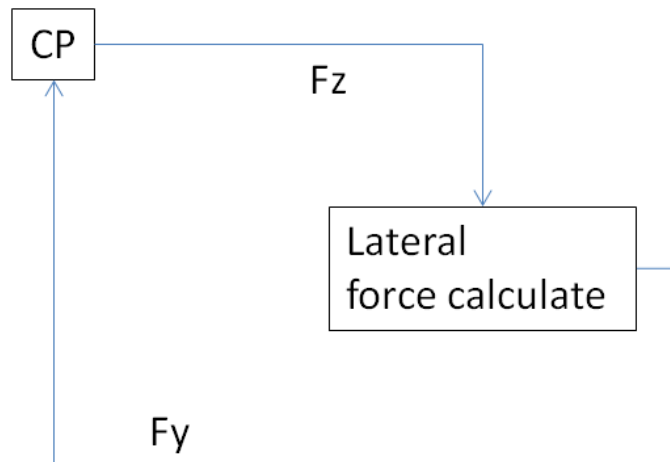


Figure 5-12. Lateral force loop

For the block that calculate the lateral force the same thing happens as in the previous case. Instead of the longitudinal force, the transverse force is calculated.

These closed loops make heavy the numerical calculation and force the introduction of transfer functions to mitigate possible errors due to discontinuities, also due to the presence of analytical functions used for the calculation of torques and contact forces.

5.2 Description of the simplified tire model

Up to this point the simplified model has not undergone substantial changes with respect to the one with the entire car.

See now the links introduced with the “HUB” to simulate the presence of the rest of the car.

To study its dynamic behavior, the need arose to reintroduce kinematic links with respect to the global reference defined for simplicity “WORD” in the image below.

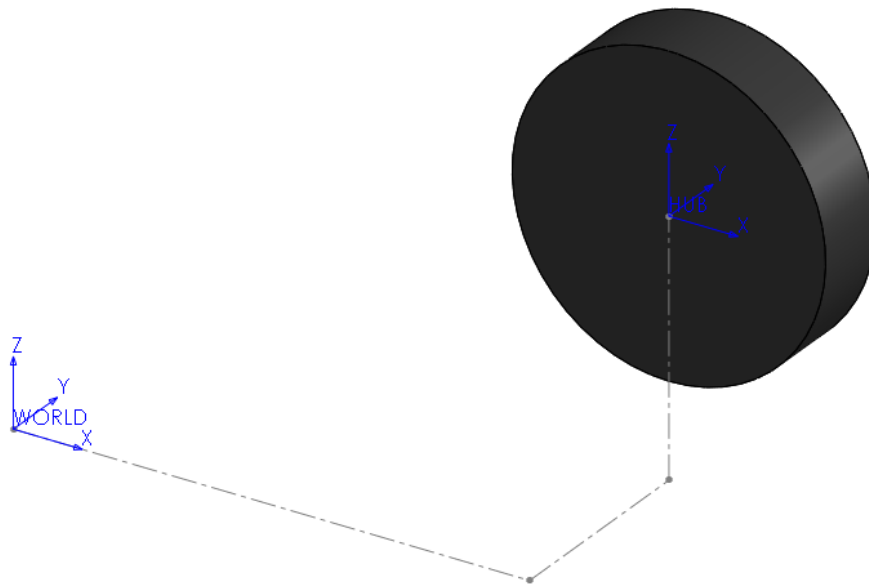


Figure 5-13. WORLD – HUB

Compared to this absolute reference system the local one defined “HUB” can translate along the three axes.

A rotation is then assigned with respect to the local reference system “HUB”. This movement around the Z axis allows us to simulate steering.

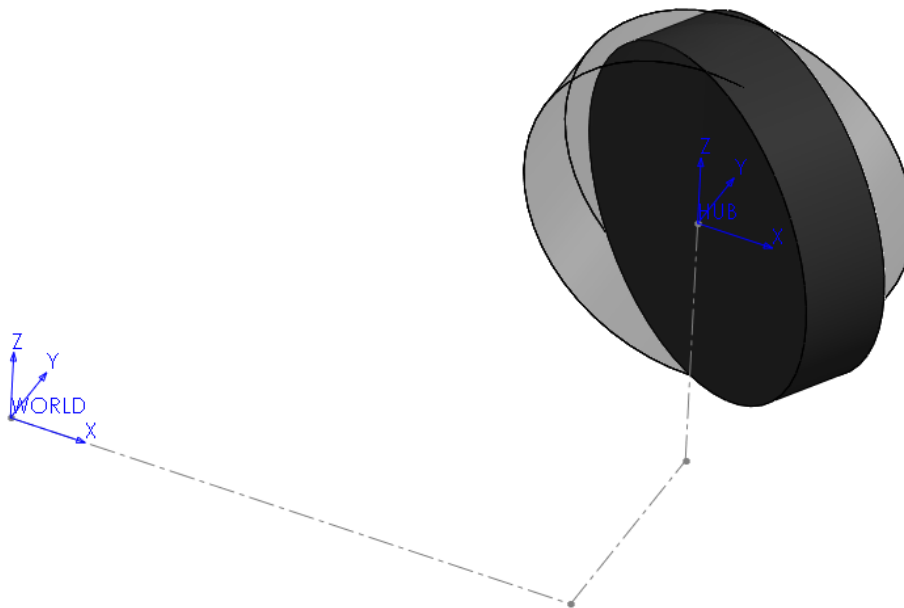


Figure 5-14. Steering

The new local reference system obtained will be called “STEERING”. The steering angle is therefore managed with the rotation between the two “HUB” and “STEERING” reference systems. It is possible to apply a constant or variable angle over time.

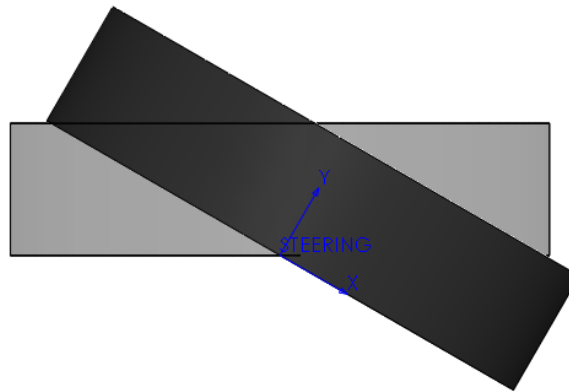


Figure 5-15. Local reference coordinate system for steering

Compared to this new reference system, a further rotation has been assigned around the X axis. In this way, the camber angle can also be simulated.

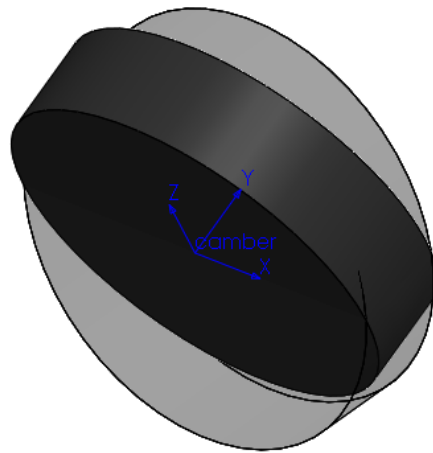


Figure 5-16. Local reference coordinate system for camber

Now we summarize, with a diagram, all the links described until now, outside the tyre model:

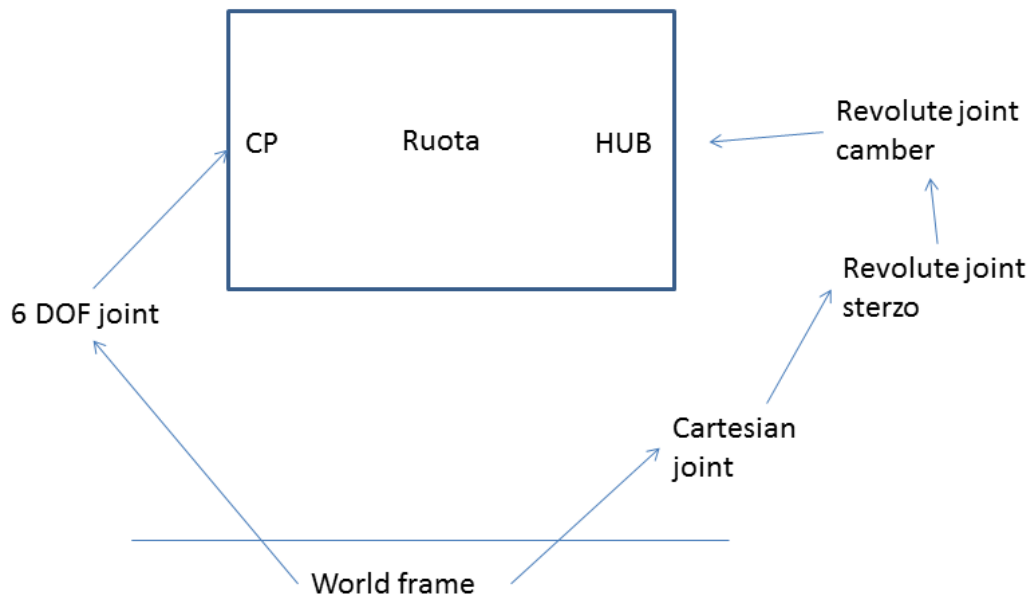


Figure 5-17. Wheel simplified model scheme

This configuration makes it possible to test all the characteristics of the tyre quickly and light from a computational point of view.

5.3 Vertical load behavior

First of all it occurs that by increasing the vertical load on the tyre the contact forces generated by friction increase. Indirectly, therefore, the wheel that enter in the cornering will suffer reduced lateral shifts (less slippage along the y axis).

Two simple cases are examined:

- Vertical load on the tyre equal to $\frac{1}{4}$ of the weight of the entire car, equal to 300 kg.
- Vertical load doubled compared to the previous case.

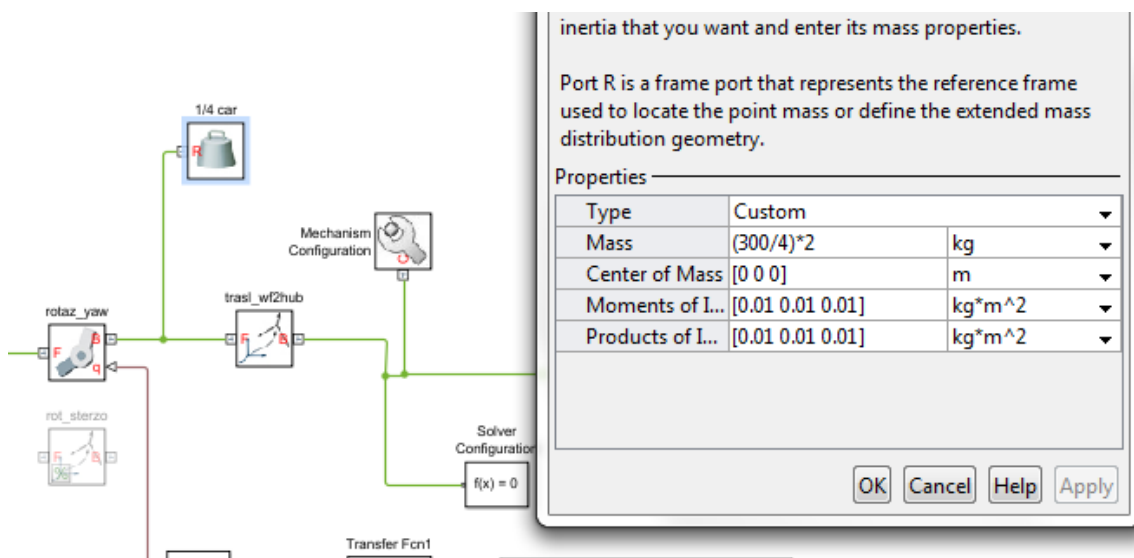


Figure 5-18. Simple case studio

Note the results obtained in the figure below:

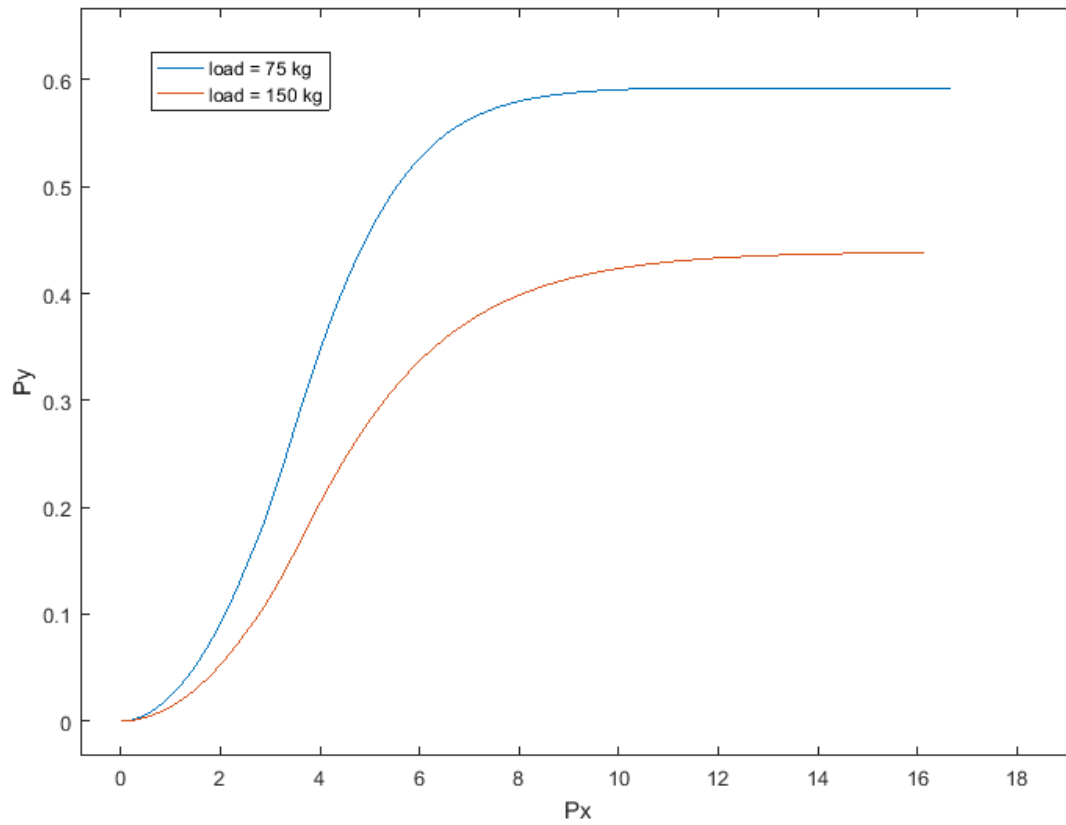


Figure 5-19. Normal load

As you can see, with the same trajectory set, very different results (paths) are obtained.

As the applied load increases, the transverse friction increases and therefore the wheel follow a narrower trajectory, with less transversal sliding.

5.4 Transverse force depending on the slip angle

We now want to check the trend of the transverse contact force F_y depending to the slip angle.

To make the treatment clearer, we normalize the lateral force with respect to the vertical load.

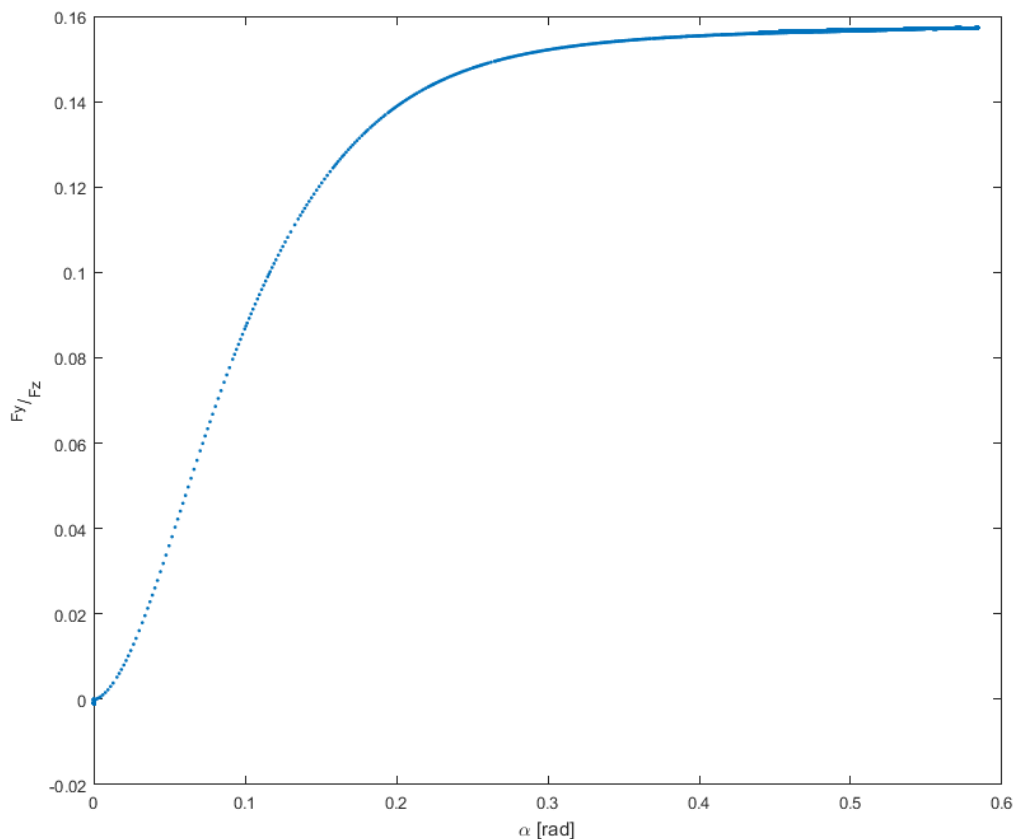


Figure 5-20. Transverse load depending on the side slip angle

As can be seen, the entire drift angle, beyond 0.2 rad, does not show any further transverse force increases.

The curve remains linear up to about 0.15 rad or about 8.5°. This linear part represents the cornering stiffness assigned through experimental data implemented in the Pacejka formulas.

In situations of high transversal sliding the tyre therefore does not significantly increase the lateral force it transfers to the vehicle. In a more detailed physical model a decrease in force is required for the high sideslip angles, however for the level of detail to which we want to get the answer is considered adequate.

As a further verification of the trend of transverse contact force as a function of the slip angle, we decided to go under steady state conditions.

The boundary conditions are changed by assigning a fixed steering angle (which in this case coincides with the slip angle) and the wheel is slid sideways at a constant speed. Thus transversal sliding is imposed and force is measured.

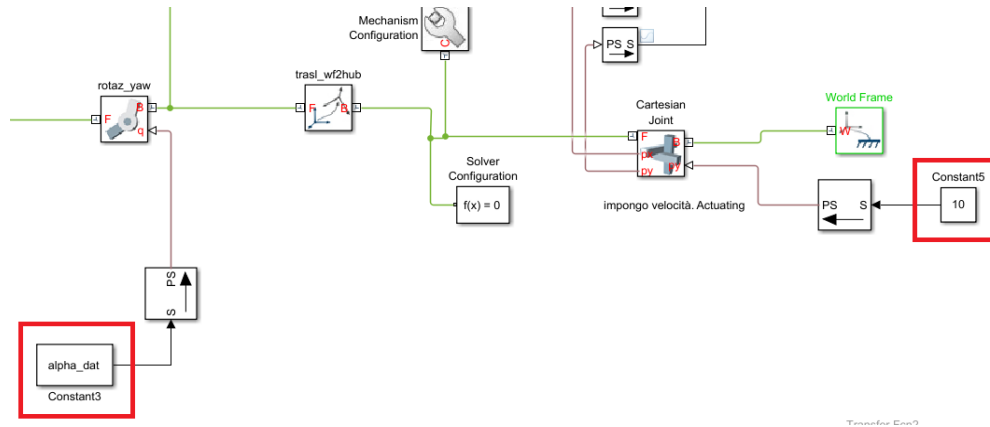


Figura 5-1. Sliding at a constant speed

The test is made for several slip angles and the force is measured in steady-state speed conditions.

The plot thus obtained is the following:

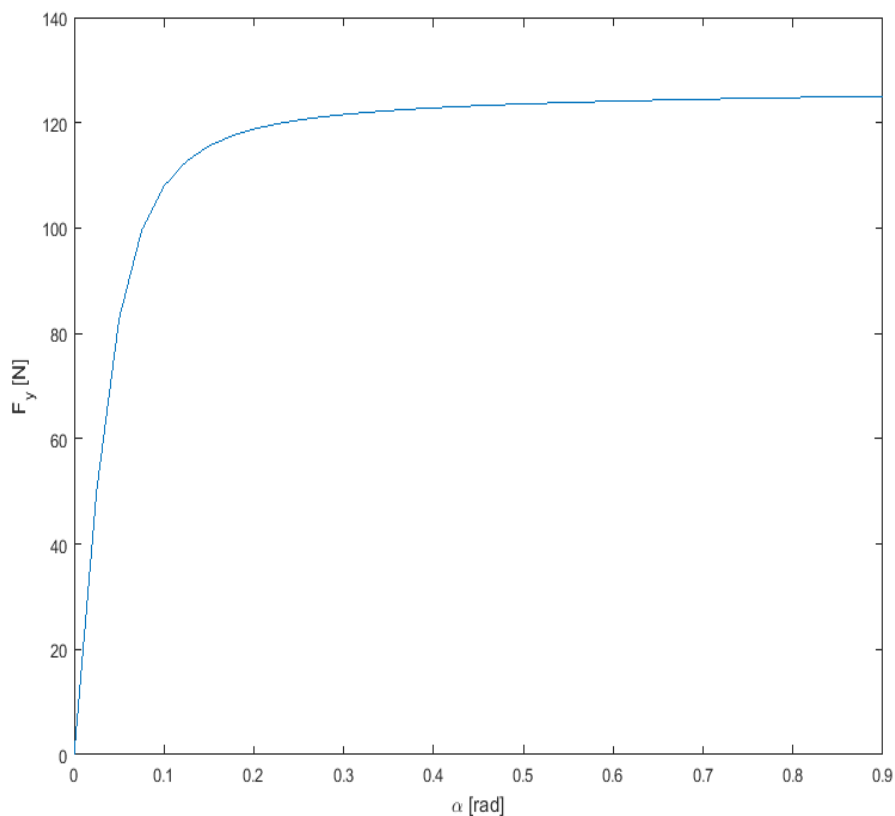


Figura 5-2. Steady state transversal load

5.5 Transverse force depending on the sliding coefficient

The longitudinal sliding is defined as:

$$k = \frac{\omega * R_0 - V_x}{V_x}$$

Note that the speed component x is about the local wheel reference system.

The evaluation of the longitudinal force trend in relation to the sliding was done with the straight-line wheel. In this way it is possible to analyze the longitudinal contributions without possible influences from the transverse ones.

The graph obtained is the following:

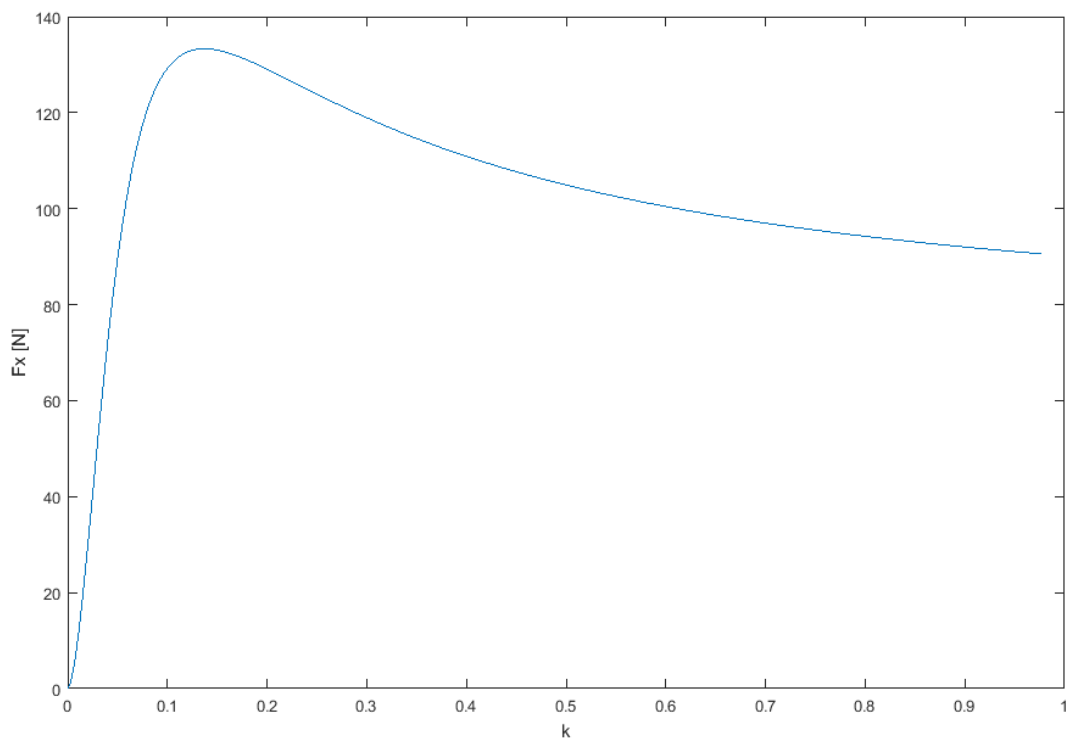


Figura 5-3. Longitudinal force depending to the sliding

After a first part in which the F_x rises almost linearly with the k there is a gradual descent due to high sliding.

To get this graph on the wheel only a very low torque has been assigned. On the other hand, the blocks generating the forces due to the rolling resistance have been deactivated. Also the braking torque and the constraining reaction of the longitudinal force itself are deactivated.

5.6 Response to camber variations

To validate the contribution of the camber, a simple curve was chosen by varying the camber angle by 5° at a time.

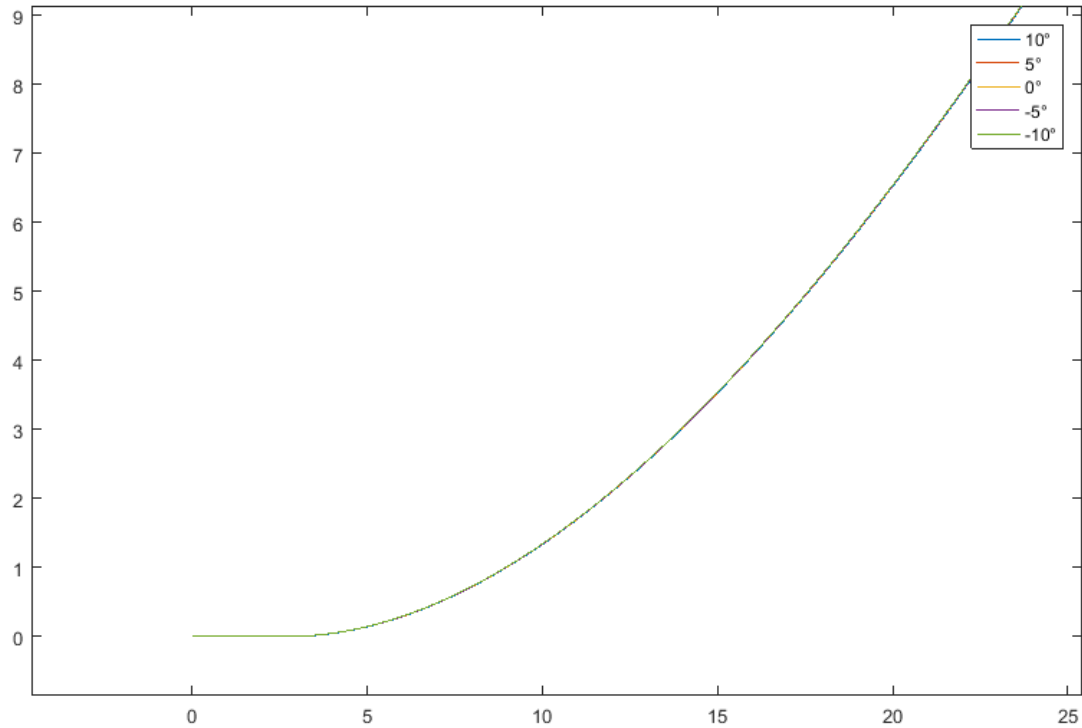


Figura 5-4. Path traveled to verify the camber

Seeing the different paths in detail, we obtain that the narrowest path, with respect to the assigned curvature, is obtained with a negative camber angle of 10° .

Going first towards the 0° and then towards positive angles the path becomes wider. Therefore the lateral sliding increase.

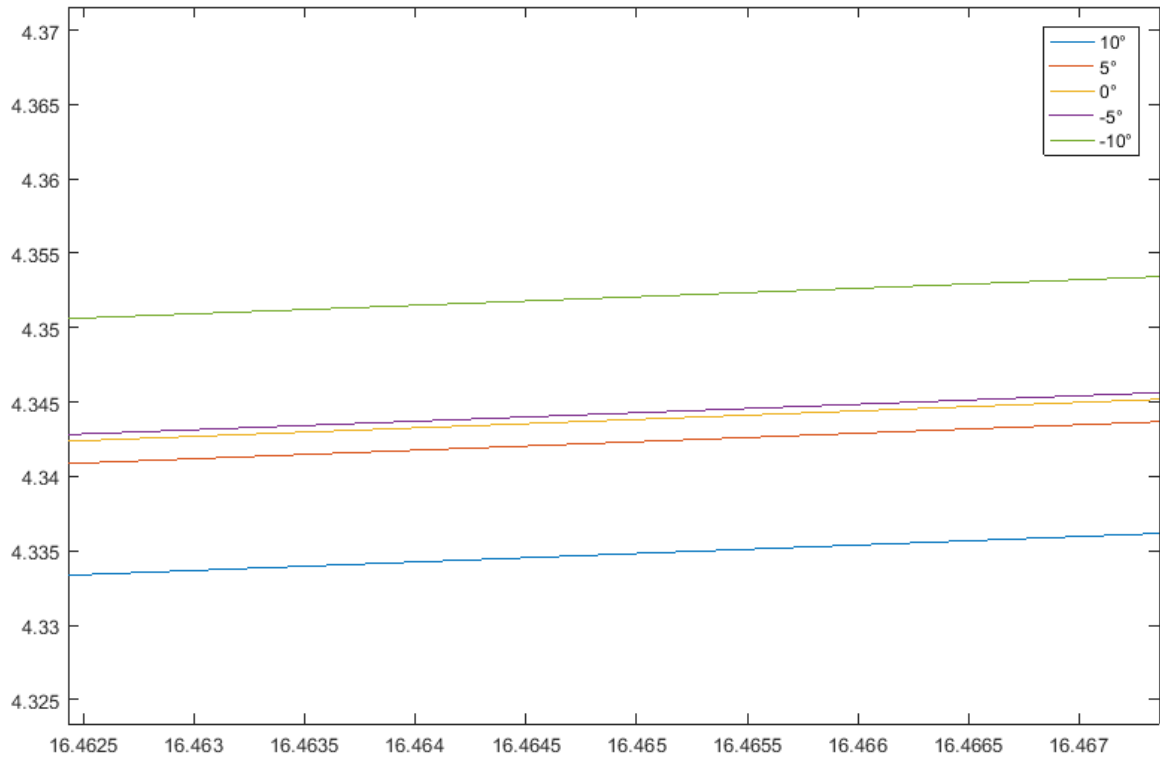


Figura 5-5. Camber depending to the path

6 Full model study

Getting plausible results with the tyre model is now possible to analyze the behavior of the complete model.

6.1 Steady state maneuvers

We decided to use maneuvers in a steady state in accordance with ISO-4138. In this way we can define standard maneuvers that can be used to study the behavior of the vehicle. Clearly this standard is not specific to racing vehicles but provides initial feedback on the operation of the model.

There are three parameters to consider for this type of test:

$\delta = \textit{steering angle}$

$v = \textit{speed}$

$R = \textit{corner radius}$

For each test a parameter is imposed as a constant, a second is changed while the third is measured, thus remaining free.

By analyzing the parameter variations we use three combinations.

1. Constant speed: in this case the steering is increased linearly and the radius of the curve obtained is measured.
2. Constant curvature radius: the speed is linearly increased, keeping the radius of curvature constant. To obtain this result it is necessary to introduce a control on the steering angle.
3. Constant steering angle: the speed is increased linearly and the increase of the cornering radius is measured, without any control (open loop).

6.1.1 Constant speed cornering

For the first case study a constant speed of 4 m / s was considered. However, the model is actuated by acting on the torques applied to the individual wheels. Since the resisting forces are present it was necessary to introduce a control logic in order to maintain a constant speed.

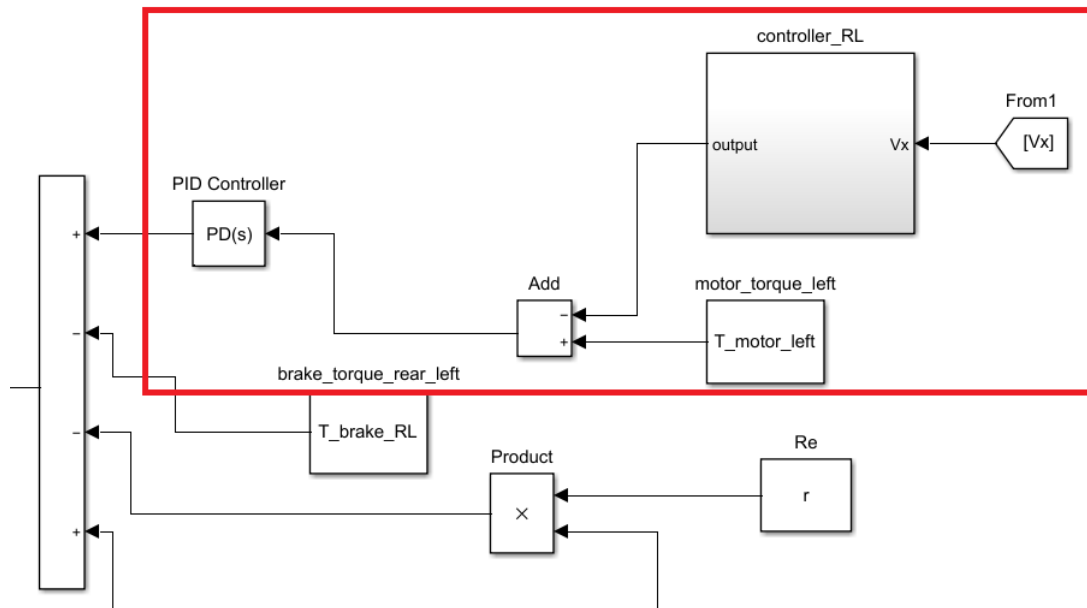


Figure 6-1. Velocity PD controller

The work carried out on the left rear wheel is taken as an example, considering that for the right there is the same situation. Another constant block is added to the constant motor torque, whose only input is the longitudinal speed measured on the vehicle's center of gravity.

We now enter the "controller RL" block to explain how the speed is regulated using as feedback the only available input (V_x), in addition to the constant speed v , which we want to maintain.

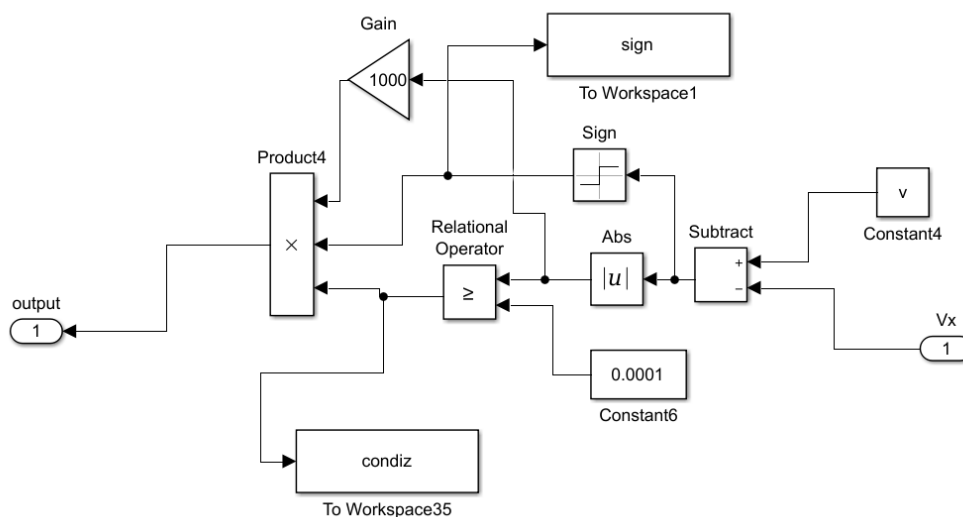


Figure 6-2. Controller-RL

We assess whether the difference in absolute value between the set speed and the current speed is greater than or equal to a certain tolerance (0.0001).

$$\text{If } |V - V_x| \geq 0.0001 = 1 \text{ else } = 0$$

If the difference is less than our tolerance, the null result (0) is multiplied by the other values, canceling the contribution of the control. In this way, being within the selected tolerance, we do not act on the motor torque.

Otherwise we are moving too far from the set speed. The unit value, result of the previous conditional, is multiplied by $|V - V_x|$, in turn multiplied by a gain (1000) and by the sign of the difference between the speeds.

The control in this second case adds or removes torque to the motor depending on the sign extrapolated and depending on how far it is deviating from the set speed, allowing to return to tolerance.

The torque to be added or subtracted from the motor is first processed by a proportional-derivative control that allows for a cleaner and more stable signal. We will not go any further into the detail of the choice of this type of control, nor of its values which are in any case reported below.

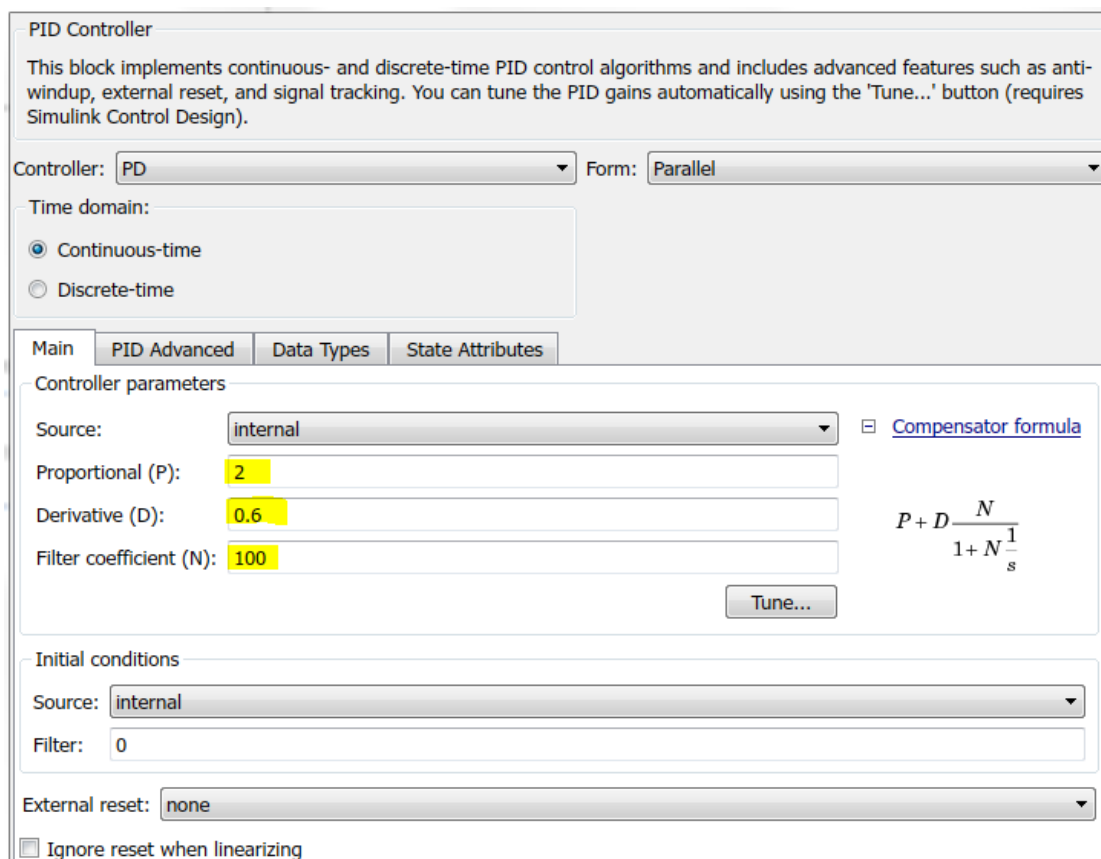


Figura 6-3. PD controller

The simulation was done keeping the speed as constant as possible.

Setting a speed of 4 m / s, the one actually held by the controlled system is visible in the graph below.

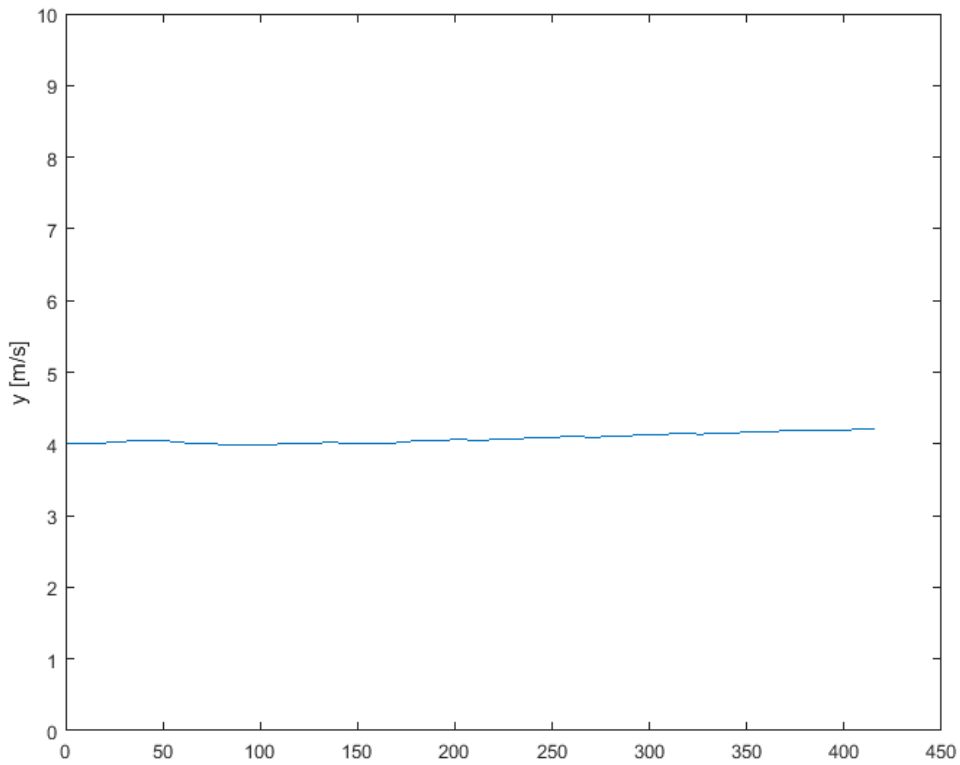


Figura 6-4. Constant speed

In these conditions, the simulation is cycled with different steering angles. Keep in mind that the vehicle has a constant steering ratio, so at each steering angle there is only one wheel angle.

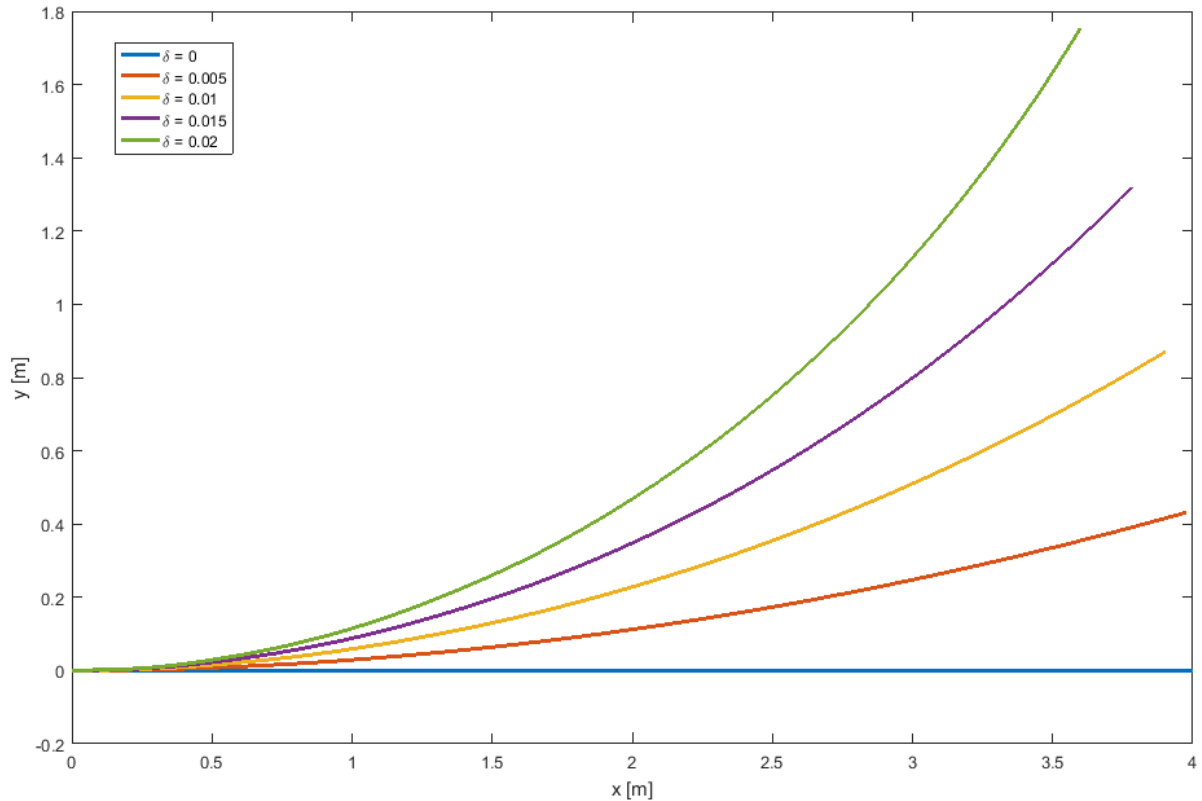


Figure 6-5. Steering angle increase/constant speed

The plot obtained shows the vehicle trajectory for various wheel angles (and therefore steering angles). As it was easy to expect the cornering radius is inversely proportional to the steering angle. By increasing the steering, curves with a lower curvature radius are obtained.

6.1.2 Constant cornering radius

In this second case, the speed is increased linearly while keeping the cornering radius constant. A steering angle control is introduced.

For the sake of simplicity, only three speeds are plotted: 2, 5 and 8 m /s. Once the first curve has been set at the lower speed to guarantee a similar trajectory with higher speeds (within a certain tolerance) it is necessary to increase the steering angle.

In detail, the following steering angles correspond to the speeds of 2, 5 and 8 m /s: 0.004, 0.009 and 0.026. The following plot shows the trajectories obtained with the different speeds.

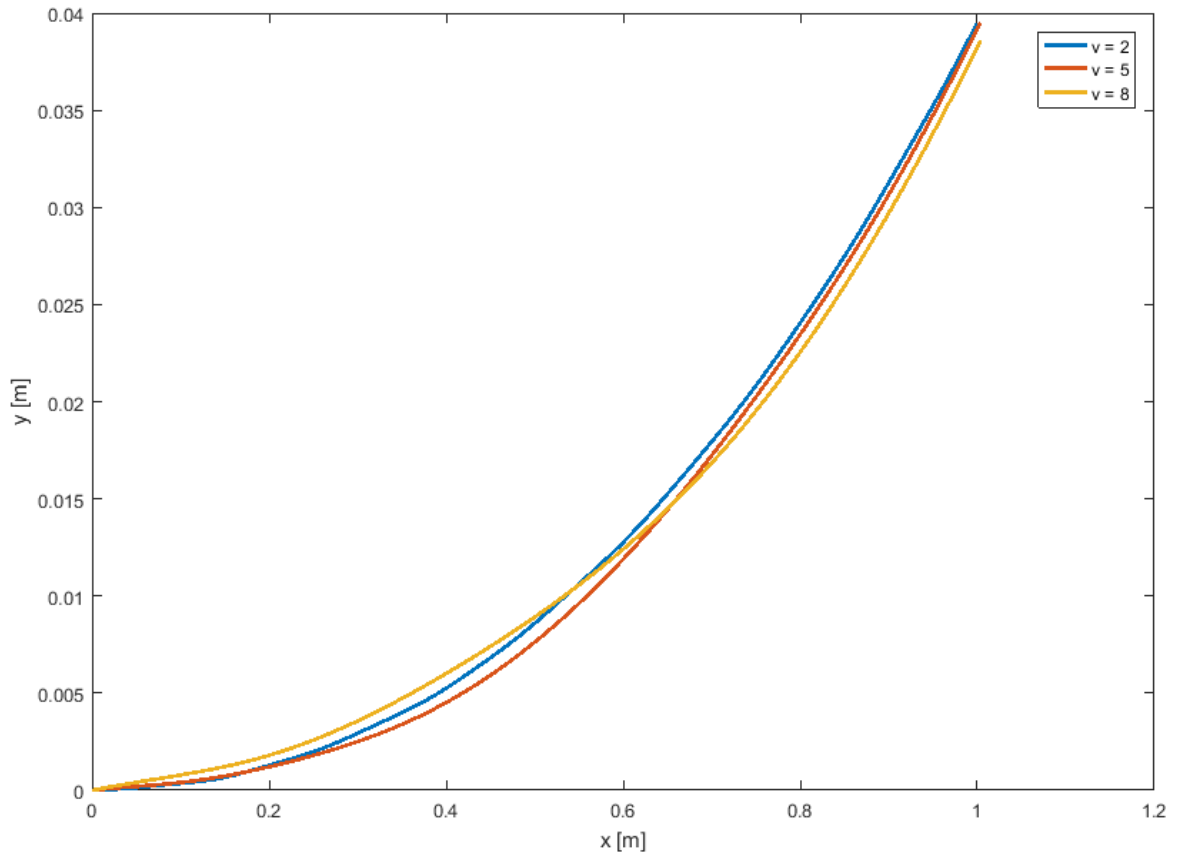


Figura 6-6. Trajectories with different speed and steering angle

It is important to note that a linear increment of the speed corresponds to a non-linear increment of the steering angle.

The slip angle rises increasing the speed. Therefore the vehicle's behavior to increase the cornering radius is consistent with the physical model. To correct the behavior of the car the pilot will be forced to steer even more for cornering taken at higher speeds.

6.1.3 Constant steering radius

The last case is similar to the previous one except that any control on the steering is removed. We linearly increase the speed and measure the increase of the cornering radius. In this case, the steering angle is set to 0.01 for each speed.

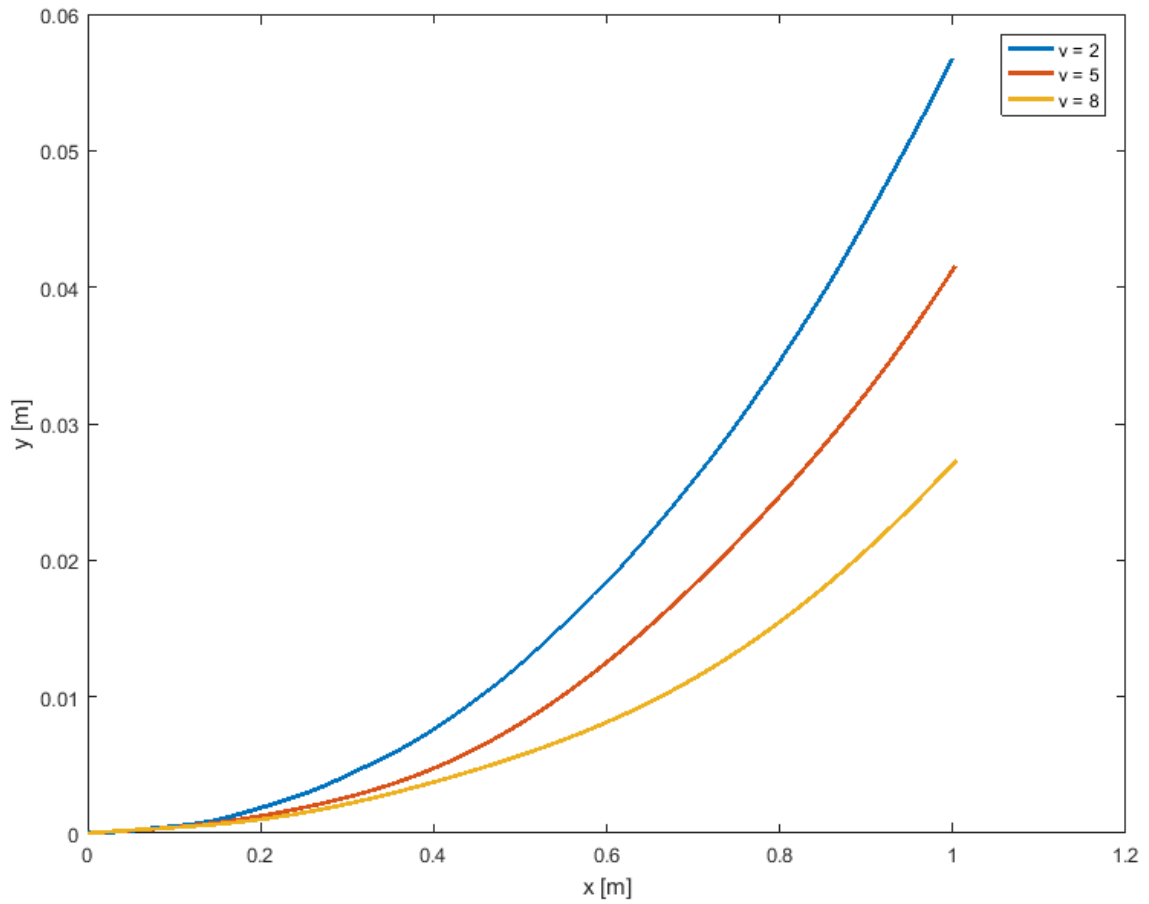


Figura 6-7. Trajectories with different speed and the same steering angle

As expected also from the previous case, we see that, once the steering control is removed, the car makes a trajectory with a greater cornering radius as the speed increases.

6.2 Transient maneuvers

Once the steady-state cases have been examined, we proceed to the study of maneuvers with the presence of transients.

6.2.1 Braking in a turn

The standard ISO 7975:1996 specifies an open-loop test procedure to determine the effect of braking during a steady-state corner.

During a circle with a given radius at a constant velocity the driver give a fast braking. The aim of this test is to understand the behavior of the car in a situation in which the ratio between longitudinal and lateral grip has an instantaneous change.

In our case we make two corner at the same speed. The first without braking and the second one with braking. Below we can see the different paths obtained.

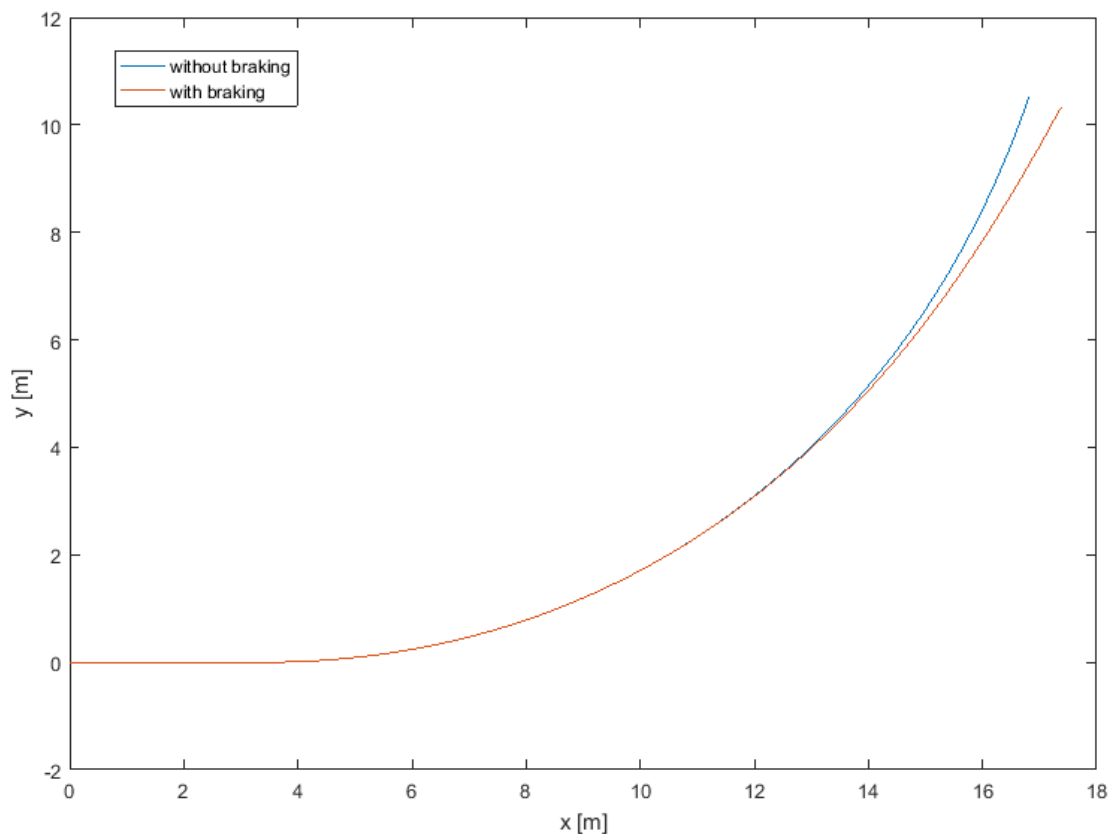


Figura 6-8. Path with and without braking

As we can see in the case with braking the corner radius increases. This behavior is due by a diminution of the transversal grip with respect to the other case.

This behavior is in accordance with the physical one of a real vehicle. So, also in this test, the model give a realistic output.

6.2.2 VDA test

This test, initially named “moose or elk test”, was designed to give a criterion to test the stability of a vehicle.

The aim of the moose test designers is to generate a reproducible method that allow to compare different vehicles. Moreover this test must be comprehensible for the customers and demonstrable.

VDA test procedure is described in the standard ISO 3888-2 :2011. It is a test track for a closed-loop lane-change maneuver . The aim of the test is to simulate an obstacle avoidance.

We report an image that allow to understand the lane-change maneuver.

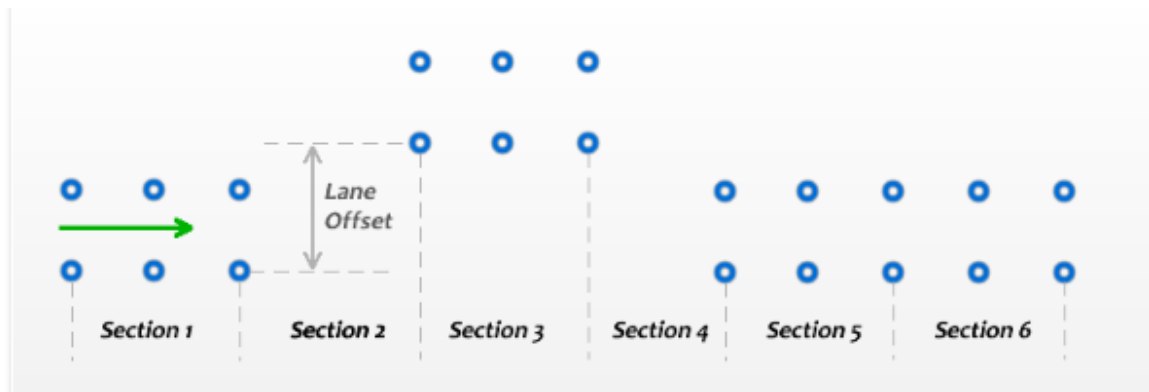


Figura 6-9. VDA test

As we can see the path is divided into six sections. The section lengths are shown below:

Section 1 length = 15 m

Section 2 length = 30 m

Section 3 length = 25 m

Section 4 length = 25 m

Section 5 length = 15 m

Instead, the sections width depends to the vehicle width.

*Section 1 width = 1.1 * vehicle width + 0.25 m*

*Section 3 width = 1.2 * vehicle width + 0.25 m*

*Section 5 width = 1.3 * vehicle width + 0.25 m*

The lane offset is equal to 3.5 m.

In our case, to perform the indicated maneuver it was necessary to introduce a control on the steering actuator to follow the set trajectory.

A proportional control is used which acts on the error with respect to the set path and the yaw measure of the vehicle.

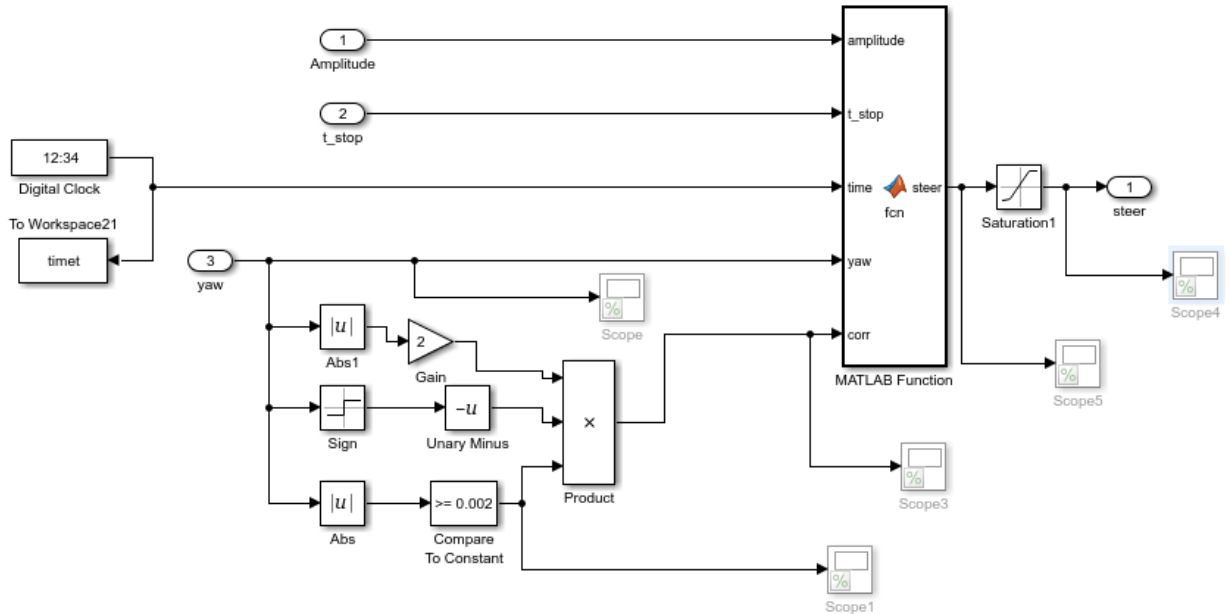


Figura 6-10. Actuator control

The “MATLAB Function” block communicates to the system the time instants in which to start steering. The maneuver continues until the difference between the target yaw angle and the instantaneous angle is not less than 0.002 rad.

This difference is used as a multiplicative coefficient for reaching the assigned trajectory.

The purpose of this thesis is not to faithfully recreate the VDA test but to use a similar maneuver to see the response of the model, so we don't care about the layout of the pins imposed by the regulations or even the standard speed.

Now we can see the response of a simulation at about 4 m/s. We obtain the following trajectory.

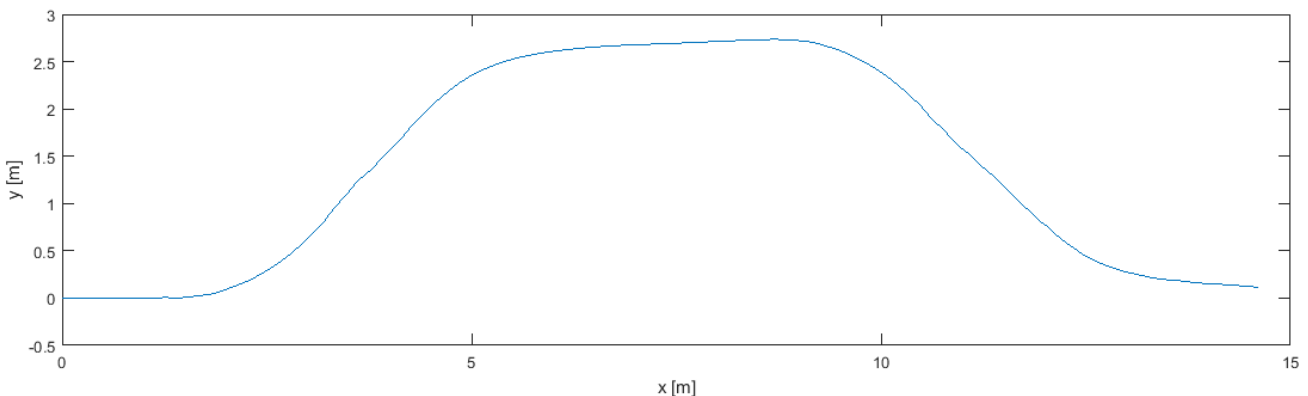


Figura 6-11. Trajectory in VDA test at 4m/s

Now we can see the plot of the steering. In the parts circled in red we can see that the path has a non-impulsive course as in the other sections. The trend is more gradual. This feature is due to the steering control which returns the car to the right direction.

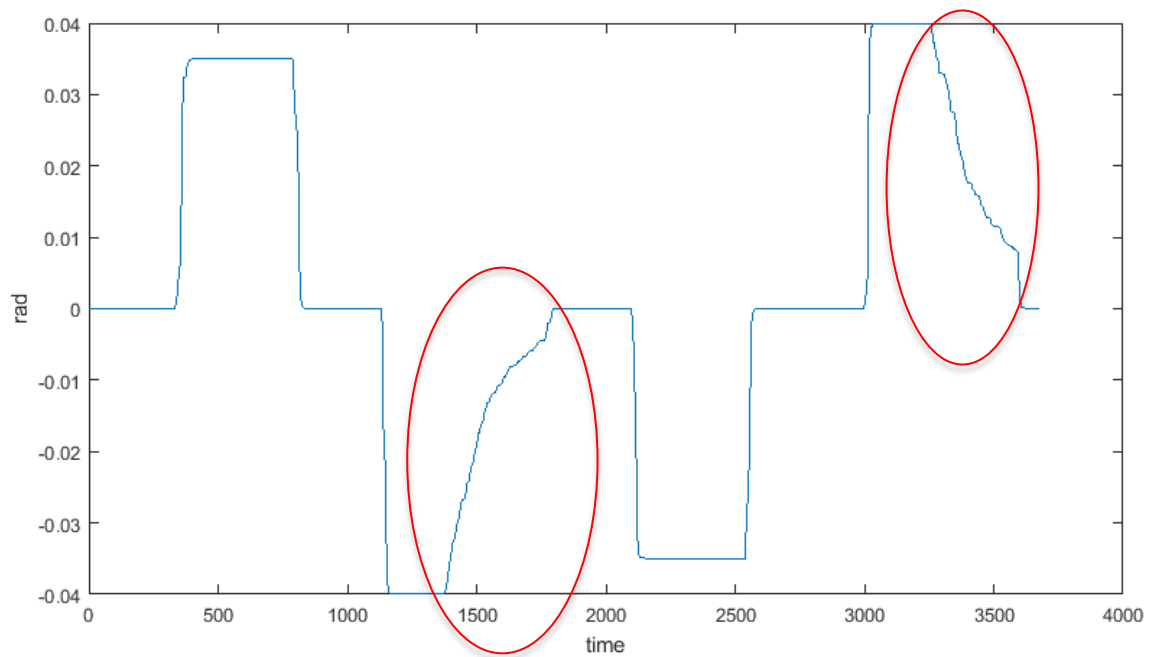


Figure 6-12. Steer in VDA test at 4 m/s

After the previous test we can try to increase the speed up to 8 m/s. The other inputs rest the same.

Like in the previous case we can see the path:

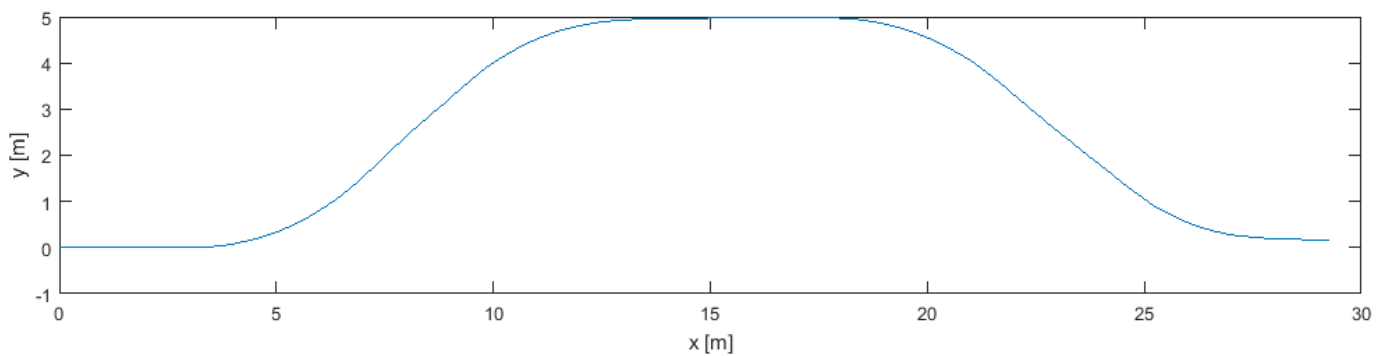


Figure 6-13. Figure 6-14. Trajectory in VDA test at 8 m/s

And the steering:

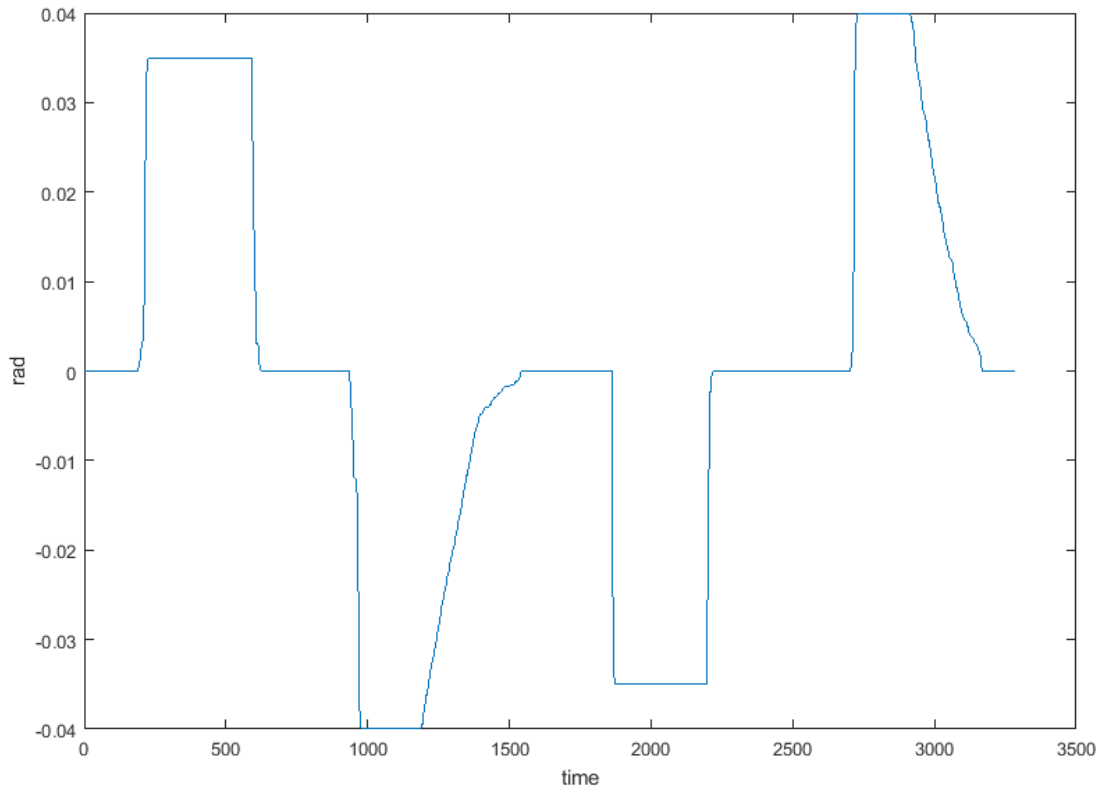


Figura 6-15. Steer in VDA test at 8 m/s

As we notice in the above plot in this second case the actuator has a fast response to achieve the required path.

With respect to the standard maneuver it was decided to select a lower speed but with a narrower maneuver to better understand the behavior of the vehicle between the cones of a dynamic test of the student formula.

7 Conclusions

Regarding the first part of the thesis we had mounted in the car the transmission and we can use it without problem in the operations of development of the motor controls.

In the image below we can see some transmission components before their mount. In this phases we dimensionally check the parts to ensure the right mount.

The respect of the dimensional tolerances is important to guarantee the correct interface with the supply components, like bearings for examples. Otherwise the assembly can be impossible.



Figura 7-1. Transmission components

Now we can see the transmission assembled in the car, the only missing parts in the photos are the two chains.

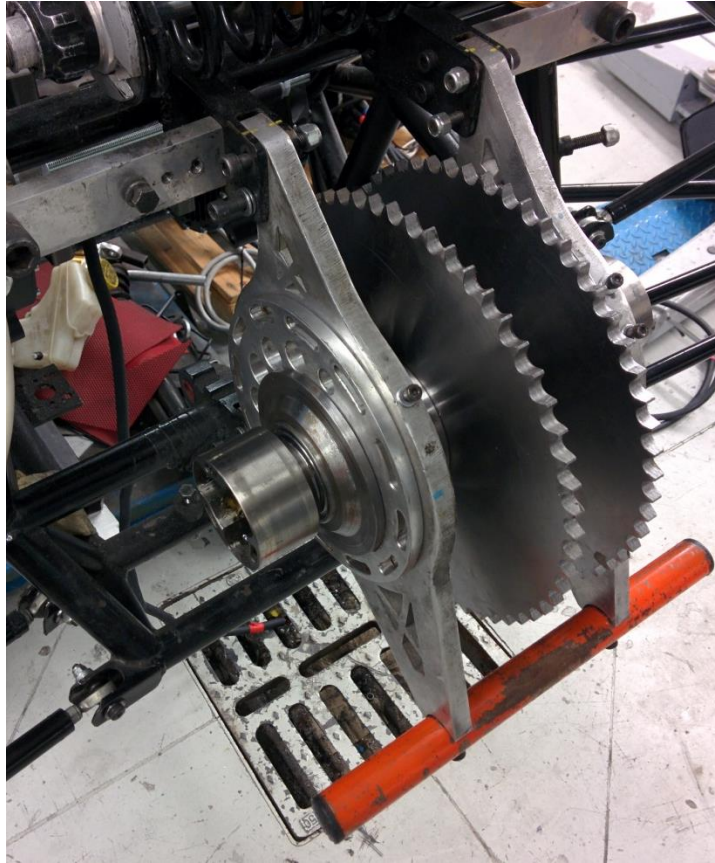


Figura 7-2. Transmission assembly in the car 1/2

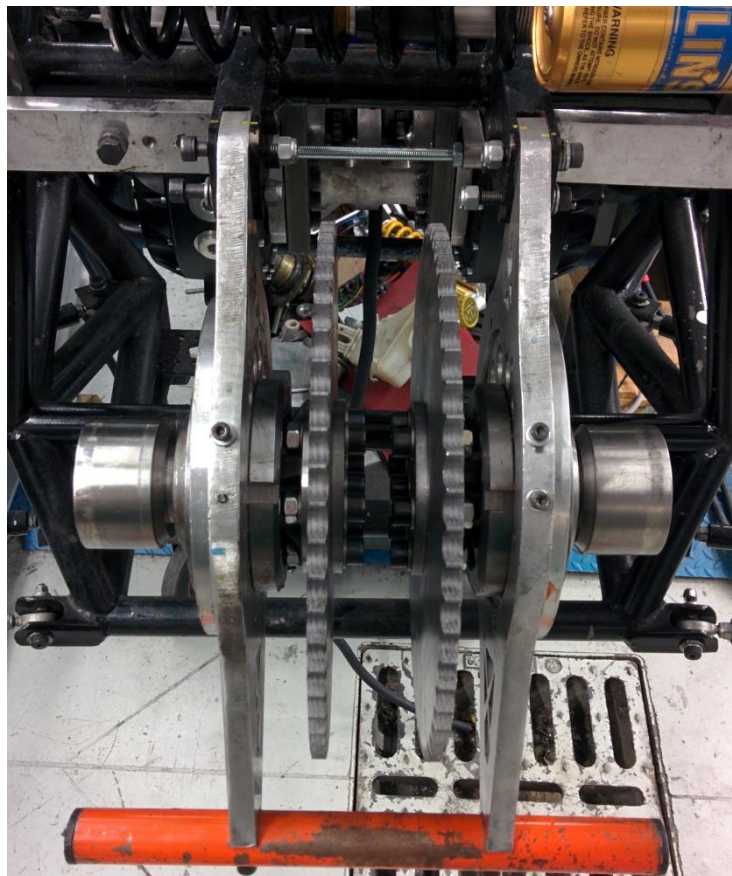


Figura 7-3. Transmission assembly in the car 2/2

Respect to the second part of the thesis the multibody model can be used, also with other future modification of layout, with simple corrections of the geometry in the model itself.

For the inertial behavior of the car the batteries accommodation is the most important thing, consider the weight of this components. The battery brackets welded to the previous DP5 frame allow us to develop a car to test the new motor layout but is clear that this solution are not applicable for a formula race car.

A study of a new frame optimized with the electrical layout will be necessary to develop a competitive car and a modification of the multibody model, to represent futures layout, will be the natural consequence.

In the images below we can see different phases of the design of the actual layout that the new multibody model represent.



Figura 7-4. Study of the new battery brackets



Figura 7-5. Battery brackets



Figura 7-6. New layout

So this model can be seen like a design instrument that simplify the develop of a future formula student car. The next step will be to compare physical data obtained by the real car with the output of the model. In this way we can calibrate the output to obtain a validated and affordable model.

8 Bibliography

- Dinamica dei sistemi meccanici [volume 1 e 2];G.Diana,F.Cheli.
- Corso ADAMS, D.Catalani.
- Standard ISO-4138:2012.
- Standard CNR-UNI 10011.
- Abaqus user's manual.
- Simulink user's manual.
- Standard ISO 3888-2 :2011
- Standard ISO 7975:1996